ABSTRACT

ZHU, JIANXI. Mathematical Modeling of Single Phase Flow and Particulate Flow Subjected to Microwave Heating. (Under the direction of Dr. Andrey V. Kuznetsov).

The purpose of this research is to numerically investigate heat transfer in liquids and liquids with carried solid particles as they flow continuously in a duct that is subjected to microwave irradiation. During this process, liquid flows in an applicator tube. When flow passes through the microwave cavity, the liquid absorbs microwave power and its temperature quickly increases. The spatial variation of the electromagnetic energy and temperature fields in the liquid was obtained by solving coupled momentum, energy and Maxwell's equations. A finite difference time domain method (FDTD) is used to solve Maxwell's equations simulating the electromagnetic field. The effects of dielectric properties of the liquid, the applicator diameter and its location, as well as the geometry of the microwave cavity on the heating process are analyzed. For modeling particulate flow subjected to microwave heating, the hydrodynamic interaction between the solid particle and the carrier fluid is simulated by the force-coupling method (FCM). The Lagrangian approach is utilized for tracking particles. The electromagnetic power absorption, temperature distribution inside both the liquid and the particles are taken into account. The effects of dielectric properties and the inlet position of the particle on electromagnetic energy and temperature distributions inside the particle are studied. The effect of the particle on power absorption in the carrier liquid is analyzed. The effect of the time interval between consecutive injections of two groups of particles on power absorption in particles is analyzed as well.

MATHEMATICAL MODELING OF SINGLE PHASE FLOW AND PARTICULATE FLOW SUBJECTED TO MICROWAVE HEATING

By

JIANXI ZHU

A dissertation submitted to the Graduate Faculty of
North Carolina State University
in partial fulfillment of the
requirements for the Degree of
Doctor of Philosophy

MECHANICAL ENGINEERING

Raleigh

2006

APPROVED BY:

_____	_____
ANDREY V. KUZNETSOV Chair of Advisory Committee	K. P. SANDEEP
_____	_____
WILLIAM L. ROBERTS	TAREK ECHEKKI

BIOGRAPHY

Jianxi (Jason) Zhu was born in Xi'an, China on March 9, 1979. He received his Bachelor of Science degree in Automotive Engineering from Xi'an Jiaotong University in July 2001. Wishing to further his education, he enrolled in the department of Mechanical, Industrial and Manufacturing Engineering at University of Toledo, Ohio, and obtained his Master of Science degree in December 2003. He continued his education at North Carolina State University to earn his Doctor of Philosophy degree in Mechanical Engineering in January 2004.

ACKNOWLEDGEMENTS

My sincere gratitude should be first delivered to my advisor, Dr. Andrey V. Kuznetsov for his continuous support and guidance during my studies at NC State University. His enthusiasm in research and encouragement has been the driving force for the successful completion of my research and dissertation.

I gratefully acknowledge the support of this work by a USDA grant and Dr. K. P. Sandeep, for suggesting the project in the first place, and for critical advice and help for my research. My thanks would extend to Dr. William L. Roberts and Dr. Tarek Echekki for serving on my Ph.D. committee.

This major undertaking has received the generous support from my officemates, Ms. Ping Xiang. Her assistance, suggestions and encouragement are very important to me.

I would like to especially thank my family and friends for their unconditional love and inspiration. This study would not have been possible without the assistance and dedication of a great many people. To them this dissertation is dedicated.

TABLE OF CONTENTS

LIST OF TABLES

LIST OF FIGURES

1 INTRODUCTION

1.1 MICROWAVE HEATING

Microwave heating is utilized to process materials for decades. The ability of microwave radiation to penetrate the material directly without the need for any intermediate heat transfer medium provides a new and significantly different tool for processing a variety of industrial materials. When compared with conventional heating methods, where heat is conducted from surface into the interior volume of the specimen, microwave energy causes volumetric heat generation in the material, which results in high energy efficiency and a reduction in heating time. This is especially desirable for specimen of thick section and materials with low thermal conductivities, where surface heat may require much time to diffuse though the specimen.

Microwave processing of materials has been utilized in a wide range of industrial applications. In 1949, microwave heating of materials was first discovered, and the commercial microwave oven was first introduced by Raytheon in 1952. During the past two decades, microwave heating of food product has been extensively used in the world. Other important microwave applications on processing of materials include industrial heating (large volume drying of textiles, rubber, and ceramic), material development (polymer matrix composites curing, ceramic sintering and plasma processing), and microwave removing of volatile constituents deep within materials [1]. In addition to these applications available, microwave processing has been considered for processing of radioactive wastes [2]. Microwave energy evaporates the liquid in the waste solution, which contains glass forming additives. Once the liquid have evaporated the remaining

mixture continues to absorb microwave energy until it fuses and vitrifies. In a similar process, infectious medical wastes can be irradiated prior to disposal, eliminating the need for incineration and off-sit treatment [3]. All these extensive applications of microwave heating stem from the great advantages of microwave heating over the traditional heating methods.

1.2 MICROWAVE PROCESSING DEVICE

Microwaves are defined as electromagnetic waves with frequencies in the range from 300 MHz to 300 GHz. The corresponding wavelengths are from 10 cm to 0.1 cm. A microwave system typically consists of a generator to produce the microwaves, a waveguide to transport the microwaves and a cavity to manipulate microwaves for a specific purpose. Microwave cavities are classified as either single-mode, where a single standing electromagnetic wave fills the cavity, or multimode, where the cavity dimensions and microwave source frequency produce multiple standing waves. Single-mode cavities have had limited applications in industry because of a limited processing volume over which the electric field is useful, but have been particularly effective in plasma processing, joining and fiber curing. In a multimode system, the fixed frequency microwaves yield resonant modes over a narrow frequency band around the operating frequency. The modes result in regions of high and low electric fields within the cavity. In general, the uniformity of the field increases as the cavity size increase, but the uniformity also is dependent on the overall cavity dimensions [4].

Magnetrons, gyrotrons, klystrons and traveling wave tubes are used to generate microwaves. Each has its advantages. Klystrons offer precise control in amplitude,

frequency and phase. Gyrotrons offer the possibility of providing much higher power output (megawatts) and beam focusing. The traveling wave tubes can provide variable and controlled frequencies of microwave energy. Magnetrons are by far the most widely used microwave source for home microwave ovens and industrial microwave systems, due to their availability and low cost. Solid state devices also are available for generating microwaves, but typically have been limited in power (few tens of watts) [5].

Certain features of microwave device have most likely hindered more widespread use of microwave energy for industrial processes;(i.e. limited and fixed frequencies, low temperature capabilities, field non-uniformity and complexity, and inability to monitor or control the internal temperatures). Although microwave energy covers a broad frequency range, to avoid interference with established telecommunication and defense frequencies, the U.S. government has defined frequency bands centered at 2.45GHz and 915MHz for industrial, scientific and medical microwave use [6, 7]. These two frequencies provide a good compromise between penetration depth, absorption and equipment costs for food processing. Water and other polar molecules couple well with these frequencies. Unfortunately for the rest of the materials processing community, they are not always the optimum frequencies for heating polymers, ceramics, composites and other materials. Most of the equipment is designed for low- temperature (few hundred °C) cooking and drying. Consequently, the equipment is not designed or properly insulated for the high temperatures (>1000°C) required to process most ceramics and composites. Field uniformity also has been a problem, especially for the lower frequency microwaves (2.45 and 915MHz), where the wavelengths are several inches. The power absorbed by the

material is strongly dependent on the internal electric field. In turn, the internal field is controlled by the field inside the cavity, which can vary widely in most cavities [5].

1.3 DIELECTRIC PROPERTIES OF MATERIALS

Microwave radiation penetrates a material and produces a volumetrically distributed heat source, due to molecular friction resulting from dipolar rotation of polar solvents and fro the conductive migration of dissolved ions. The dipolar rotation is caused by variations of the electric and magnetic fields in the material [8]. Water, a major constituent of many materials is the main source of microwave interactions due to its dipolar nature [9]. When microwaves are applied to the material, forces on the charged particle from the oscillating electric field cause charged particles to move away from their equilibrium positions. This gives rise to induced dipoles which respond to the applied field. These dipoles are inclined to reoriented themselves in response to the changing electric field. The resistance to the reorientations of the dipole causes losses, attenuating the electric field and heating the material volumetrically. When a specimen is placed in a microwave cavity, the propagating microwave will penetrate and travel through the specimen. Once a steady root-mean-square electric field is achieved in the microwave cavity and specimen, the oscillating electric field within the material serves as a volumetric heat source. If the frequency of the electric field is near the natural frequency at which dipole reorientation occurs, the amount of heat generated within the material is maximized [2].

The propagation of microwave in air and other materials depends on the dielectric properties of the medium. The important properties that describe the behavior of

microwave propagation in a dielectric material are complex permittivity, ε, and the complex permeability, μ :

$$\varepsilon = \varepsilon' - i\varepsilon'' \tag{1.1}$$

$$\mu = \mu' - i\mu'' \tag{1.2}$$

The real part of the complex permittivity, ε', is the relative permittivity, and the imaginary part, ε'', is called the effective loss factor. The real part of the complex permeability, μ', is referred to as the relative permeability, and the imaginary part, μ'', is the magnetic loss factor.

The amount of microwave energy that the specimen absorbs depends strongly on the dielectric properties of the material. For insulating (non-magnetic) materials, the complex permittivity, ε, indicates the ability of the material to store and absorb energy from the oscillating electric source field. The relative permittivity, ε', indicates the penetration of microwave into the material. And the effective loss factor, ε'', characterizes the ability to store energy.

In addition, two alternative parameters, the loss tangent, , and the absorption coefficient, , are used to characterize the ability of the material to absorb microwave energy. They are defined as [10]:

$$\tan\delta = \frac{\varepsilon''}{\varepsilon'} \tag{1.3}$$

$$\sigma = 2\pi f \varepsilon_0 \varepsilon'' + \sigma_e \tag{1.4}$$

where f is the microwave frequency, ε_0 is the permittivity of free space or vacuum, and σ_e is the electric conductivity ($\sigma_e = 0$ for a nonconductor dielectric). From Eq. (1.4), it is

evident that the absorption of microwave energy is not only proportional to the effective permittivity but also the microwave frequency.

1.4 NUMERICAL MODELING OF MICROWAVE HEATING PROCESS

The intensity and spatial distribution of microwave energy throughout a material specimen is dictated by the complexity of electromagnetic waves scattering and reflecting in the microwave unit, as well as absorption of electromagnetic waves within the material [11]. Factors that influence microwave heating include dielectric properties, volume, and shape of the material, as well as design and geometric parameters of the microwave unit [12]. These factors make it difficult to precisely control the heating process in order to obtain the desired temperature distribution in the material. Due to complexity of the physical process, numerical modeling has been widely utilized to study microwave heating [13].

Modeling of microwave heating requires solving the energy equation with a source term, which describes microwave power absorption in the material. The power absorption can be evaluated by two methods, using the Lambert's law or by directly solving Maxwell's equations. Lambert's law has been extensively used in recent literature [14-16], mostly when the heated sample is large. In large samples microwave power absorption decays exponentially from the surface into the material. In small size samples, since the heat is generated by the resonance of standing waves, which Lambert's law can not adequately describe, the solution of Maxwell's equations is necessary to accurately determine the microwave power absorption.

In the past, a number of studies [17-24] have been documented that dealt with numerical modeling of microwave heating process by solving Maxwell's equations. The finite difference time domain (FDTD) method developed by Yee [25] has been used to provide a full description of electromagnetic scattering and absorption and gives detailed spatial and temporal information of wave propagation. Due to its versatility in handling complex shaped objects, a wide range of frequencies and stimuli, and a variety of materials, including those which exhibit frequency and temperature dependence, the FDTD method has received increased attention. A comparison of the FDTD method and other widely used methods for simulating microwave propagation and electromagnetic-material interactions are be found in refs. [26,27]. Solutions of Maxwell's equations using the FDTD method for a number of simplified cases are reported in Webb et al. [28]. Three-dimensional simulations of microwave propagation and energy deposition are presented in Liu et al. [19], Zhao and Turner [29], and Zhang et al. [30].

Success in the numerical simulation of electromagnetic propagation has recently generated interest in numerical modeling of heat transfer induced by microwave radiation. Clemens and Saltiel [16] developed a model of microwave heating of a solid specimen. Their model accounts for temperature dependent dielectric properties, which causes coupling between the Maxwell's and energy equations. Effects of the microwave frequency, dielectric properties of the specimen, and the size of the sample on the microwave energy deposition were investigated in a two-dimensional formulation. Other important papers addressing modeling of microwave heating processes include Ayappa et al. [31-33], Basak et al. [34], and Ratannadecho et al. [35-36].

Although most previous studies of microwave heating focused on conduction heat transfer in a specimen, a few recent papers investigated natural convection induced by microwave heating of liquids; mathematical models utilized in these papers included the momentum equation. Datta et al. [37] investigated natural convection in a liquid subjected to microwave heating. In their study, the microwave energy deposition was assumed to decay exponentially into the sample based on Lambert's law, which is valid only for a high loss dielectric material and a sample of large size.

Ratanadecho et al. [38] were the first who investigated, numerically and experimentally, microwave heating of a liquid layer in a rectangular waveguide. The movement of liquid particles induced by microwave heating was taken into account. Coupled electromagnetic, hydrodynamic and thermal fields were simulated in two dimensions. The spatial variation of the electromagnetic field was obtained by solving Maxwell's equations with the FDTD method. Their work demonstrated the effects of microwave power level and liquid electric conductivity on the degree of penetration and the rate of heat generation within the liquid layer. Furthermore, an algorithm for resolving the coupling of Maxwell's, momentum, and energy equations was developed and validated by comparing with experimental results.

1.5 DISSERTATION STRUCTURE

The organization of this dissertation involves a total of six chapters. The present chapter provides a general introduction to the microwave heating, microwave processing device, dielectric properties of materials, and numerical modeling of microwave heating process, as well as the structure of the dissertation itself. Chapter 2 (published as ref.

[39]) investigates forced convection in a rectangular duct subjected to microwave heating. Three types of non-Newtonian fluids flowing through the duct are considered, specifically, apple sauce, skim milk, and tomato sauce. A finite difference time domain method is used to solve Maxwell's equations simulating the electromagnetic field. The three-dimensional temperature field is determined by solving the coupled momentum, energy, and Maxwell's equations. Chapter 3 (published as ref. [40]) investigates heat transfer in liquids as they flow continuously in a circular duct that is subjected to microwave heating. The transient Maxwell's equations are solved by the Finite Difference Time Domain (FDTD) method to describe the electromagnetic field in the microwave cavity and the waveguide. Simulations aid in understanding the effects of dielectric properties of the fluid, the applicator diameter and its location, as well as the geometry of the microwave cavity on the heating process. Chapter 4 (published as ref. [41]) investigates microwave heating of a food particle and carrier liquid as they flow continuously in a circular pipe. The electromagnetic power and temperature distributions in both the liquid and the particle are taken into account. The hydrodynamic interaction between the solid particle and the carrier fluid is simulated by the force-coupling method (FCM). This chapter explores the effects of dielectric properties and the inlet position of the particle on microwave energy and temperature distributions inside the particle. The effect of the particle on power absorption in the carrier liquid is studied as well. Chapter 5 (published as ref. [42]) investigates microwave heating of a liquid and large particles that it carries while continuously flowing in a circular applicator pipe. Computational results are presented for the microwave power absorption, temperature distribution inside the liquid and the particles, as well as the velocity distribution in the applicator pipe and

trajectories of particles. The effect of the time interval between consecutive injections of two groups of particles on power absorption in particles is studied. The influence of the position of the applicator pipe in the microwave cavity on the power absorption and temperature distribution inside the liquid and the particles is investigated as well.

REFERENCES

1. Venkateswaran, S., Merkle, C.L. (1991) Numerical modeling of waveguide heated microwave plasmas, *Multidisciplinary Applications of Computational Fluid Dynamics, ASME,* 129: 1-12.
2. Smith, S.E. (2001): *Numerical modeling of hybrid dielectric heating within a multi mode microwave cavity,* MS thesis, Indiana University-Purdue University at Indianapolis, IN.
3. Lagos, L.E., Li, W., Ebadian, M.A. (1995) Heat transfer within a concrete slab with a finite microwave heating source, *International Journal of Heat and Mass Transfer*, 38(5): 887-897.
4. Clark, D.E., Folz, D.C., West, J.K. (2000) Processing materials with microwave energy, *Journal of Materials Science and Engineering*, A287: 153-158.
5. Clark, D.E., Sutton, W.H. (1996) Microwave processing of materials, *Annual Review of Materials Science*, 26: 299-331.
6. Saltiel, C. Fathi, Z., Sutton, W. (1995) Materials processing with microwave energy, *Mechanical Engineering*, 117: 102-105.
7. Chamchong, M., Datta, A.K. (1999) Thawing of foods in a microwave oven: I. effect of power levels and power cycling, *Journal of Microwave Power and Electromagnetic Energy*, 34: 9-21.
8. Alton, W.J. (1998) Microwave pasteurization of liquids, *Society of Manufacturing Engineers Paper*, No. EM98-211.

9. Oliveira, M.E.C., Franca, A.S. (2002) Microwave heating of foodstuffs, *Journal of Food Engineering*, 53: 347-359.

10. Metaxas, A.C. Meredith, R.J. (1983) *Industrial Microwave Heating*, Peter Peregrinus Ltd., London.

11. Clemens, J., Saltiel, C. (1995) Numerical modeling of materials processing microwave furnaces, *International Journal of Heat and Mass Transfer*, 39: 1665-1675.

12. Anantheswaran, R.C., Liu, L. (1994) Effect of viscosity and salt concentration on microwave heating of model non-Newtonian liquid foods in a cylindrical container, *Journal of Microwave Power and Electromagnetic Energy*, 29: 119-126.

13. Zhang, Q., Jackson, T.H., Ungan, A. (2000) Numerical modeling of microwave induced natural convection, *International Journal of Heat and Mass Transfer*, 43: 2141-2154.

14. Saltiel, C., Datta, A. (1997) Heat and mass transfer in microwave processing, *Adv. Heat Transfer*, 30: 1-94.

15. Franca, A.S., Haghighi, K. (1996) Adaptive finite element analysis of microwave driven convection, *International Communications in Heat and Mass Transfer*, 23: 177-186.

16. O'Brien, K.T., Mekkaoui, A.M. (1993) Numerical simulation of the thermal fields occurring in the treatment of malignant rumors by local hyperthermia, *Journal of Biomechanical Engineering*, 115: 247-253.

17. Jia, X., Bialkowski, M. (1992) Simulation of microwave field and power distribution in a cavity by a three dimensional finite element method, *Journal of Microwave Power and Electromagnetic Energy*, 27: 11-22.

18. Deepak, Evans, J.W. (1993) Calculation of temperatures in microwave-heated two-dimensional ceramic bodies, *Journal of American Ceramic Society*, 76: 1915-1923.
19. Liu, F., Turner, I., Bialkowski, M. (1994) A finite-difference time-domain simulation of power density distribution in a dielectric loaded microwave cavity, *Journal of Microwave Power and Electromagnetic Energy*, 29: 138-147.
20. Iwabuchi, K., Kubota, T., Kashiwa, T., Tagashira, H. (1997) Analysis of electromagnetic fields using the finite-difference time-domain method in a microwave oven loaded with high-loss dielectric, *Electronics and Communications in Japan*, 78: 41-50.
21. Dibben, D.C., Metaxas, A.C. (1997) Frequency domain vs. time domain finite element methods for calculation of fields in multimode cavities, *IEEE Transaction on Magnetics*, 33: 1468-1471.
22. Dibben, D.C., Metaxas, A.C. (1994) Finite element time domain analysis of multimode applicators using edge elements, *Journal of Microwave Power and Electromagnetic Energy*, 29: 243-251.
23. Kriegsmann, G.A. (1997) Cavity effects in microwave heating of ceramics, *Journal of Applied Mathematics*, 57: 382-400.
24. Araneta, J.C., Brodwin, M.E., Kriegsmann, G.A. (1984) High-temperature microwave characterization of dielectric rods, *IEEE Transactions on Microwave Theory and Techniques*, 32: 1328-1335.
25. Yee, K.S. (1966) Numerical solution of initial boundary value problem involving Maxwell's equations in isotropic media, *IEEE Trans. on Antennas and Propagation*, 14: 302-307.

26. Miller, E.K. (1994) Time-domain modeling in electromagnetics, *Journal of Electromagnetic Waves and Applications*, 8: 1125-1172.

27. Iskander, M.F. (1992) Computer modeling and numerical techniques for quantifying microwave interactions with materials, *Microwave Processing of Materials II*, 189: 149-171.

28. Webb, J.P., Maile, G.L., Ferrari, R.L. (1983) Finite element implementation of three dimensional electromagnetic problems, *IEEE Proceedings*, 78: 196-200.

29. Zhao, H., Turner, I.W. (1996) An analysis of the finite-difference time-domain method for modeling the microwave heating of dielectric materials within a three-dimensional cavity system, *Journal of Microwave Power and Electromagnetic Energy*, 31: 199-214.

30. Zhang, H., Taub, A.K., Doona, I.A. (2001) Electromagnetics, heat transfer and thermokinetics in microwave sterilization, *AIChE Journal*, 47: 1957-1968.

31. Ayappa, K.G., Davis, H.T., Davis, E.A., Gordon, J. (1992) Two-dimensional finite element analysis of microwave heating, *AIChE Journal*, 38: 1577-1592.

32. Ayappa, K.G., Brandon, S., Derby, J.J., Davis, H.T., Davis, E.A. (1994) Microwave driven convection in a square cavity, *AIChE Journal*, 40: 1268-1272.

33. Ayappa, K.G., Sengupta, T. (2002) Microwave heating in multiphase systems: evaluation of series solutions, *Journal of Engineering Mathematics*, 44: 155-171.

34. Basak, T., Ayappa, K.G. (1997) Analysis of microwave thawing of slabs with effective heat capacity method, *AIChE Journal*, 43: 1662-1667.

35. Ratanadecho, P., Aoki, K., Akahori, M. (2002) The characteristics of microwave melting of frozen packed beds using a rectangular waveguide, *IEEE Trans. on Microwave Theory and Techniques*, 50: 1495-1502.

36. Ratanadecho, P., Aoki, K., Akahori, M. (2002) Influence of irradiation time, particle sizes, and initial moisture content during microwave drying of multi-layered capillary porous materials, *Journal of Heat Transfer*, 124: 151-161.

37. Datta, A., Prosetya, H., Hu, W. (1992) Mathematical modeling of batch heating of liquids in a microwave cavity, *Journal of Microwave Power and Electromagnetic Energy*, 27: 38-48.

38. Ratanadecho, P., Aoki, K., Akahori, M. (2002) A Numerical and experimental investigation of the modeling of microwave heating for liquid layers using a rectangular wave guide (effects of natural convection and dielectric properties), *Applied Mathematical Modeling*, 26: 449-472.

39. Zhu, J., Kuznetsov, A.V., Sandeep, K.P. (2005) Numerical simulation of forced convection in a duct subjected to microwave heating, *Heat and Mass Transfer*, http://dx.doi.org/10.1007/s00231-006-0105-y (online first).

40. Zhu, J., Kuznetsov, A.V., Sandeep, K.P. (2005) Mathematical modeling of continuous flow microwave heating of liquids (effects of dielectric properties and design parameters), *International Journal of Thermal Sciences*, In press.sdfs

41. Zhu, J., Kuznetsov, A.V., Sandeep, K.P. (2006) Numerical modeling of a moving particle in a continuous flow subjected to microwave heating, *Numerical Heat Transfer, Part A*, Submitted.

42. Zhu, J., Kuznetsov, A.V., Sandeep, K.P. (2006) Investigation of a particulate flow subjected to microwave heating, *Heat and Mass Transfer*, Submitted.

2 NUMERICAL SIMULATION OF FORCED CONVECTION IN A DUCT SUBJECTED TO MICROWAVE HEATING

ABSTRACT

In this chapter, forced convection in a rectangular duct subjected to microwave heating is investigated. Three types of non-Newtonian fluids flowing through the duct are considered, specifically, apple sauce, skim milk, and tomato sauce. A finite difference time domain method is used to solve Maxwell's equations simulating the electromagnetic field. The three-dimensional temperature field is determined by solving the coupled momentum, energy, and Maxwell's equations. Numerical results show that the heating pattern strongly depends on the dielectric properties of the fluid in the duct and the geometry of the microwave heating system.

Nomenclature

A area, m^2

C_p specific heat capacity, $J/(kg \cdot K)$

c phase velocity of the electromagnetic propagation wave, m/s

E electric field intensity, V/m

f frequency of the incident wave, Hz

h effective heat transfer coefficient, $W/(m^2 \cdot K)$

H magnetic field intensity, A/m

L standard deviation of temperature, ^oC

k thermal conductivity, $\mathrm{W/(m \cdot K)}$

m fluid consistency coefficient

n flow behavior index

N_t number of time steps

p pressure, Pa

q electromagnetic heat generation intensity, $\mathrm{W/m^3}$

Q volume flow rate, $\mathrm{m^3/s}$

T temperature, $^{o}\mathrm{C}$

t time, s

$\tan\delta$ loss tangent

w velocity component in the z direction, m/s

W width of the cavity, m

Z_{TE} wave impedance, Ω

Greek symbols

η apparent viscosity, $\mathrm{Pa \cdot s}$

ε electric permittivity, F/m

ε' dielectric constant

ε'' effective loss factor

λ_g wave length in the cavity, m

μ magnetic permeability, H/m

ρ density, kg/m^3

σ electric conductivity, S/m

Superscripts

τ instantaneous value

Subscripts

∞ ambient condition

0 free space, air

in input

x,y,z projection on a respective coordinate axis

2.1 INTRODUCTION

Microwave heating has been utilized in the food industry for decades. It has been used predominantly as a batch processing and sporadically as a continuous process. Microwave heating has well-known advantages over traditional heating methods, such as fast heating and high energy efficiency as well as heating without direct contact with high temperature surfaces. However, microwave heating has also been known to heat products

non-uniformly [1-3]. Several factors affect the magnitude and uniformity of absorption of electromagnetic energy. These include dielectric properties, ionic concentration, volume, and shape of a product [4]. The power and temperature distributions inside the product can be predicted by solving the coupled momentum, energy, and Maxwell's equations. Due to a large number of factors that affect heating and the complexity of the equations involved, numerical modeling is the only viable approach for conducting realistic process simulations [5].

A number of studies have been reported that dealt with numerical modeling of the microwave heating problem in a cavity containing a lossy material. Solutions of Maxwell's equations for a number of simplified cases are presented in de Pourcq [2], Webb et al. [6], and Ayappa et al. [7]. Electromagnetic field and microwave power distributions for three-dimensional cavities are obtained in Liu et al. [8], Zhao and Turner [9], and Zhang et al. [10]. As for the simulation of heat transfer induced by microwave treatment, most previous works focused on the solid lossy material inside the microwave cavity. Zhang and Datta [11] coupled two separate finite element softwares to predict the temperature distribution inside solid foods due to heating in a domestic microwave oven. Liu et al. [8] applied a finite difference time domain (FDTD) algorithm to a three-dimensional problem and investigated heating inside a partially loaded cavity, demonstrating the significant effect of relative location of the dielectric material within the cavity. There are also recent studies of a multi-dimensional heating process of a liquid by a microwave field. Zhang et al. [5] developed a three-dimensional model by coupling the momentum, energy, and Maxwell's equations to investigate natural convection of a contained liquid induced by microwave heating. In their model, the local microwave

power dissipation in a liquid is predicted by employing an FDTD method and the transient temperature and flow patterns in the liquid are simulated using the "SIMPLER" algorithm [12]; the two modules are coupled by temperature dependent dielectric properties of the liquid. A similar algorithm is adopted in the present study.

This chapter reports a numerical prediction of forced convection heat transfer occurring in a rectangular applicator within a three-dimensional microwave cavity. Three types of liquid foods are considered in this chapter to investigate the effect of dielectric properties on heating by simulating the steady-state temperature distributions in various liquids.

2.2 GEOMETRY OF THE SYSTEM

The microwave heating system, as illustrated in Figure 2.1, consists of a single mode microwave resonant cavity and a vertical applicator tube. The liquid flows through the applicator tube vertically upward, absorbing microwave energy during the process which heats the liquid.

As shown in Figure 1, the cavity dimensions ($Cx \times Cy \times Cz$) are 406 × 305 × 124mm. The applicator tube dimensions ($Ax \times Ay \times Az$) are 46 × 46 × 124mm. The applicator is located in the center of the cavity so that the centerline of the applicator is located at $Dx = Cx/2 = 203$mm and $Dy = Cy/2 = 152.5$mm. The microwave cavity is excited in TE_{10} mode [13] operating at a frequency of 915 MHz by imposing a plane polarized source at the incident plane ($x = 21$mm). The reflected microwave energy is absorbed at the absorbing plane ($x = 0$mm).

2.3 MATHEMATICAL MODEL FORMULATION

2.3.1 ELECTROMAGNETIC FIELD

The equations governing the electromagnetic field are based on the Maxwell curl relation. The three-dimensional unsteady Maxwell's equations in Cartesian coordinates are:

$$\frac{\partial H_x}{\partial t} = \frac{1}{\mu}\left(\frac{\partial E_y}{\partial z} - \frac{\partial E_z}{\partial y}\right) \tag{2.1}$$

$$\frac{\partial H_y}{\partial t} = \frac{1}{\mu}\left(\frac{\partial E_z}{\partial x} - \frac{\partial E_x}{\partial z}\right) \tag{2.2}$$

$$\frac{\partial H_z}{\partial t} = \frac{1}{\mu}\left(\frac{\partial E_x}{\partial y} - \frac{\partial E_y}{\partial x}\right) \tag{2.3}$$

$$\frac{\partial E_x}{\partial t} = \frac{1}{\varepsilon}\left(\frac{\partial H_z}{\partial y} - \frac{\partial H_y}{\partial z} - \sigma E_x\right) \tag{2.4}$$

$$\frac{\partial E_y}{\partial t} = \frac{1}{\varepsilon}\left(\frac{\partial H_x}{\partial z} - \frac{\partial H_z}{\partial x} - \sigma E_y\right) \tag{2.5}$$

$$\frac{\partial E_z}{\partial t} = \frac{1}{\varepsilon}\left(\frac{\partial H_y}{\partial x} - \frac{\partial H_x}{\partial y} - \sigma E_z\right) \tag{2.6}$$

where E and H are the electric and magnetic field intensities, σ is the electric conductivity, μ is the magnetic permeability, and ε is the electric permittivity.

The boundary conditions for the electromagnetic fields are:

- At the surface of the wall of the cavity, a perfect conducting condition is utilized. Therefore, normal components of magnetic fields and tangential components of electric fields are assumed to vanish:

$$H_n = 0, \quad E_t = 0 \tag{2.7}$$

At the absorbing plane, Mur's [14] first order absorbing condition is utilized:

$$\left(\frac{\partial}{\partial z} - \frac{1}{c}\frac{\partial}{\partial t} \right) E_z \Big|_{x=0} = 0 \tag{2.8}$$

where c is the phase velocity of the propagation wave.

- At the incident plane, the input microwave source is simulated by the following equations:

$$E_{Z,inc} = -E_{in} \sin\left(\frac{\pi y}{W} \right) \cos\left[2\pi \left(ft - \frac{x_{in}}{\lambda_g} \right) \right] \tag{2.9}$$

$$H_{Y,inc} = \frac{E_{in}}{Z_{TE}} \sin\left(\frac{\pi y}{W} \right) \cos\left[2\pi \left(ft - \frac{x_{in}}{\lambda_g} \right) \right] \tag{2.10}$$

where E_{in} is the input value of the electric field intensity, W is the width of the cavity, Z_{TE} is the wave impedance, and λ_g is the wave length of a microwave in the cavity.

2.3.2 HEAT AND MASS TRANSPORT EQUATIONS

The flow in the applicator is assumed to be hydrodynamically fully developed; only the streamwise velocity component is non-zero. The momentum equation is then presented as:

$$\frac{\partial}{\partial x}\left(\eta \frac{\partial w}{\partial x} \right) + \frac{\partial}{\partial y}\left(\eta \frac{\partial w}{\partial y} \right) - \frac{dp}{dz} = 0 \tag{2.11}$$

where η is the apparent viscosity for the non-Newtonian fluid, which in this chapter is assumed to obey the power-law. The apparent viscosity for the power-law fluid is given by:

$$\eta = m\left[\left(\frac{\partial w}{\partial x}\right)^2 + \left(\frac{\partial w}{\partial y}\right)^2\right]^{(n-1)/2} \tag{2.12}$$

where m and n are the fluid consistency coefficient and the flow behavior index, respectively.

The temperature distribution in the liquid is obtained by solving the following energy equation wherein the microwave power absorption is accounted for by an electromagnetic heat source term:

$$\rho C_p\left(\frac{\partial T}{\partial t} + w\frac{\partial T}{\partial z}\right) = k\left(\frac{\partial^2 T}{\partial x^2} + \frac{\partial^2 T}{\partial y^2}\right) + q \tag{2.13}$$

where q stands for the local electromagnetic heat generation intensity term, which is a function of dielectric properties of the liquid and the electric field intensity:

$$q = 2\pi f \varepsilon_0 \varepsilon'(\tan\delta)E^2 \tag{2.14}$$

In Eq. (2.14), ε_0 is the permittivity of the air, ε' is the dielectric constant of the liquid, and $\tan\delta$ is the loss tangent, a dimensionless parameter defined as:

$$\tan\delta = \frac{\varepsilon''}{\varepsilon'} \tag{2.15}$$

where ε'' stands for the effective loss factor. The dielectric constant, ε', characterizes the penetration of the microwave energy into the product, while the effective loss factor, ε'', indicates the ability of the product to convert the microwave energy into heat. Both ε' and ε'' are dependent on the microwave frequency and the temperature of the product. $\tan\delta$ indicates the ability of the product to absorb microwave energy.

The following boundary conditions are utilized. At the inner surface of the applicator tube, a hydrodynamic no-slip boundary condition is used. At the inlet to the applicator, a uniform, fully developed velocity profile is imposed; it is specified by the inlet volume flow rate, Q. Heat transfer at the applicator wall is modeled as follows. The wall is assumed to lose heat by natural convection, which is modeled by the following equations:

at the walls normal to the x direction :

$$-k\frac{\partial T}{\partial x} = h\left(T - T_{\infty}\right) \tag{2.16}$$

at the walls normal to the y direction :

$$-k\frac{\partial T}{\partial y} = h\left(T - T_{\infty}\right) \tag{2.17}$$

where k is the thermal conductivity of the liquid and h is the effective heat transfer coefficient defined as:

$$h = \frac{1}{1/h_{air} + L_{wall}/k_{wall} + 1/h_{liquid}} \tag{2.18}$$

where h_{air} stands for the heat transfer coefficient from the applicator wall to the air in the cavity and h_{liquid} stands for the heat transfer coefficient from the liquid inside the applicator to the wall. L_{wall} is the thickness of the applicator wall and k_{wall} is the thermal conductivity of the wall. The inlet liquid temperature is set uniform and equal to the temperature of the free space outside the applicator, T_{∞}. The initial temperature of the liquid is defined as:

$$T = T_\infty \quad \text{at} \quad t = 0 \tag{2.19}$$

2.4 COMPUTATIONAL PROCEDURE

Two different time steps are utilized to update the electromagnetic and thermal-flow fields. An FDTD method [15] is used to solve Maxwell's equations (2.1)-(2.6). The obtained electromagnetic fields are used to calculate the electromagnetic heat source, given by Eq. (2.14), which represents the heating effect of the microwave field on the liquid. Since in Eq. (2.14) the dielectric constant, ε', and the loss tangent, $\tan\delta$, are temperature dependent, an iterative scheme is required to resolve the coupling of the energy and Maxwell's equations. The time scale for electromagnetic transients (a nanosecond scale) is much smaller than that for the flow and thermal transport (a second scale). A time step in the block of the code that solves Maxwell's equations must satisfy the stability requirement of the FDTD scheme [16] written as:

$$\Delta t \le \frac{1}{c\sqrt{\frac{1}{\Delta x^2} + \frac{1}{\Delta y^2} + \frac{1}{\Delta z^2}}} \tag{2.20}$$

The momentum and energy equations are solved by applying an implicit scheme; a time step of one second is utilized in these computations. The electromagnetic heat source, q, defined by Eq. (2.14), is computed in terms of the time average field, $\overline{E}$, which is treated as a constant over one time step for the thermal-flow computation, and defined as:

$$\overline{E} = \frac{1}{N_t}\sum_{\tau=1}^{N_t} E^\tau \tag{2.21}$$

where N_t is the number of time steps in each period of the microwave and E^τ is the instantaneous E field. The details of the numerical scheme used in this chapter are given in ref. [17].

2.5 RESULTS AND DISCUSSION

Table 2.1 shows electromagnetic and thermo-physical properties used in computations. The temperature-dependent data for the dielectric constant and loss tangent are plotted versus temperature in Figure 2.2.

2.5.1 HEATING PATTERNS FOR LIQUIDS WITH DIFFERENT DIELECTRIC PROPERTIES

Figure 2.3 displays steady-state temperature distributions at the outlet of the applicator for the three different liquids as well as the corresponding electromagnetic heat generation intensity distributions. The heat generation intensity is also shown at the applicator outlet; however, its dependence on z (different from that of the temperature) is insignificant. This figure illuminates the interaction of the electromagnetic field and forced convection in the liquid. It illustrates that the temperature and electromagnetic heat generation intensity are nonuniformly distributed at the applicator outlet for all liquids. For the apple sauce, from Figure 2.3-a(1), the electromagnetic heat generation intensity distribution at the applicator outlet exhibits two well-defined peaks near the central area. Since the electromagnetic heat generation intensity determines the temperature distribution, Figure 2.3-a(2) depicts two hot spots around the central area and four hot spots at the corners of the applicator tube. Similar behavior of electromagnetic heat generation intensity and temperature can be observed in Figure 2.3-b(1-2) for the

skim milk, while the intensities of the hot spots near the center of the tube are smaller. For the tomato sauce, from Figure 2.3-c(1-2), the peaks of the electromagnetic heat generation intensity disappear and there are no hot spots of the temperature in the central area of the applicator tube, only four hot spots at the corners. From this analysis it can be concluded that although the difference of dielectric properties of these three liquids is not great (see Figure 2.2), it causes a significant difference in their heating as they pass through the microwave cavity. In order to evaluate the uniformity of the temperature distribution quantitatively, a standard deviation of temperature is introduced as:

$$L = \sqrt{\frac{1}{A}\iint \left(T - T_m\right)^2 dA} \tag{2.22}$$

where A is the area of a cross-section perpendicular to the streamwise direction, and T_m is the mean temperature. Figure 2.4 displays the standard deviation of temperature versus the streamwise locations for the three liquids considered in this chapter. A larger standard deviation of temperature corresponds to a more nonuniform temperature distribution. Figure 2.4 shows that at the outlet of the applicator, the apple sauce has the most uniform temperature distribution and the tomato sauce has the most nonuniform temperature distribution. This can be attributed to the difference of their dielectric properties. From Figure 2.2, one can see that the dielectric constants ε' of the three liquids are almost the same; however, the loss tangent, $\tan\delta$, is significantly different for these three products. Consider the heat generation intensity equation, Eq. (2.14), if the frequency of the microwave and the dielectric constant are held constant. In this case the electromagnetic heat generation is proportional to the loss tangent. Thus, being a high loss liquid (with a large loss tangent), the tomato sauce absorbs more microwave energy than the skim milk

(which is characterized by a medium loss tangent) and the apple sauce (which is characterized by the smallest loss tangent of the three products), which results in the peak value of the electromagnetic heat generation intensity; also, the temperature range (T_{max}-T_{min}) for the tomato sauce is larger than that for the skim milk and the apple sauce. The result is that the tomato sauce has the largest standard deviation of temperature at the outlet (the most nonuniform temperature distribution at the outlet) and the apple sauce has the most uniform temperature distribution.

2.5.2 *Effect of Different Locations of the Applicator on the Heating Process*

This section discusses the effect of positioning the applicator at different locations in the microwave cavity. As previously mentioned, Figure 2.3 shows the heat generation intensity and temperature distributions at the outlet of the applicator for the three liquids when the applicator is located at the center of the microwave cavity (which is considered as its base position). Figure 2.5 shows similar distributions with the applicator displaced by 141mm forward in the x direction from the base position (see Figure 2.1). A comparison between Figures 2.3 and 2.5 suggests that there is a great difference between the distributions and magnitudes of the electromagnetic heat generation intensity and temperature for the two cases. In particular, in Figure 2.3-a(2), which shows the temperature distribution at the outlet of the applicator for the apple sauce, there are two hot spots near the center of the applicator while in Figure 2.5-a(2) there is only one hot spot positioned almost exactly in the center of the applicator. Also, the peak value of the temperature in Figure 2.5-a(2) is about 1.7 times greater than that in Figure 2.3-a(2). Comparing Figures 2.3-a(1) and 2.5-a(1), one can find similar differences in the

distributions of the electromagnetic heat generation intensity. This proves the significant effect of positioning the applicator tube in the microwave cavity on heating the product.

2.5.3 EFFECT OF THE SIZE OF THE APPLICATOR

The effect of the size of the applicator tube on heating patterns for the apple sauce is discussed in this paragraph. Figure 2.6 shows the electromagnetic heat generation intensity and temperature distributions of the three liquids at the outlet of the applicator with dimensions of 60×60×124mm. This applicator is larger than the applicator of the base size (46×46×124mm) although the enlarged applicator is positioned similarly in the center of the cavity, at the same location as the applicator of the base size. Comparing Figures 2.3 and 2.6, the distributions of the electromagnetic heat generation intensity and temperature are greatly affected by enlarging the applicator. For example, in the skim milk the peak value of the electromagnetic heat generation intensity and temperature in the applicator of a larger size are twice and three times larger than those in the applicator of the base size, respectively. This can be attributed to the fact that the larger applicator has a larger cross-sectional area allowing for more absorption of the microwave energy; also, for the same inlet volume flow rate, the flow in a larger applicator has a lower flow rate thus allowing fluid particles have larger residence time, which makes it possible for them to absorb more microwave energy.

2.6 CONCLUSIONS

A numerical model is developed to simulate forced convection in a rectangular duct subjected to microwave heating. The results reveal a complicated interaction between electromagnetic field and convection. Dielectric properties of a liquid flowing in

the applicator tube play an important role in the heating process. Even a small difference in dielectric properties can result in a completely different heating pattern. It is also found that the electromagnetic heat generation intensity and the temperature distributions in the liquid are sensitive to the size and the location of the applicator. Both the magnitude and the distribution of the electromagnetic heat generation intensity and the temperature depend strongly on the geometry of the microwave heating system. This illustrates the importance of numerical modeling to design an optimal microwave heating device.

Table 2.1 Parameter values utilized in computations.

	Apple Sauce	Skim Milk	Tomato Sauce
f, MHz	915	915	915
E_0, V/m	9000	9000	9000
μ, H/m	$4\pi\times10^{-7}$	$4\pi\times10^{-7}$	$4\pi\times10^{-7}$
ε_0, F/m	8.854×10^{-12}	8.854×10^{-12}	8.854×10^{-12}
k, W/(m·K)	0.5350	0.5678	0.5774
c_p, J/(kg·K)	3703.3	3943.7	4000.0
h, W/(m^2·K)	30	30	30
ρ, kg/m^3	1104.9	1047.7	1036.9
Q, m^3/s	6.0×10^{-6}	6.0×10^{-6}	6.0×10^{-6}
m	32.734	0.0059	3.9124
n	0.197	0.98	0.097

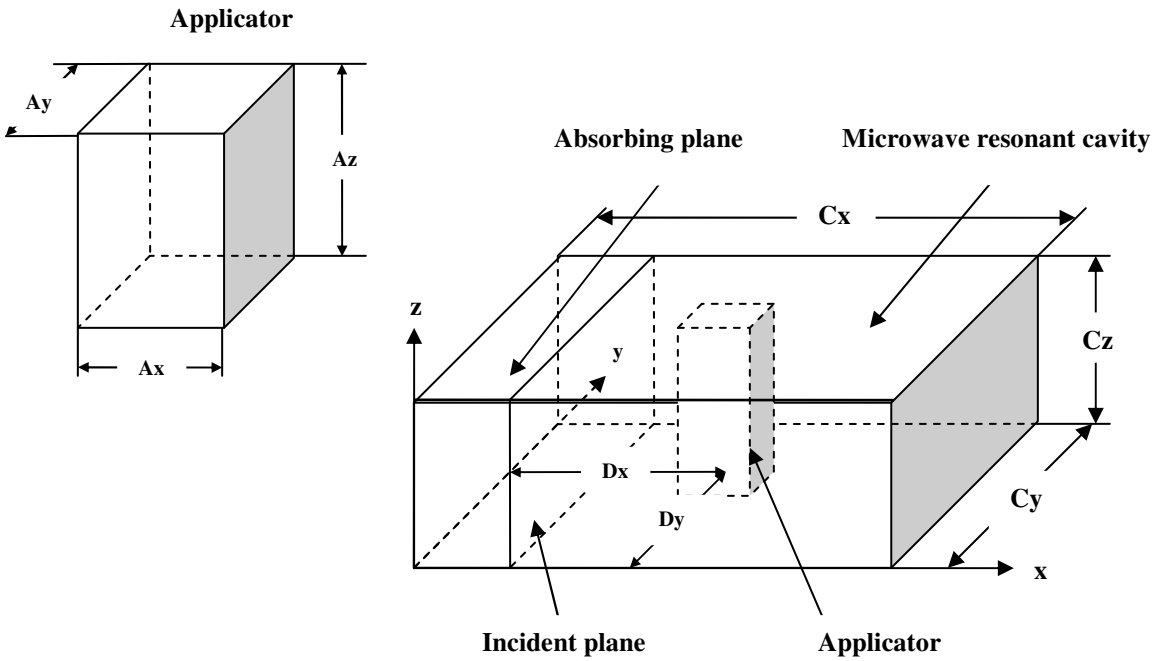

Figure 2.1 Schematic diagram of the microwave cavity and the applicator.

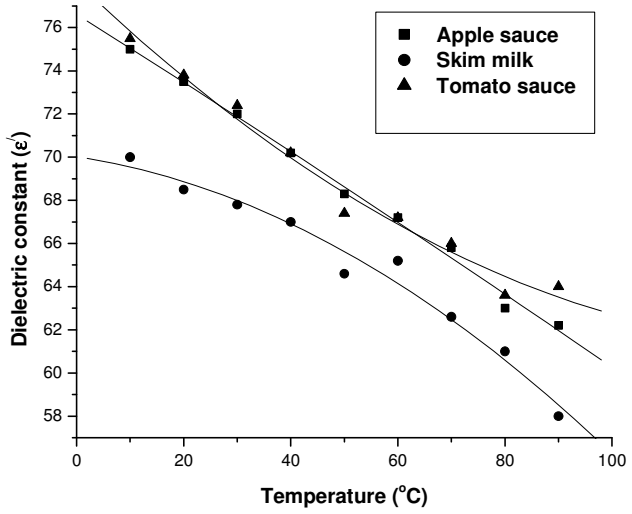

(a)

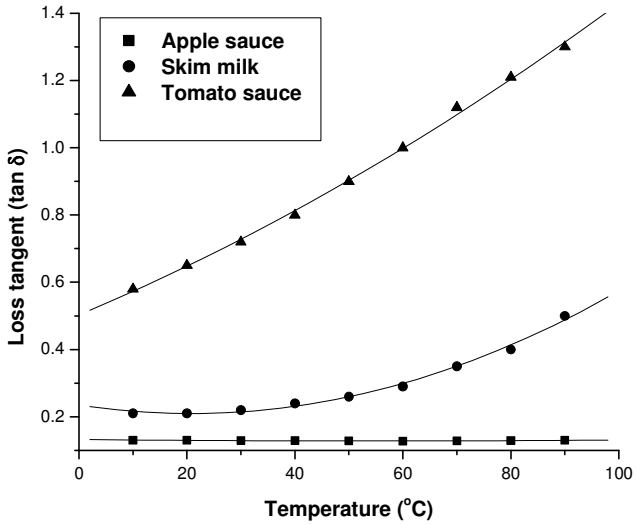

(b)

Figure 2.2 Temperature dependence of the dielectric properties: (a) dielectric constant, ε'; (b) loss tangent, $\tan\delta$.

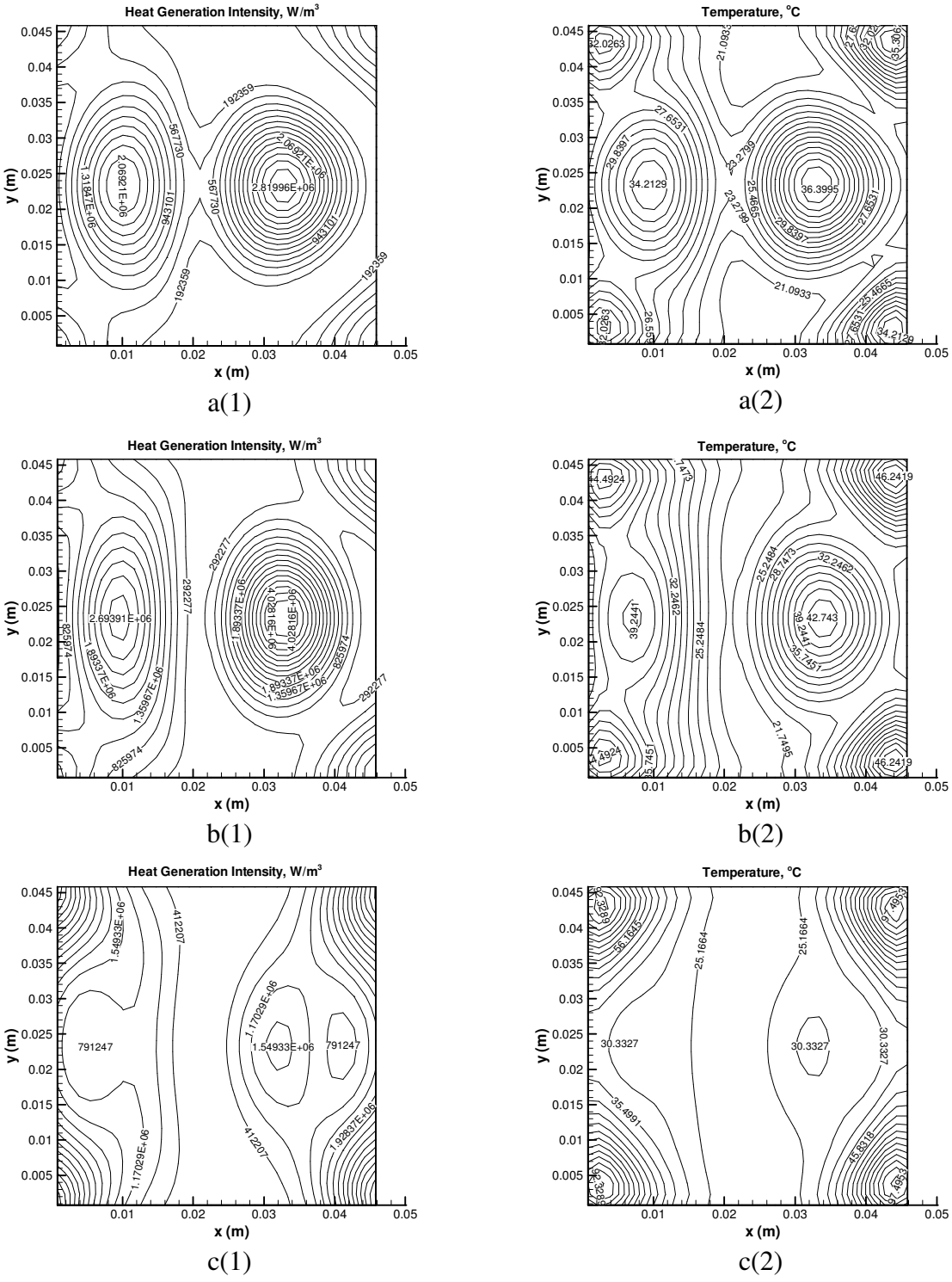

Figure 2.3 Electromagnetic heat generation intensity and temperature distributions at the outlet of the applicator: (a(1) – c(1)) electromagnetic heat generation intensity distributions (W/m^3) for the apple sauce (a), skim milk (b), and tomato sauce (c), respectively; (a(2) – c(2)) temperature distributions (^{o}C) for the apple sauce (a), skim milk (b), and tomato sauce (c), respectively.

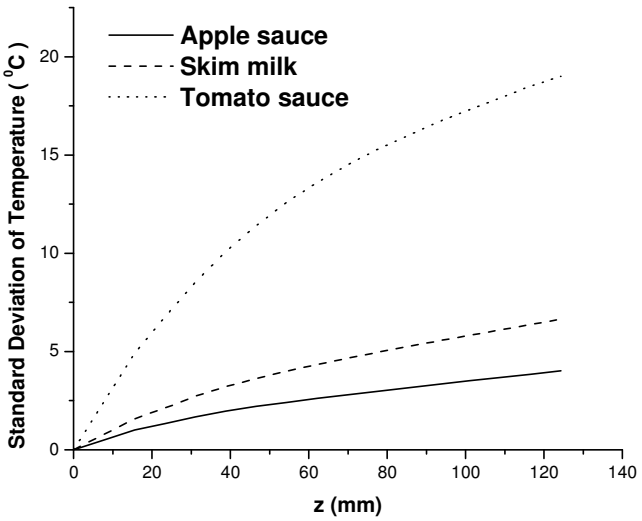

Figure 2.4 Standard deviation of the temperature distribution for the apple sauce, skim milk, and tomato sauce.

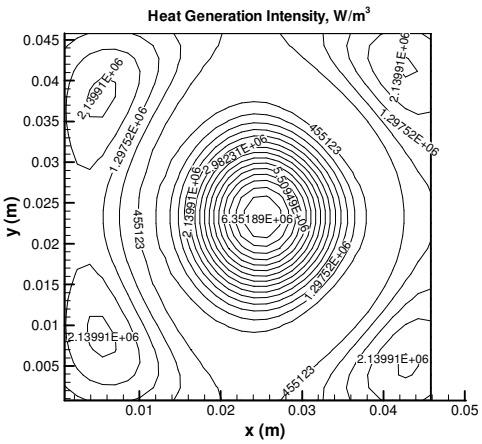

a(1)

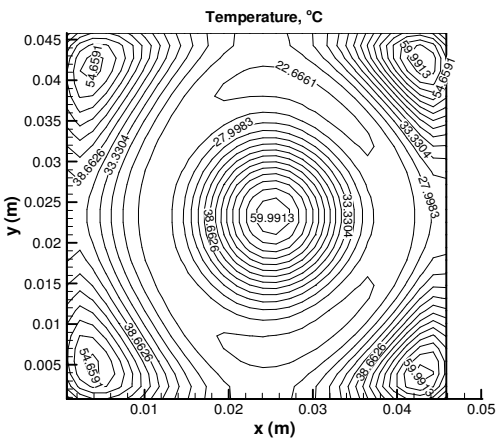

a(2)

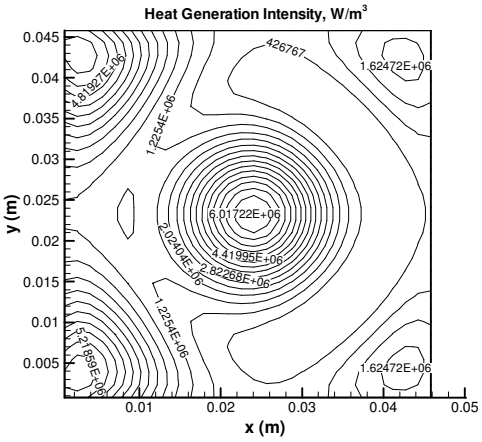

b(1)

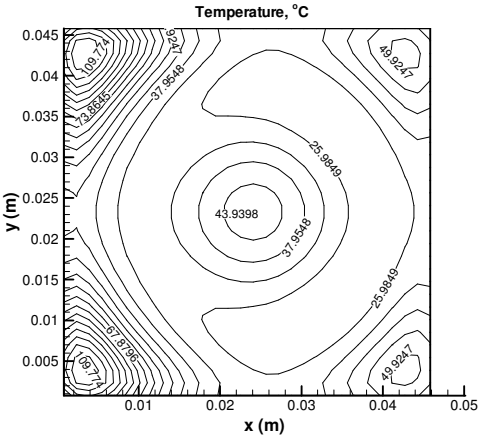

b(2)

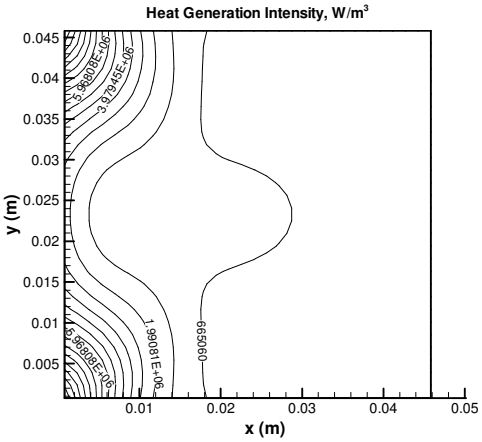

c(1)

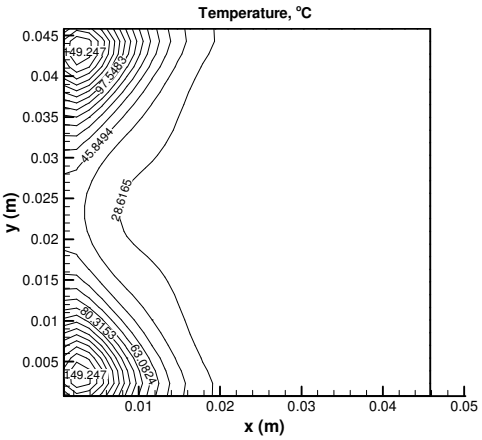

c(2)

Figure 2.5 Effect of the location of the applicator on heating the product: (a(1) – c(1)) electromagnetic heat generation intensity (W/m^3) distributions at the outlet for the apple sauce (a), skim milk (b), and tomato sauce (c), respectively; (a(2) – c(2)) temperature (^{o}C) distributions at the outlet for the apple sauce (a), skim milk (b), and tomato sauce (c), respectively, for the applicator having 141 mm off the original location in the *x* direction.

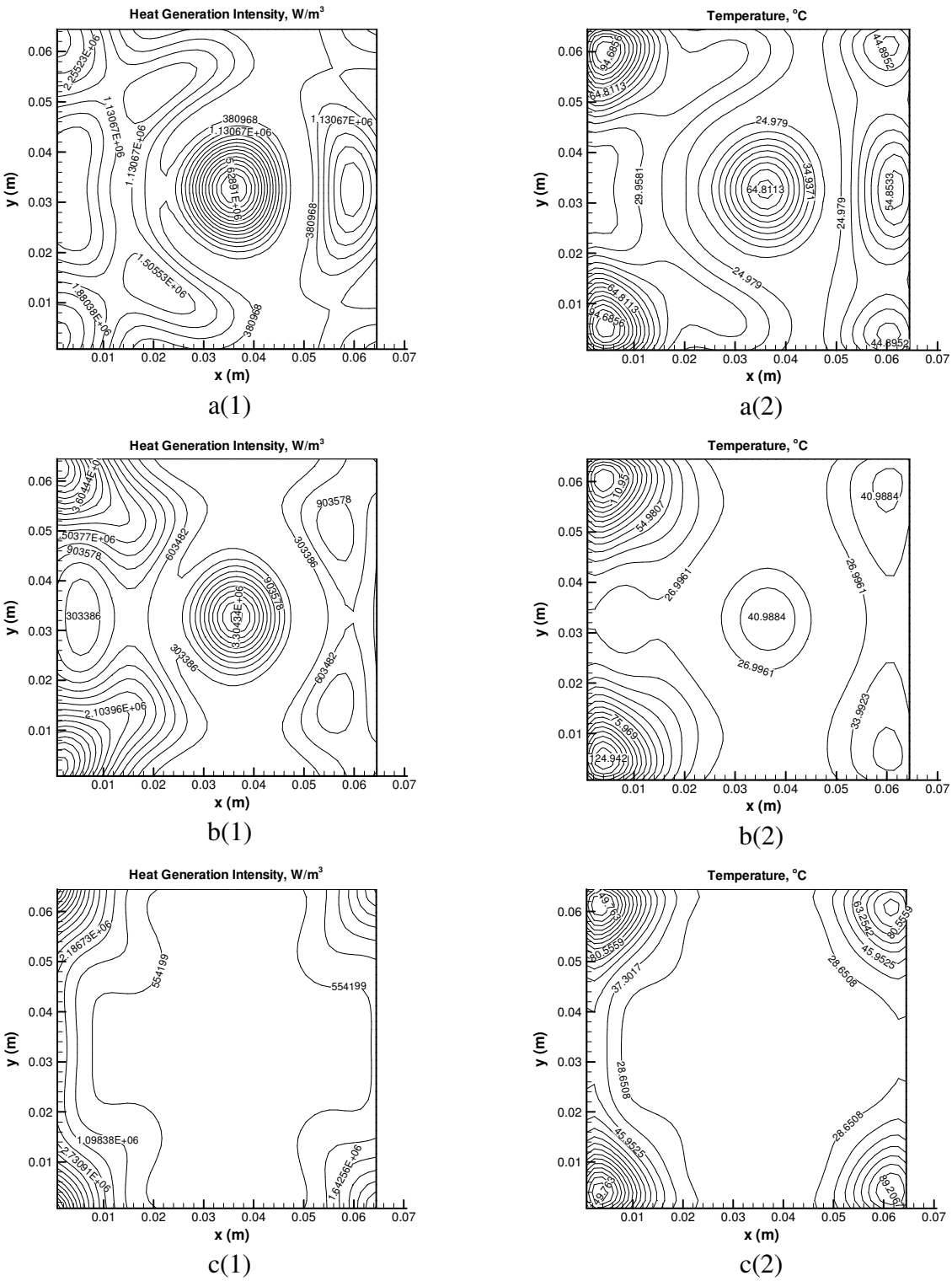

Figure 2.6 Effect of the size of the applicator on heating the product: (a(1) – c(1)) electromagnetic heat generation intensity (W/m^3) distributions at the outlet for the apple sauce (a), skim milk (b), and tomato sauce (c), respectively; (a(2) – c(2)) temperature (^{o}C) distributions at the outlet for the apple sauce (a), skim milk (b), and tomato sauce (c), respectively, for the applicator size of 60×60×124mm.

REFERENCES

1. Dibben, D.C., Metaxas, A.C. (1995) Time domain finite element analysis of multimode microwave applicators loaded with low and high loss materials, *Proceedings of the International Conference on Microwave and High Frequency Heating*, vol. 1-3, no. 4.
2. De Pourcq, M. (1985) Field and power density calculation in closed microwave system by three-dimensional finite difference, *IEEE Proceedings*, 132 (11): 361-368.
3. Jia, X., Jolly, P. (1992) Simulation of microwave field and power distribution in a cavity by a three dimensional finite element method, *Journal of Microwave Power and Electromagnetic Energy*, 27(1): 11-22.
4. Anantheswaran, R.C., Liu, L. (1994) Effect of viscosity and salt concentration on microwave heating of model non-Newtonian liquid foods in a cylindrical container, *Journal of Microwave Power and Electromagnetic Energy*, 29(2): 119-126.
5. Zhang, Q., Jackson, T.H., Ungan, A. (2000) Numerical modeling of microwave induced natural convection, *International Journal of Heat and Mass Transfer*, 43: 2141-2154.
6. Webb, J.P., Maile, G.L., Ferrari, R.L. (1983) Finite element implementation of three dimensional electromagnetic problems, *IEEE Proceedings*, 78: 196-200.
7. Ayappa, K.G., Davis, H.T., Davis, E.A., Gordon, J. (1992) Two-dimensional finite element analysis of microwave heating, *AIChE Journal*, 38: 1577-1592.
8. Liu, F., Turner, I., Bialkowski, M. (1994) A finite-difference time-domain simulation of power density distribution in a dielectric loaded microwave cavity, *Journal of Microwave Power and Electromagnetic Energy*, 29(3): 138-147.

9. Zhao, H., Turner, I.W. (1996) An analysis of the finite-difference time-domain method for modeling the microwave heating of dielectric materials within a three-dimensional cavity system, *Journal of Microwave Power and Electromagnetic Energy*, 31(4): 199-214.
10. Zhang, H., Taub, A.K., Doona, I.A. (2001) Electromagnetics, heat transfer and thermokinetics in microwave sterilization, *AIChE Journal*, 47: 1957-1968.
11. Zhang, H., Datta, A.K. (2000) Coupled electromagnetic and thermal modeling of microwave oven heating of foods, *Journal of Microwave Power and Electromagnetic Energy*, 35(2): 71-85.
12. Patankar, S.V. (1980) *Numerical heat transfer and fluid flow*, Hemisphere, New York
13. Cheng, D.K. (1992) *Field and wave electromagnetics*, second ed., Addison-Wesley, New York.
14. Mur, G. (1981) Absorbing boundary conditions for the finite difference approximation of the time domain electromagnetic field equations, *IEEE Trans. Electromag. Compat*., EC-23: 377.
15. Yee, K.S. (1966) Numerical solution of initial boundary value problem involving Maxwell's equations in isotropic media, *IEEE Trans. On Antennas and Propagation*, 14: 302-307.
16. Kunz, K.S., Luebbers, R. (1993) *The finite difference time domain method for electromagnetics*, CRC, Boca Raton, FL.
17. Zhang, Q. (1998): *Numerical simulation of heating of a containerized liquid in a single-mode microwave cavity*. MS thesis, Indiana University-Purdue University at Indianapolis, IN.

3 MATHEMATICAL MODELING OF CONTINUOUS FLOW MICROWAVE HEATING OF LIQUIDS (EFFECTS OF DIELECTRIC PROPERTIES AND DESIGN PARAMETERS)

ABSTRACT

In this chapter, a detailed numerical model is presented to study heat transfer in liquids as they flow continuously in a circular duct that is subjected to microwave heating. Three types of food liquids are investigated: apple sauce, skim milk, and tomato sauce. The transient Maxwell's equations are solved by the Finite Difference Time Domain (FDTD) method to describe the electromagnetic field in the microwave cavity and the waveguide. The temperature field inside the applicator duct is determined by the solution of the momentum, energy, and Maxwell's equations. Simulations aid in understanding the effects of dielectric properties of the fluid, the applicator diameter and its location, as well as the geometry of the microwave cavity on the heating process. Numerical results show that the heating pattern strongly depends on the dielectric properties of the fluid in the duct and the geometry of the microwave heating system.

Nomenclature

A area, m^2

C_p specific heat capacity, $J/(kg \cdot K)$

c phase velocity of the electromagnetic propagation wave, m/s

E electric field intensity, V/m

f frequency of the incident wave, Hz

h effective heat transfer coefficient, $\mathrm{W/(m^2 \cdot K)}$

H magnetic field intensity, A/m

L standard deviation of temperature, $^{o}\mathrm{C}$

k thermal conductivity, $\mathrm{W/(m \cdot K)}$

m fluid consistency coefficient, $\mathrm{Pa\ s^n}$

n flow behavior index

N number of time steps

p pressure, Pa

q electromagnetic heat generation intensity, $\mathrm{W/m^3}$

Q microwave power absorption, W

T temperature, $^{o}\mathrm{C}$

t time, s

$\tan\delta$ loss tangent

$\mathbf{v}$ fluid velocity vector, m/s

w velocity component in the z direction, m/s

W width of the incident plane, m

Z_{TE} wave impedance, Ω

Greek symbols

η apparent viscosity, $Pa \cdot s$

ε electric permittivity, F/m

ε' dielectric constant

ε'' effective loss factor

ε_{rad} emissivity

λ_g electromagnetic wavelength in the cavity, m

μ magnetic permeability, H/m

ρ density, kg/m^3

σ electric conductivity, S/m

σ_{rad} Stefan-Boltzmann constant, $W/(m^2 K^4)$

Superscripts

τ instantaneous value

Subscripts

∞ ambient condition

0 free space, air

t time

in input

X,Y,Z projection on a respective coordinate axis

3.1 INTRODUCTION

Microwave heating is utilized to process materials for decades. In contrast to other conventional heating methods, microwave heating allows volumetric heating of materials. Without the need for any intermediate heat transfer medium, microwave radiation penetrates the material directly. Microwave energy causes volumetric heat generation in the material, which results in high energy efficiency and a reduction in heating time.

A distinct drawback to microwave heating is the lack of uniformity in material heating [1-3]. Both the magnitude and spatial distribution of microwave energy are dictated by the complexity of electromagnetic waves scattering and reflecting in the microwave unit, as well as absorption of electromagnetic waves within the material [4]. Factors that influence microwave heating include dielectric properties, volume, and shape of the material, as well as design and geometric parameters of the microwave unit [5]. These factors make it difficult to precisely control the heating process in order to obtain the desired temperature distribution in the material. Due to complexity of the physical process, numerical modeling has been widely utilized to study microwave heating [6].

In the past, a number of studies [7-14] have been documented that dealt with numerical modeling of microwave heating process in a cavity. Generally, prediction of microwave energy deposition requires the solution of Maxwell's equations, which

determines the electromagnetic field in the microwave cavity and waveguide. The finite difference time domain (FDTD) method developed by Yee [15] has been widely utilized to solve Maxwell's equations. Solutions of Maxwell's equations using the FDTD method for a number of simplified cases are reported in Webb et al. [16]. Three-dimensional simulations of microwave propagation and energy deposition are presented in Liu et al. [9], Zhao and Turner [17], and Zhang et al. [18].

Success in the numerical simulation of electromagnetic propagation has recently generated interest in numerical modeling of heat transfer induced by microwave radiation. Clemens and Saltiel [4] developed a model of microwave heating of a solid specimen. Their model accounts for temperature dependent dielectric properties, which causes coupling between the Maxwell's and energy equations. Effects of the microwave frequency, dielectric properties of the specimen, and the size of the sample on the microwave energy deposition were investigated in a two-dimensional formulation. Other important papers addressing modeling of microwave heating processes include Ayappa et al. [19-21], Basak et al. [22], and Ratannadecho et al. [23-24].

Although most previous studies of microwave heating focused on conduction heat transfer in a specimen, a few recent papers investigated natural convection induced by microwave heating of liquids; mathematical models utilized in these papers included the momentum equation. Datta et al. [25] investigated natural convection in a liquid subjected to microwave heating. In their study, the microwave energy deposition was assumed to decay exponentially into the sample based on Lambert's law, which is valid only for a high loss dielectric material and a sample of large size. Therefore, for small

size samples or low loss dielectric materials, coupled Maxwell's, momentum, and energy equations must be solved.

Ratanadecho et al. [26] were the first who investigated, numerically and experimentally, microwave heating of a liquid layer in a rectangular waveguide. The movement of liquid particles induced by microwave heating was taken into account. Coupled electromagnetic, hydrodynamic and thermal fields were simulated in two dimensions. The spatial variation of the electromagnetic field was obtained by solving Maxwell's equations with the FDTD method. Their work demonstrated the effects of microwave power level and liquid electric conductivity on the degree of penetration and the rate of heat generation within the liquid layer. Furthermore, an algorithm for resolving the coupling of Maxwell's, momentum, and energy equations was developed and validated by comparing with experimental results.

Microwave heating of a liquid flowing in a rectangular duct passing through a cubic cavity was studied in [27]. Temperature distributions in different liquids were simulated. The aim of this research is to investigate heating of a liquid in a geometry which better approximates that of real industrial systems. The geometry is similar to that investigated in [28] and [29], but extended to three dimensions. Numerical simulations of microwave heating of a liquid continuously flowing in a circular pipe are reported. Velocity distribution is assumed to be that of a fully developed non-Newtonian flow in a circular pipe. If more microwave energy is released in the center of the pipe and less is released near the wall, the outlet temperature distribution may be closer to uniform. In this chapter, a microwave cavity designed to generate exactly such energy distribution is investigated. An algorithm similar to that reported in [26] is utilized in this chapter to

couple Maxwell's and energy equations. In order to optimize the design of the microwave system, the effects of the diameter of the applicator tube, the location of the applicator tube in the microwave cavity, and the shape of the microwave cavity are investigated.

3.2 MODEL GEOMETRY

Figure 3.1 shows the schematic diagram of the microwave system examined in this research. The system consists of a waveguide, a resonant cavity, and a vertically positioned applicator tube that passes through the cavity. A liquid food, which is treated as a non-Newtonian fluid, flows through the applicator tube in the upward direction, absorbing the microwave energy as it passes through the tube. It is assumed that no phase change occurs during the heating process. The microwave operates in TE_{10} [30] mode at a frequency of 915 MHz; the microwave energy is generated at the incident plane by imposing a plane polarized source. The microwave is transmitted through the waveguide towards the applicator tube located in the center of the resonant cavity. An absorbing plane is placed behind the incident plane to absorb the microwave energy reflected from the cavity. Two computational domains are utilized. The first domain, used for electromagnetic computations, includes the region enclosed by the wall of the waveguide, resonant cavity, and incident plane. The second domain, used for solving the momentum and energy equations, coincides with the region inside the applicator tube. The origin of the coordinate system for the electromagnetic computational domain lies at a corner of the waveguide, as shown in Figure 3.1. The origin of the coordinate system for the inside of the applicator tube is in the center of the tube at the tube entrance. Parameters characterizing system's geometry are listed in Table 3.1.

3.3 MATHEMATICAL MODEL FORMULATION

3.3.1 ELECTROMAGNETIC FIELD

Maxwell's equations governing the electromagnetic field are expressed in terms of the electric field, **E**, and the magnetic field, **H**. In the Cartesian coordinate system, (*X*, *Y*, *Z*), they are presented as:

$$\frac{\partial H_x}{\partial t} = \frac{1}{\mu}\left(\frac{\partial E_y}{\partial z} - \frac{\partial E_z}{\partial y}\right) \tag{3.1}$$

$$\frac{\partial H_y}{\partial t} = \frac{1}{\mu}\left(\frac{\partial E_z}{\partial x} - \frac{\partial E_x}{\partial z}\right) \tag{3.2}$$

$$\frac{\partial H_z}{\partial t} = \frac{1}{\mu}\left(\frac{\partial E_x}{\partial y} - \frac{\partial E_y}{\partial x}\right) \tag{3.3}$$

$$\frac{\partial E_x}{\partial t} = \frac{1}{\varepsilon}\left(\frac{\partial H_z}{\partial y} - \frac{\partial H_y}{\partial z} - \sigma E_x\right) \tag{3.4}$$

$$\frac{\partial E_y}{\partial t} = \frac{1}{\varepsilon}\left(\frac{\partial H_x}{\partial z} - \frac{\partial H_z}{\partial x} - \sigma E_y\right) \tag{3.5}$$

$$\frac{\partial E_z}{\partial t} = \frac{1}{\varepsilon}\left(\frac{\partial H_y}{\partial x} - \frac{\partial H_x}{\partial y} - \sigma E_z\right) \tag{3.6}$$

where σ is the electric conductivity, μ is the magnetic permeability, and ε is the electric permittivity. Subscripts *X*, *Y*, and *Z* denote respective components of the vectors **E** and **H**.

Boundary and initial conditions for the electromagnetic fields are:

(a) At the walls of the waveguide and cavity, a perfect conducting condition is utilized. Therefore, normal components of the magnetic field and tangential components of the electric field vanish at these walls:

$$H_n = 0, \quad E_t = 0 \tag{3.7}$$

(b) At the absorbing plane, Mur's first order absorbing condition [31] is utilized:

$$\left(\frac{\partial}{\partial Z} - \frac{1}{c} \frac{\partial}{\partial t} \right) E_Z \big|_{X=0} = 0 \tag{3.8}$$

where c is the phase velocity of the propagation wave.

(c) At the incident plane, the input microwave source is simulated by the equations:

$$E_{Z,inc} = -E_{Zin} \sin\left(\frac{\pi Y}{W} \right) \cos\left[2\pi \left(ft - \frac{X_{in}}{\lambda_g} \right) \right] \tag{3.9}$$

$$H_{Y,inc} = \frac{E_{Zin}}{Z_{TE}} \sin\left(\frac{\pi Y}{W} \right) \cos\left[2\pi \left(ft - \frac{X_{in}}{\lambda_g} \right) \right] \tag{3.10}$$

where f is the frequency of the microwave, W is the width of the incident plane, Z_{TE} is the wave impedance, λ_g is the wave length of a microwave in the waveguide, and E_{Zin} is the input value of the electric field intensity. By applying the Poynting theorem [26], the input value of the electric field intensity is evaluated by the microwave power input as:

$$E_{Zin} = \sqrt{\frac{4 Z_{TE} P_{in}}{A}} \tag{3.11}$$

where P_{in} is the microwave power input and A is the area of the incident plane.

(d) The applicator wall is assumed to be electromagnetically transparent.

(e) At $t = 0$ all components of **E** and **H** are zero.

3.3.2 *ENERGY AND MOMENTUM EQUATIONS*

The temperature distribution in the applicator tube is obtained by the solution of the following energy equation with a source term which accounts for internal energy generation due to the absorption of the microwave energy:

$$\rho C_p \left(\frac{\partial T}{\partial t} + w \frac{\partial T}{\partial z} \right) = \nabla \cdot \left(k \nabla T \right) + q(x, y, z, t) \tag{3.12}$$

where ρ is the density; C_p is the specific heat; k is the thermal conductivity; T is the temperature; w is the axial velocity of the fluid; t is the time; and x, y, and z are the Cartesian coordinates. q represents the local electromagnetic heat generation intensity term, which depends on dielectric properties of the liquid and the electric field intensity:

$$q = 2\pi f \varepsilon_0 \varepsilon' (\tan \delta) E^2 \tag{3.13}$$

In Eq. (3.13), ε_0 is the permittivity of the air; ε' is the dielectric constant of the liquid; and $\tan \delta$ is the loss tangent, a dimensionless parameter defined as:

$$\tan \delta = \frac{\varepsilon''}{\varepsilon'} \tag{3.14}$$

where ε'' stands for the effective loss factor. The dielectric constant, ε', characterizes the penetration of the microwave energy into the product, while the effective loss factor, ε'', indicates the ability of the product to convert the microwave energy into heat [32]. Both ε' and ε'' are dependent on the microwave frequency and the temperature of the product. $\tan \delta$ indicates the ability of the product to absorb microwave energy.

The velocity of the fluid flow is determined by the solution of the following continuity and momentum equations:

$$\nabla \cdot \mathbf{v} = 0 \tag{3.15}$$

$$\rho \frac{D\mathbf{v}}{Dt} = -\frac{1}{p} + \nabla \cdot \eta \nabla \mathbf{v} \tag{3.16}$$

where $\mathbf{v}$ is the velocity vector; p is the pressure; and η is the apparent viscosity of the non-Newtonian fluid, which in this chapter is assumed to obey the power-law [33], as:

$$\eta = m\left(\dot{\gamma}\right)^{n-1} \tag{3.17}$$

where m and n are the fluid consistency coefficient and the flow behavior index, respectively.

In this chapter, it is assumed that the flow is hydrodynamically fully developed; only the axial velocity component is non-zero. The momentum equation is then simplified as:

$$\frac{\partial}{\partial x}\left(\eta \frac{\partial w}{\partial x}\right) + \frac{\partial}{\partial y}\left(\eta \frac{\partial w}{\partial y}\right) - \frac{dp}{dz} = 0 \tag{3.18}$$

The apparent viscosity, η, is expressed as:

$$\eta = m\left[\left(\frac{\partial w}{\partial x}\right)^2 + \left(\frac{\partial w}{\partial y}\right)^2\right]^{(n-1)/2} \tag{3.19}$$

The following boundary conditions are utilized to determine the velocity and temperature distributions. At the inner surface of the applicator tube, a hydrodynamic no-slip boundary condition is used. At the inlet to the applicator, a uniform, fully developed velocity profile is imposed, and specified by the inlet mean velocity, V_{mean}.

The following thermal boundary condition is proposed at the applicator wall. The wall is assumed to lose heat by natural convection and radiation:

$$-k\left.\frac{\partial T}{\partial n}\right|_{surface} = h\left(T - T_{\infty}\right) + \sigma_{rad}\varepsilon_{rad}\left(T^4 - T_{\infty}^4\right) \tag{3.20}$$

where T_{∞} is the ambient air temperature (the waveguide walls are assumed to be in thermal equilibrium with the ambient air), σ_{rad} is the Stefan-Boltzmann constant, ε_{rad} is the surface emissivity of the wall of the applicator tube, n is the normal direction to the surface of the wall, and h is the effective heat transfer coefficient defined as:

$$h = \frac{1}{1/h_{air} + L_{wall}/k_{wall} + 1/h_{liquid}} \tag{3.21}$$

In Eq. (3.21), h_{air} is the heat transfer coefficient between the applicator wall and the air in the cavity, h_{liquid} is the heat transfer coefficient between the liquid inside the applicator and the wall, L_{wall} is the thickness of the applicator wall, and k_{wall} is the thermal conductivity of the wall. The inlet liquid temperature is assumed to be uniform and equal to the temperature in the free space outside the applicator, T_{∞}. The initial temperature of the liquid is defined as:

$$T = T_{\infty} \quad \text{at} \quad t = 0 \tag{3.22}$$

Table 2 lists thermo-physical properties of the liquids considered in this chapter and other pertinent system parameters.

3.4 NUMERICAL SOLUTION PROCEDURE

Maxwell's equations (3.1)-(3.6) are solved utilizing the FDTD method [34] on a uniform rectangular grid consisting of 2,472,000 cells in the electromagnetic computational domain. A leapfrog scheme [34] is applied to Maxwell's equations so that the components of the electric field intensity vector are one half cell offset in the direction of their corresponding components, while the magnetic field intensity components are one half cell offset in each direction orthogonal to their corresponding components [4]. The electric and magnetic fields are evaluated at alternate half time steps. The time step, Δt , must satisfy the Courant stability condition [34]:

$$\Delta t \leq \frac{1}{c\sqrt{\frac{1}{\Delta X^2}+\frac{1}{\Delta Y^2}+\frac{1}{\Delta Z^2}}} \tag{3.23}$$

In this research, a time step of $\Delta t = 1.56\times10^{-12}\,s$ is used to solve Maxwell's equations. Since a portion of the boundary of the resonant cavity surface is curved, a staircase grid is utilized to approximate this curved surface. The grid size is $dx = dy = 1.28\text{mm}$ and dz = 6.25mm. A contour-path integral FDTD method [35] is utilized to deal with the curved surface of the microwave cavity using traditional rectangular cells.

Energy and momentum equations (3.12) and (3.18) are discretized using a cell centered finite volume approach and are solved implicitly in the Cartesian coordinate system using the time step of 0.1s. An upwind scheme is adopted to represent advection in the thermal fluid flow domain. To approximate a cylindrically shaped applicator tube, a staircase grid with rectangular cells is utilized.

Since in Eq. (3.13) the dielectric constant, ε', and the loss tangent, $\tan\delta$, are temperature dependent, an iterative scheme is required to resolve the coupling between the energy and Maxwell's equations. Since the time scale for electromagnetic transients (a nanosecond scale) is much smaller than that for the flow and thermal transport (0.1s), the electromagnetic heat source, q, defined by Eq. (3.13), is computed in terms of the time average field, $\overline{E}$, which is treated as a constant over one time step for the thermal-flow computation, and defined as:

$$\overline{E} = \frac{1}{N}\sum_{\tau=1}^{N} E^{\tau} \tag{3.24}$$

where N is the number of time steps in each period of the microwave and E^{τ} is the instantaneous electric field intensity. The details of the numerical scheme used in this chapter are given in [4]. Energy equation (3.13) is solved by an implicit scheme, at each time step iterations are continued until the following convergence criterion is met:

$$\left|\frac{T_{i,j,k,t}^{k+1} - T_{i,j,k,t}^{k}}{T_{i,j,k,t}^{k}}\right| \le 10^{-6} \tag{3.25}$$

where the superscript k refers to the kth iteration. Since this chapter is focused on steady-state temperature profiles, iterative computations of electromagnetic and thermal fields continue until the temperature distribution does not change with time. The convergence criterion is defined as $\Delta = \left|\frac{T_{i,j,k}^{t+1} - T_{i,j,k}^{t}}{T_{i,j,k}^{t}}\right|$ and convergence to steady-state, similarly to Eq. (3.25), is declared when $\Delta \le 10^{-6}$.

3.5 RESULTS AND DISCUSSION

In this chapter, three liquid food products are considered, specifically, apple sauce, skim milk, and tomato sauce. The temperature-dependent data for the dielectric constant and loss tangent for the three liquids are plotted versus temperature in Figure 3.2. In order to compare the results obtained for variant system geometries, the base case is first defined. The base case is characterized by the following geometric parameters of the microwave system: the applicator diameter is 38mm, it is placed in the center of the resonant cavity, and the apogee distance of the resonant cavity is 154mm. Presented results correspond to the moment in time when the temperature attains its steady-state. It takes about 1,100 time steps for the temperature to reach its steady-state. The corresponding CPU time is about 50 hours on a single 208 Intel Xeon 3.0 GHz processor.

3.5.1 HEATING PATTERNS FOR LIQUIDS WITH DIFFERENT DIELECTRIC PROPERTIES

The spatial distribution of the temperature and the corresponding electromagnetic power intensity for the three liquids are presented in Figures 3.3 and 3.4. Results are shown in the vertical x-z plane ($y = 0$) and the horizontal x-y plane at the applicator outlet (z = 124mm), respectively. The system geometry corresponding to the base case is utilized. The evidence of interaction of the electromagnetic field and forced convection in the three liquids is seen in Figure 3.3. As the fluid particle enters the applicator tube, it is heated by the microwave radiation. As the temperature increases in the z-direction, dielectric properties of the liquid change in accordance with Figure 3.2, which changes the distribution of electromagnetic field in the microwave cavity and the distribution of electromagnetic power intensity in the applicator. However, since the dielectric properties

of the liquids considered in this chapter are not highly temperature dependent, the electromagnetic power intensity does not change greatly in the z-direction, as shown in Figure 3.4.

It is evident that the electromagnetic power determines the temperature distribution in the x-y plane. As expected, Figure 3.4 shows a well-defined peak of electromagnetic power intensity near the center of the applicator tube; the peak is shifted by approximately 3mm in the x-direction for all three liquids. Although most of the microwave energy is released near the center of the tube, the reduced velocity near the wall results in higher temperature in the region near the wall for all three liquids. Comparing the power density and temperature distributions for apple sauce and skim milk, it is evident that the peak value of the power density near the tube center for apple sauce is approximately half as large as that for skim milk, but the temperature of the corresponding hot spot occurring in apple sauce is larger. This is because the flow behavior index, n, for apple sauce (n = 0.197) is much smaller than that for skim milk (n = 0.98), so that the velocity profile for skim milk is sharper and the magnitude of the velocity in the core region is larger. The high velocity in the core region reduces the effect of the peak of the electromagnetic power intensity on the temperature of the corresponding hot spot in skim milk.

To illustrate the effect of dielectric properties on power absorption, Table 3.3 shows the dimensionless total electromagnetic power (nondimensionalized by the input power) absorbed by three liquids, defined as:

$$\tilde{Q} = \frac{Q_{total}}{P_{in}} \tag{3.26}$$

The total power absorbed, Q_{total}, can be calculated by integrating the electromagnetic heat generation intensity over the domain occupied by the applicator tube:

$$Q_{total} = \iiint_V q dx dy dz \tag{3.27}$$

The results confirm that a lower loss tangent liquid absorbs less microwave power as compared to a higher loss tangent liquid. The relation between the loss tangent and the microwave power absorption can be expressed by the reflection coefficient, *R*. For a normal incidence of the electromagnetic wave on a plane boundary between the material and vacuum, the reflection coefficient (the fraction of reflected power), *R*, is [36]:

$$R = \frac{1 - \sqrt{2\varepsilon'\left[1 + \sqrt{1 + (\tan\delta)^2}\right]} + \varepsilon'\sqrt{1 + (\tan\delta)^2}}{1 + \sqrt{2\varepsilon'\left[1 + \sqrt{1 + (\tan\delta)^2}\right]} + \varepsilon'\sqrt{1 + (\tan\delta)^2}} \tag{3.28}$$

Apparently, for the same dielectric constant, larger loss tangent and smaller reflection coefficient correspond to larger power absorption. From Table 3.3, it is evident that 99.8% of the electromagnetic power is absorbed by tomato sauce, 88.9% by skim milk, and 61.3% by apple sauce. The remainder of the electromagnetic power is reflected and absorbed by the absorbing plane.

3.5.2 EFFECT OF THE APPLICATOR DIAMETER

Tables 3.4 and 3.5 show the dimensionless electromagnetic power absorption and the mean temperature increase at the outlet, which is non-dimensionalized by the inlet temperature as:

$$\Delta\tilde{T} = \frac{\overline{T} - T_{\infty}}{T_{\infty}} \tag{3.29}$$

where $\overline{T}$ is the mean temperature at the outlet of the applicator. The diameters of the applicator tubes are chosen to be 30.4, 35.5, 38, 40.5, 45.6, 50.7, and 55.7mm, respectively. The effect of the diameter is investigated for the geometry of the microwave cavity corresponding to the base case. The inlet mean velocity is the same for all cases (V_{mean} = 0.03 m/s). From Table 4, it is evident that in tomato sauce the power absorption increases as the diameter of the applicator is increased from 30.4 to 38mm. This is because increasing the diameter enlarges the effective surface area for microwave penetration into the liquid. However, as the applicator diameter is further increased from 40.5 to 55.7mm, the power absorption decreases. This phenomenon is explained using the concept of the cut-off frequency, which is defined as:

$$f_c = \frac{c}{2}\lambda \tag{3.30}$$

Microwaves cannot propagate into the waveguide when the frequency is below the cut-off frequency because they cannot propagate between guiding surfaces separated by less than one half of the wavelength. Therefore, the effective surface area for microwave penetration into the liquid is reduced (microwaves cannot get to a part of the applicator surface which is too close to the walls of the resonant cavity) and the energy generation in the liquid decreases accordingly [4]. In this case, $\frac{\lambda}{2} = 164\text{mm}$, which is even larger than the perigee distance of the microwave cavity. However, since the liquid in the applicator is not a perfectly conducting material and a portion of the microwave energy can therefore penetrate through the applicator, the cut-off distance is actually smaller than

164mm in this case. Comparing the power absorption in apple sauce, skim milk, and tomato sauce, it is evident that the critical diameter, which is defined as the diameter of the applicator above which the microwave power absorption decreases with the increase of the applicator diameter, is different for the three liquids. For apple sauce and skim milk it is approximately 45.6mm, but for tomato sauce it is approximately 38mm. This is attributed to the effect of fluid dielectric properties. Since in tomato sauce the power absorption starts decreasing with the diameter increase at a smaller applicator diameter than in skim milk, for applicator diameters of 40.5 and 45.6mm the power absorption in skim milk is larger than that in tomato sauce, although tomato sauce has a higher loss tangent.

From Table 3.5, it is evident that the mean temperature increase at the outlet does not necessarily exhibit the same trend as the power absorption. For example, in apple sauce, although the power absorption increases when the diameter is increased from 30.4 to 35.5mm, the corresponding mean temperature increase becomes smaller. Recalling that the inlet mean flow velocity is the same for all applicator diameters, the mass flow rate is smaller for the applicator with a smaller diameter. Since the increase of the power absorption in the applicator with a diameter of 35.5mm is not significant, which is explained by a higher resonance in the cavity with the 30.4mm diameter applicator, temperature increases in the applicator with a smaller diameter (30.4mm) is larger. Thus in order to obtain the maximum temperature increase, one should select the applicator with the diameter of 30.4 mm.

3.5.3 *Effect of Different Locations of the Applicator on the Heating Process*

This section discusses the effect of positioning the applicator at different locations in the microwave cavity. Five different locations of the applicator are investigated. The geometry with the applicator positioned in the center of the microwave cavity is treated as the base case, other four cases correspond to -136, -68, +68, and +136mm shifts in the x-direction, respectively, from the position of the applicator in the base case. The diameter of the applicator is 38mm for all five applicator positions. Figures 3.5 and 3.6 show the temperature and electromagnetic power intensity distributions in tomato sauce at the outlet (z = 124mm) for the applicator positioned at five different locations in the microwave cavity. It is evident that the temperature and microwave power intensity decreases significantly if the applicator is shifted from the base case position. This is because the cross section of the resonant cavity is ellipsoidal, and the guiding distance of the resonant cavity is the largest for the plane corresponding to x = 0. The guiding distance is decreased by moving the applicator either forward or backward, reducing the effective surface area of the applicator available for the microwave penetration due to reduced distance between the applicator and the wall of the cavity to the extent that microwaves are not able to get to a portion of the applicator surface. In Figure 3.6, unlike the base case, most of the microwave energy is absorbed in the front ($x < 0$) half of the applicator, implying that microwaves are strongly attenuated as they propagate around the applicator and the effective surface area for the microwave penetration is reduced to the front half part of the applicator surface. The heat energy generation decreases as well. Table 3.6 shows the effect of positioning of the applicator on electromagnetic power absorption in apple sauce, skim milk and tomato sauce. It is evident that for all three

liquids the power absorption is the greatest when the applicator is in the base case position. The power absorption is greatly attenuated by shifting the applicator away from the base case position. Positioning the applicator in the center of the cavity thus provides the maximum heating rate.

3.5.4 EFFECT OF THE SHAPE OF THE CAVITY

The effect of the shape of the resonant cavity is investigated. The height and the perigee distance of the resonant cavity are kept unchanged. The shape of the cross section of the cavity is controlled by the apogee distance which is chosen to be 205, 186, 167, 154, and 128mm, respectively. An applicator diameter of 38mm is utilized. Figures 3.7 and 3.8 show the outlet (z = 124mm) temperature and electromagnetic power intensity distributions in apple sauce for different shapes of the cavity. From Figure 3.8 it is evident that the peak of the electromagnetic power intensity moves backward (in the negative x-direction) and the magnitude of the power intensity decreases with reduced apogee distance. The decreasing trend of the power intensity can be attributed to the fact that the space of the cavity is reduced by decreasing the apogee distance, which reduces the resonance of the microwaves in the cavity. The effect of the cross section shape on the electromagnetic power absorption of apple sauce, skim milk, and tomato sauce is shown in Table 3.7. It is evident that the maximum heating rate can be achieved by utilizing the microwave cavity with the apogee distance of 205 mm. However, if the goal is to obtain the most uniform temperature distribution at the outlet cross-section, the apogee distance of 186 mm should be used. For this apogee distance, the maximum power absorption occurs in the area most closely located to the applicator axis. In this

case the maximum power absorption is compensated by the smallest residence time of the liquid (because of the largest fluid velocity in the applicator center).

3.6 CONCLUSIONS

A numerical model is developed for simulating forced convection of a liquid continuously flowing in a circular applicator that is subjected to microwave heating. The results reveal a complicated interaction between electromagnetic field and convection. The effects of dielectric properties of the liquid, the diameter of the applicator tube, the location of the applicator tube in the cavity, and the shape of the cavity on heating patterns are investigated. Dielectric properties of the liquid determine the ability of the liquid to absorb the microwave energy; the geometry of the microwave system also plays an important role in the power absorption and distribution. Enlarging the diameter of the applicator increases the effective surface available to absorb the microwave energy, usually increases the power absorption in the liquid. However, beyond the critical diameter of the applicator, an opposite trend is observed. The critical diameter of the applicator depends on the geometry of the resonant cavity and dielectric properties of the liquid flowing in the applicator. The microwave power absorption is also sensitive to the location of the applicator and the shape of the resonant cavity, which affect the microwave propagation and resonance.

Table 3.1 Geometrical parameters.

Symbol	Description	Value (mm)
D	Applicator diameter	30.4-55.7
AD	Apogee distance of cavity	128-205
PD	Perigee distance of cavity	154
CH	Cavity & applicator height	125
WL	Waveguide length	347
WW	Waveguide width	244
WH1	Waveguide height	125
WH2	Waveguide height	51
TL	Total length of the system	661
IAD	Distance between the incident plane and absorbing plane	27

Table 3.2 Thermophysical and electromagnetic parameters utilized in computations.

f, MHz		915
P_{in}, W		5000
μ, H/m		$4\pi\times10^{-7}$
ε_0, F/m		8.854×10^{-12}
T_∞, ^{o}C		20
V_{mean}, m/s		0.03
h, W/(m$^2\cdot$K)		15
ε_{rad}		0.4
$Z_{TE,}\,\Omega$		377
k, W/(m$\cdot$K)	Apple Sauce	0.5350
	Skim Milk	0.5678
	Tomato Sauce	0.5774
c_p, J/(kg$\cdot$K)	Apple Sauce	3703.3
	Skim Milk	3943.7
	Tomato Sauce	4000.0
ρ, kg/m^3	Apple Sauce	1104.9
	Skim Milk	1047.7
	Tomato Sauce	1036.9
m	Apple Sauce	32.734
	Skim Milk	0.0059
	Tomato Sauce	3.9124
n	Apple Sauce	0.197
	Skim Milk	0.98
	Tomato Sauce	0.097

Table 3.3 Dimensionless power absorption in different liquids.

Liquids	Dielectric constant, ε' (50 °C)	Loss tangent, $\tan\delta$ (50 °C)	Dimensionless power absorption
Apple sauce	68.4	0.12	0.613
Skim milk	64.6	0.31	0.889
Tomato sauce	69.3	0.92	0.998

Table 3.4 Dimensionless power absorption: effect of the applicator diameter.

Liquids	Applicator Diameter, *D*, (mm)						
	30.4	35.5	38	40.5	45.6	50.7	55.7
Apple sauce	0.518	0.519	0.613	0.725	0.768	0.483	0.343
Skim milk	0.830	0.870	0.889	0.952	0.973	0.771	0.572
Tomato sauce	0.948	0.991	0.998	0.975	0.873	0.736	0.630

Table 3.5 Mean temperature increase at the outlet: effect of the applicator diameter.

Liquids	Applicator Diameter, *D*, (mm)						
	30.4	35.5	38	40.5	45.6	50.7	55.7
Apple sauce	1.35	0.846	0.926	1.026	1.072	0.560	0.302
Skim milk	2.687	1.572	1.688	1.805	1.861	1.373	0.770
Tomato sauce	2.638	2.213	2.152	1.858	1.313	0.947	0.682

Table 3.6 Dimensionless power absorption: effect of the applicator location.

Liquids	Location of Applicator				
	-136mm shift in *x*	-68mm shift in *x*	Base case (no shift)	+68mm shift in *x*	+136mm shift in *x*
Apple sauce	0.141	0.110	0.613	0.140	0.093
Skim milk	0.233	0.193	0.889	0.226	0.159
Tomato sauce	0.284	0.233	0.998	0.290	0.196

Table 3.7 Dimensionless power absorption: effect of the cavity shape.

Liquids	Apogee Distance, *AD*, (mm)				
	205	186	167	154	128
Apple sauce	0.613	0.597	0.390	0.282	0.172
Skim milk	0.889	0.784	0.533	0.404	0.267
Tomato sauce	0.998	0.822	0.578	0.459	0.325

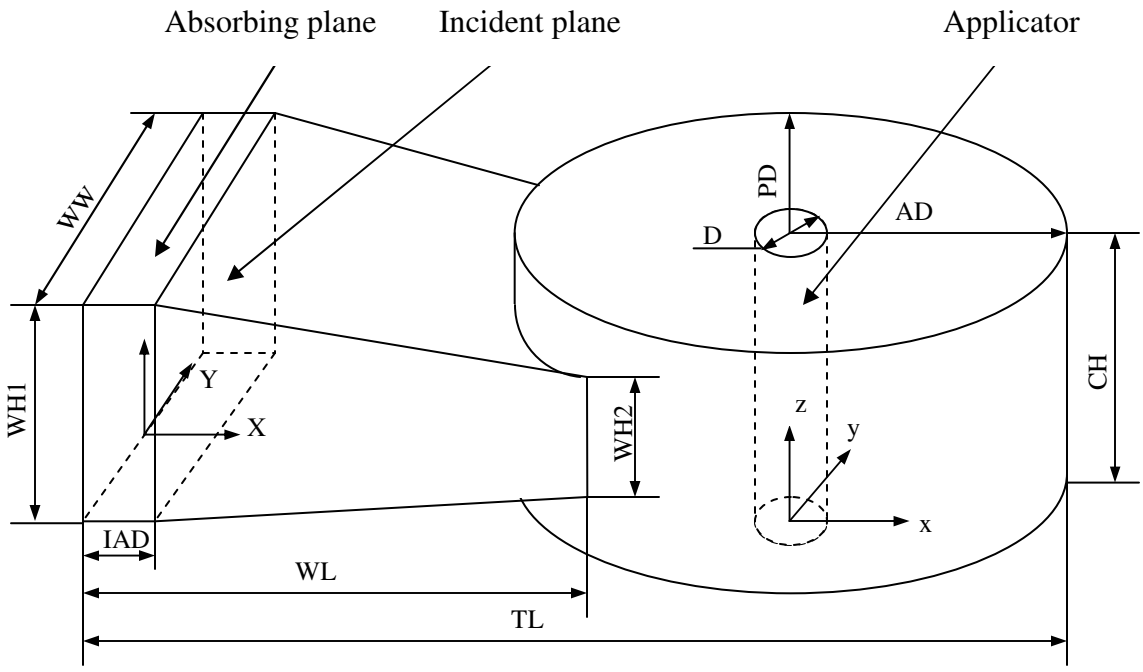

Figure 3.1 Schematic diagram of the problem.

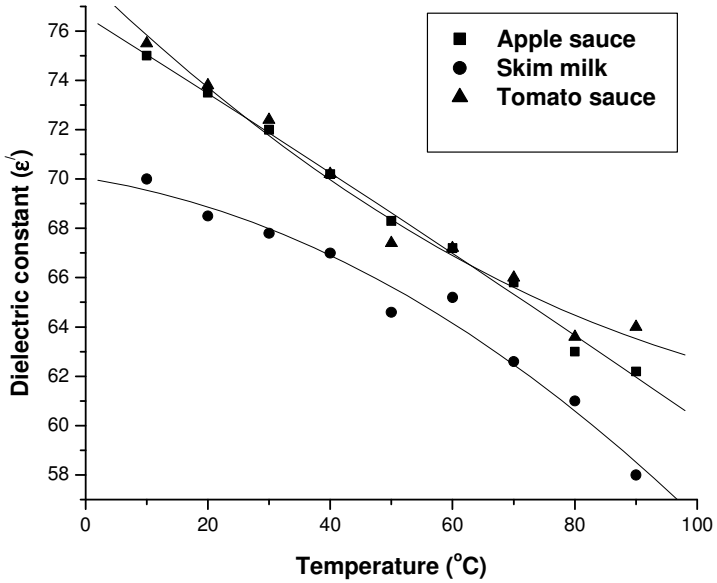

(a)

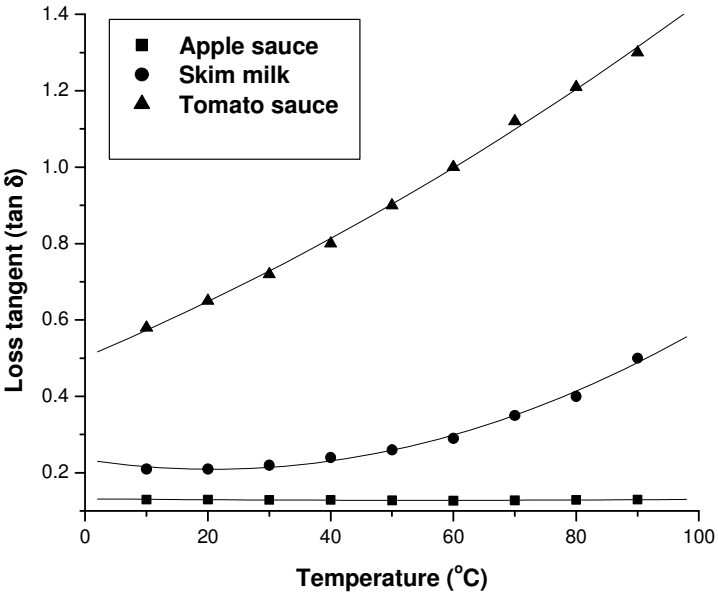

(b)

Figure 3.2 Temperature dependent dielectric properties: (a) dielectric constant, ε'; (b) loss tangent, $\tan\delta$.

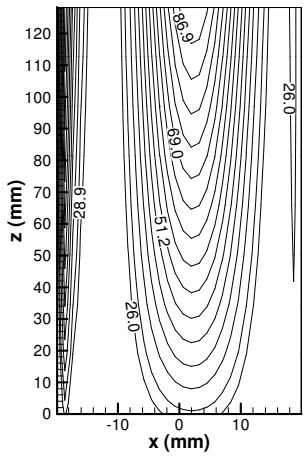

1-a

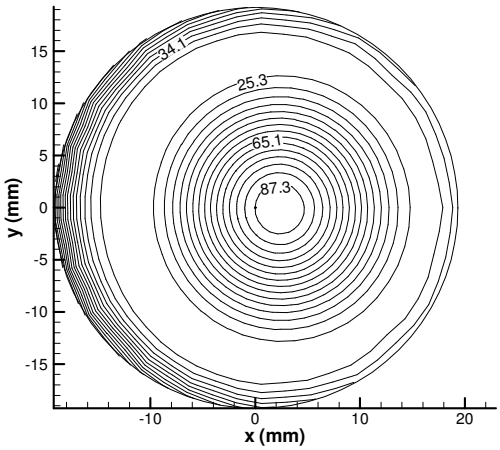

1-b

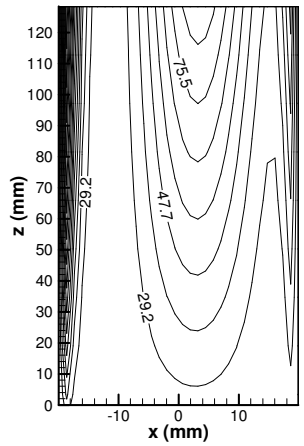

2-a

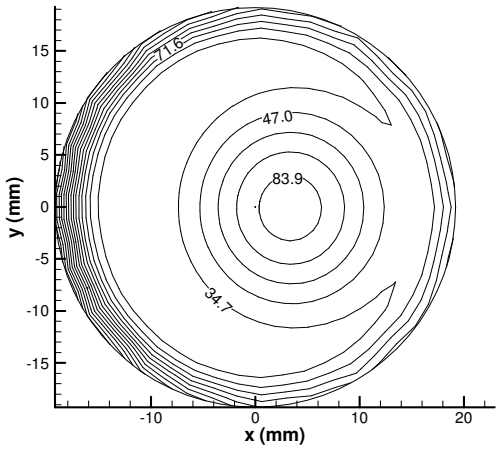

2-b

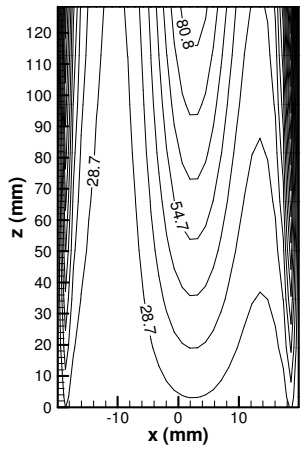

3-a

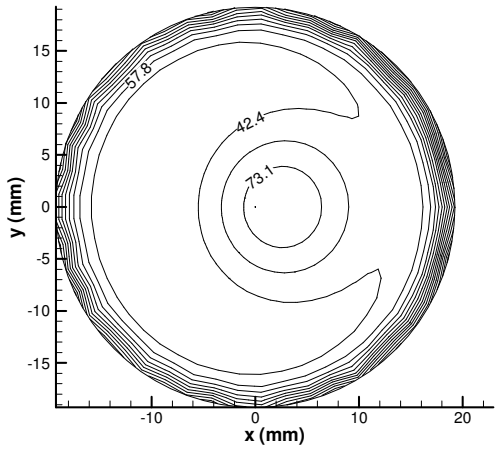

3-b

Figure 3.3 Temperature distributions (^{o}C) in (a) *x*-*z* plane (*y* = 0), and (b) *x*-*y* plane (outlet, *z* = 124mm) for apple sauce (1), skim milk (2), and tomato sauce (3), respectively.

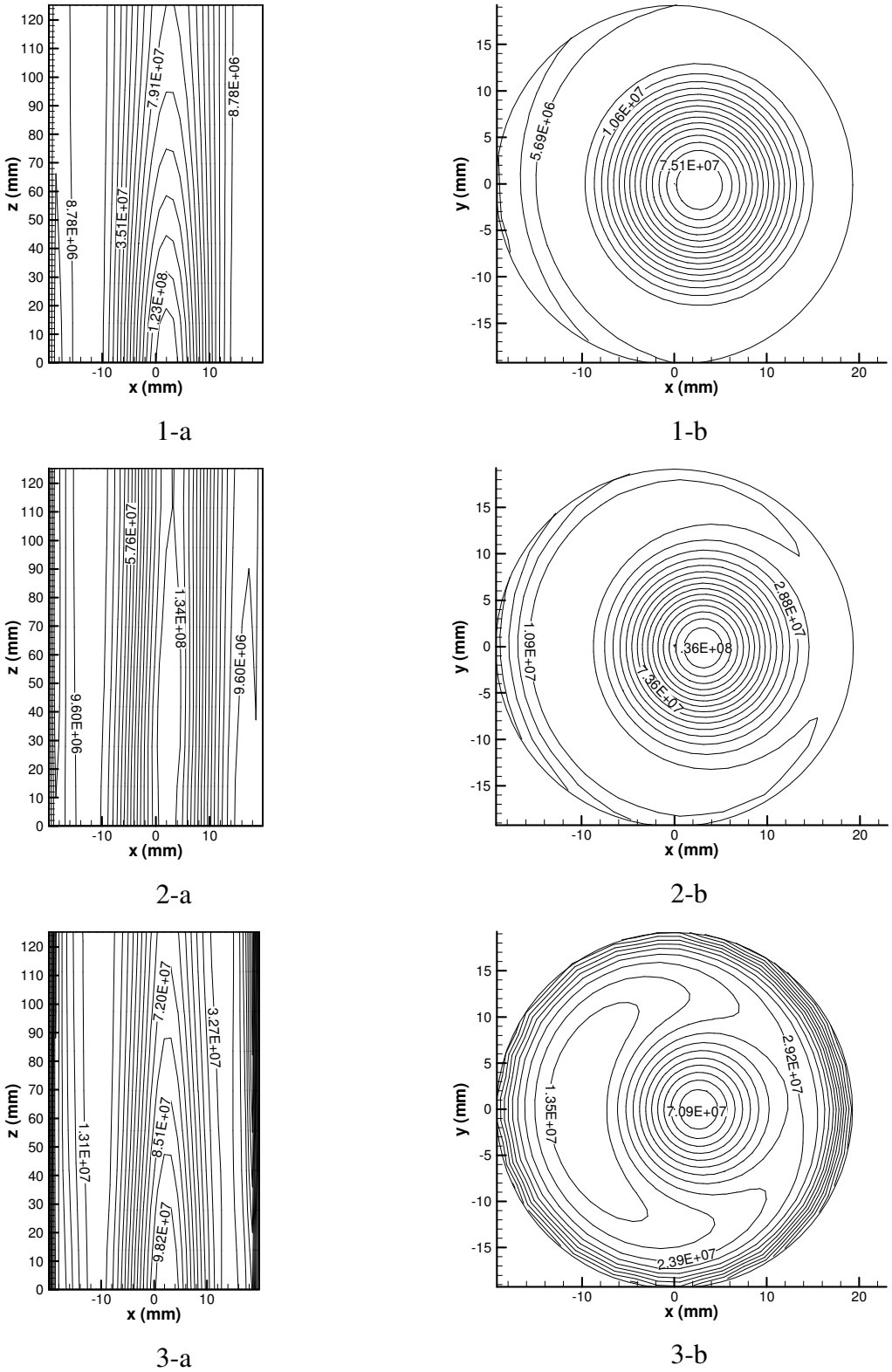

1-a 1-b

2-a 2-b

3-a 3-b

Figure 3.4 Electromagnetic power intensity distributions (W/m^3) in (a) *x*-*z* plane (*y* = 0), and (b) *x*-*y* plane (outlet, *z* = 124mm) for apple sauce (1), skim milk (2), and tomato sauce (3), respectively.

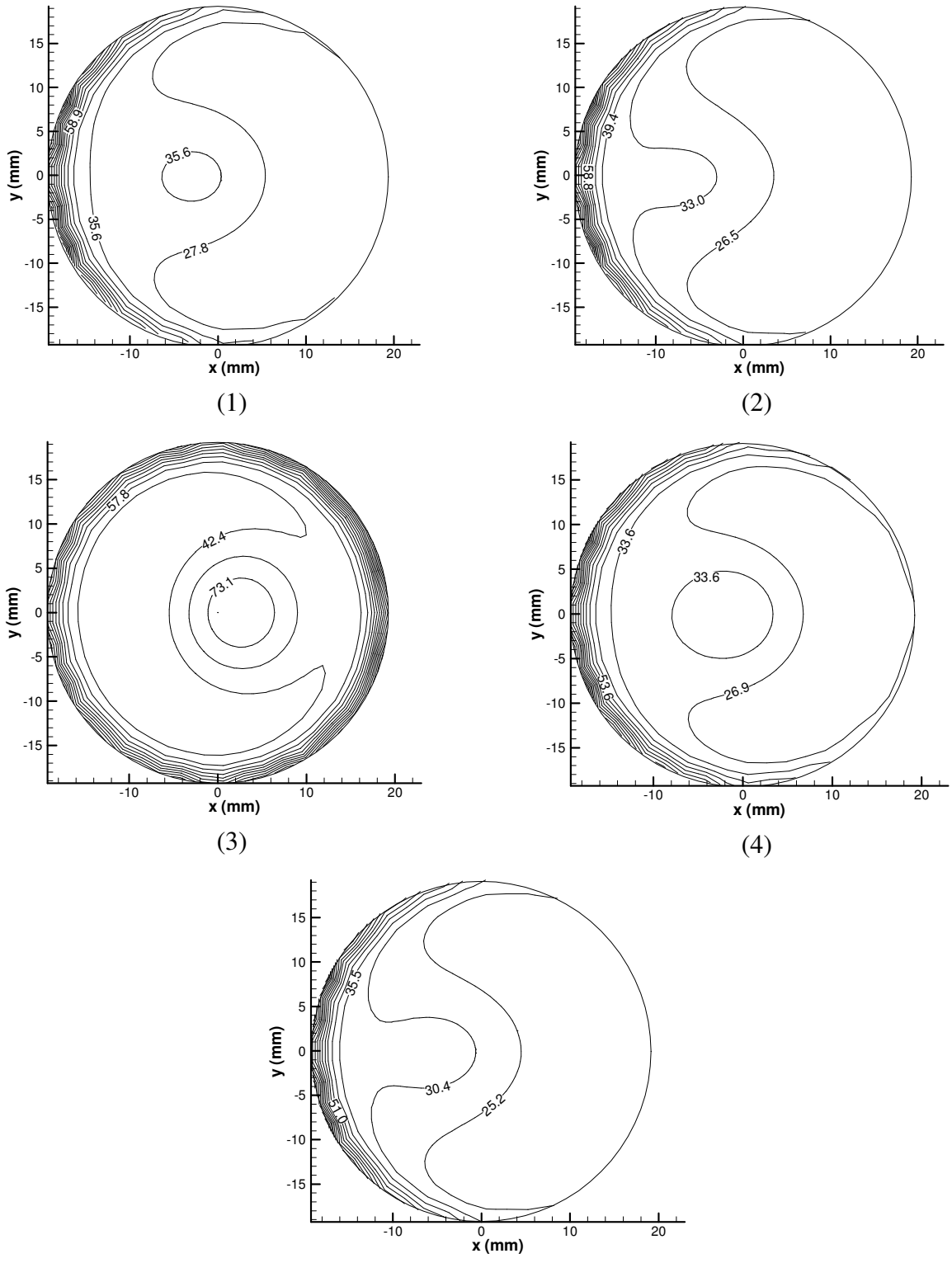

Figure 3.5 Temperature distributions for tomato sauce at the outlet (z = 124mm): effect of the applicator position; the applicator is shifted in the *x*-direction from its position in the base case by (1) -136, (2) -68, (2) 0, (4) +68, (5) +136mm, respectively.

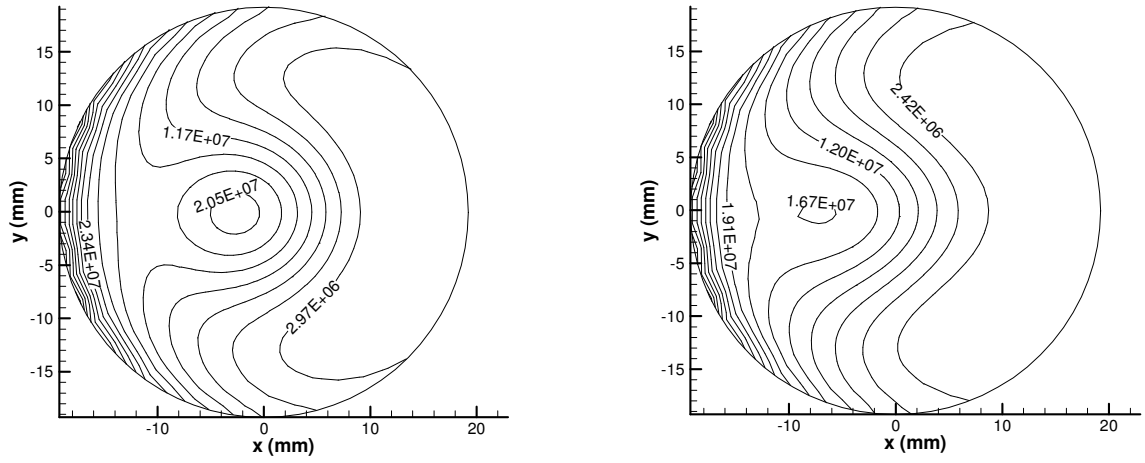

(1)

(2)

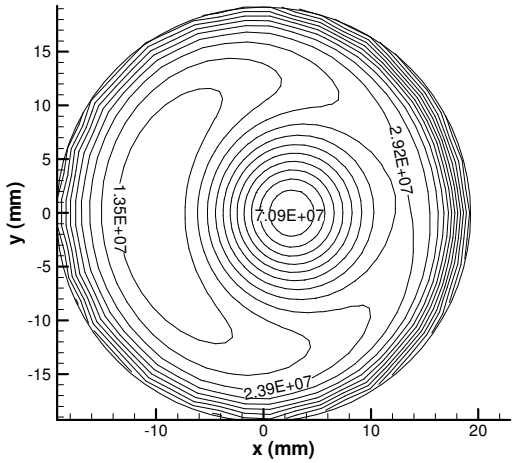

(3)

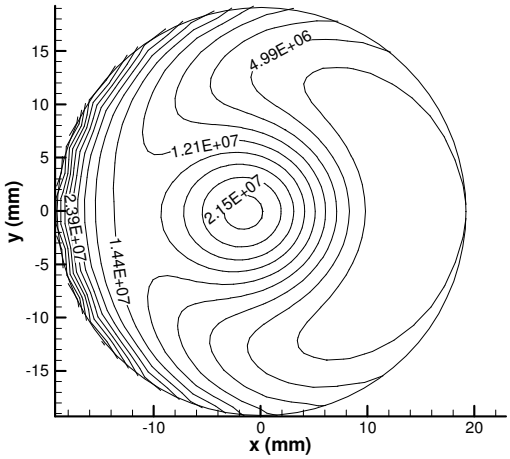

(4)

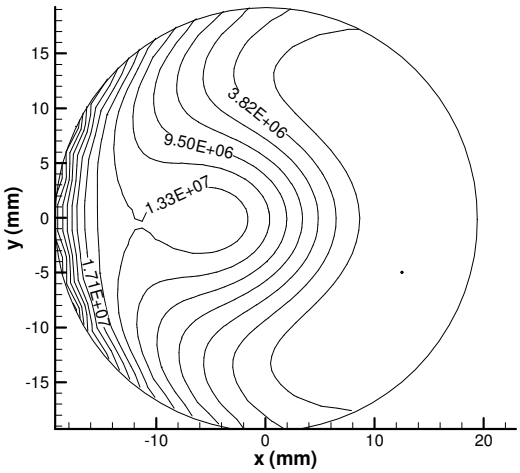

(5)

Figure 3.6 Electromagnetic power intensity distributions for tomato sauce at the outlet (z = 124mm): effect of the applicator position; the applicator is shifted in the *x*-direction from its position in the base case by (1) -136, (2) -68, (2) 0, (4) +68, (5) +136mm, respectively.

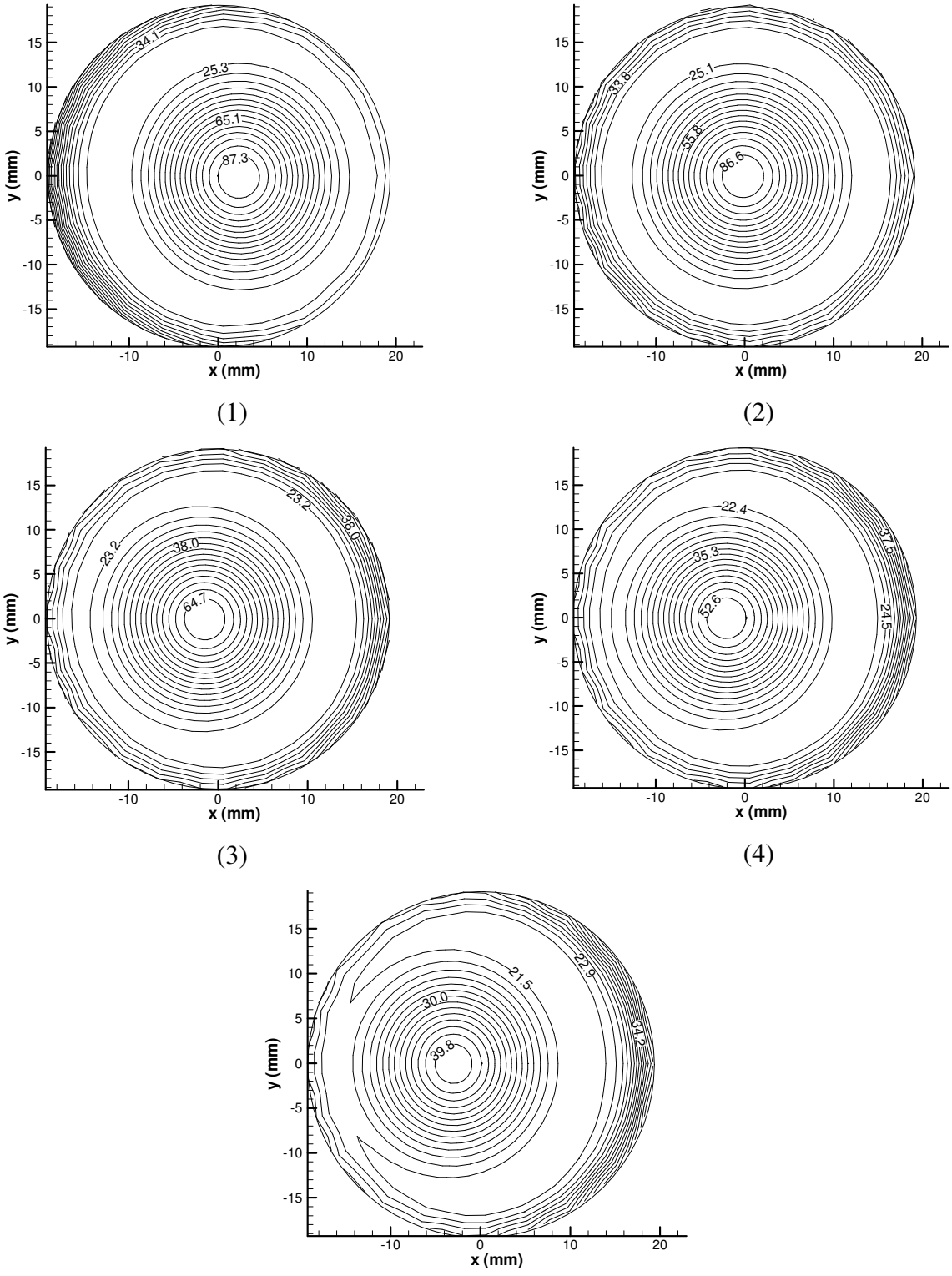

Figure 3.7 Temperature distributions for apple sauce at the outlet (z = 124mm): effect of the resonant cavity shape; (1) apogee distance of 205, (2) 186, (3) 167, (4) 154, and (5) 128mm, respectively.

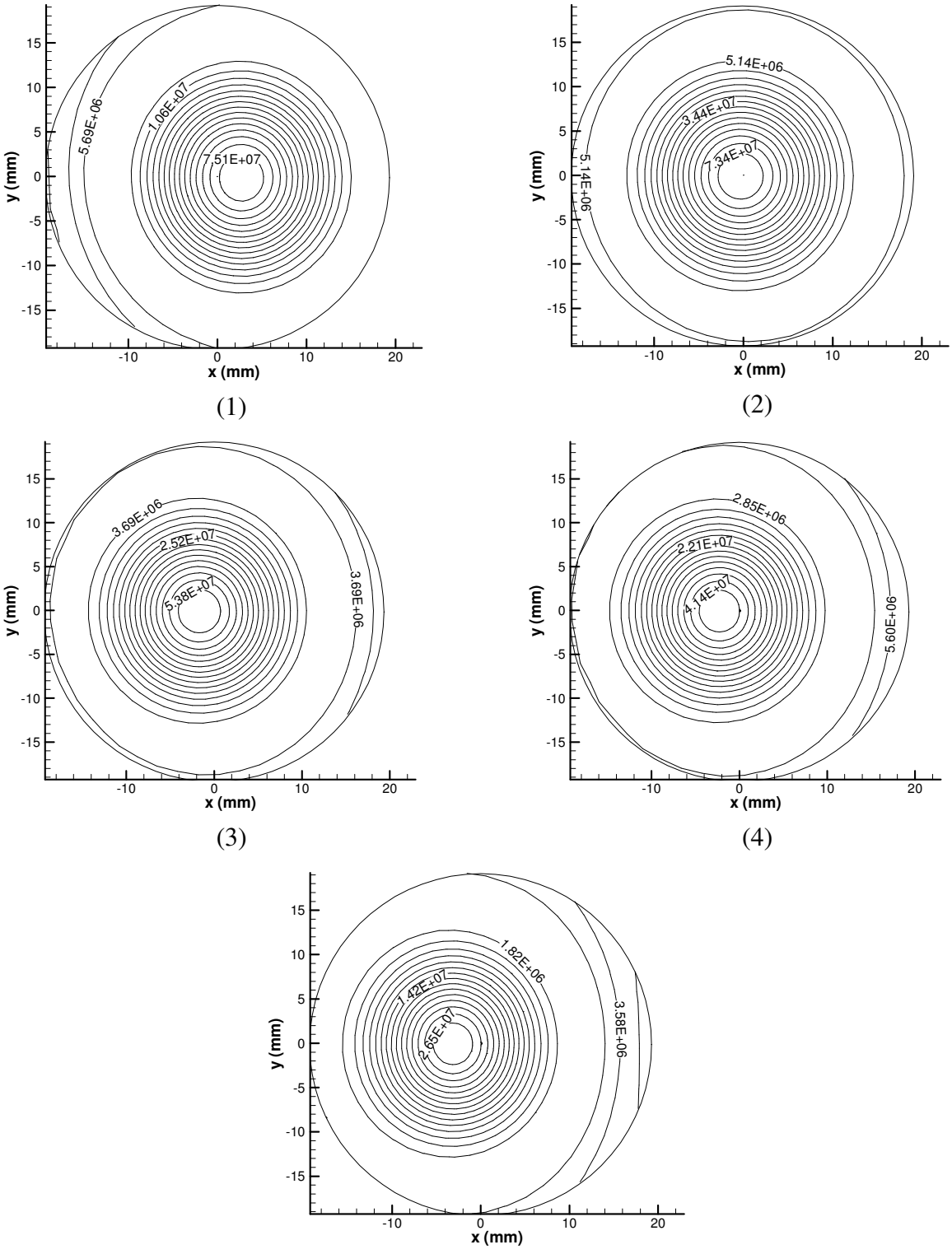

Figure 3.8 Electromagnetic power intensity distributions for apple sauce at the outlet (z = 124mm): effect of the resonant cavity shape; (1) apogee distance of 205, (2) 186, (3) 167, (4) 154, and (5) 128mm, respectively.

REFERENCES

1. Ayappa, K.G., Davis, H.T., Davis, E.A., Gordon, J. (1991) Analysis of microwave heating of materials with temperature-dependent properties, *AIChE Journal*,37: 313-322.
2. De Pourcq, M. (1985) Field and power density calculation in closed microwave system by three-dimensional finite difference, *IEEE Proceedings*, 132: 361-368.
3. Jia, X., Jolly, P. (1992) Simulation of microwave field and power distribution in a cavity by a three dimensional finite element method, *Journal of Microwave Power and Electromagnetic Energy*, 27: 11-22.
4. Clemens, J., Saltiel, C. (1995) Numerical modeling of materials processing microwave furnaces, *International Journal of Heat and Mass Transfer*, 39: 1665-1675.
5. Anantheswaran, R.C., Liu, L. (1994) Effect of viscosity and salt concentration on microwave heating of model non-Newtonian liquid foods in a cylindrical container, *Journal of Microwave Power and Electromagnetic Energy*, 29: 119-126.
6. Zhang, Q., Jackson, T.H., Ungan, A. (2000) Numerical modeling of microwave induced natural convection, *International Journal of Heat and Mass Transfer*, 43: 2141-2154.
7. Jia, X., Bialkowski, M. (1992) Simulation of microwave field and power distribution in a cavity by a three dimensional finite element method, *Journal of Microwave Power and Electromagnetic Energy*, 27: 11-22.
8. Deepak, Evans, J.W. (1993) Calculation of temperatures in microwave-heated two-dimensional ceramic bodies, *Journal of American Ceramic Society*, 76: 1915-1923.

9. Liu, F., Turner, I., Bialkowski, M. (1994) A finite-difference time-domain simulation of power density distribution in a dielectric loaded microwave cavity, *Journal of Microwave Power and Electromagnetic Energy*, 29: 138-147.
10. Iwabuchi, K., Kubota, T., Kashiwa, T., Tagashira, H. (1997) Analysis of electromagnetic fields using the finite-difference time-domain method in a microwave oven loaded with high-loss dielectric, *Electronics and Communications in Japan*, 78: 41-50.
11. Dibben, D.C., Metaxas, A.C. (1997) Frequency domain vs. time domain finite element methods for calculation of fields in multimode cavities, *IEEE Transaction on Magnetics*, 33: 1468-1471.
12. Dibben, D.C., Metaxas, A.C. (1994) Finite element time domain analysis of multimode applicators using edge elements, *Journal of Microwave Power and Electromagnetic Energy*, 29: 243-251.
13. Kriegsmann, G.A. (1997) Cavity effects in microwave heating of ceramics, *Journal of Applied Mathematics*, 57: 382-400.
14. Araneta, J.C., Brodwin, M.E., Kriegsmann, G.A. (1984) High-temperature microwave characterization of dielectric rods, *IEEE Transactions on Microwave Theory and Techniques*, 32: 1328-1335.
15. Yee, K.S. (1966) Numerical solution of initial boundary value problem involving Maxwell's equations in isotropic media, *IEEE Trans. on Antennas and Propagation*, 14: 302-307.
16. Webb, J.P., Maile, G.L., Ferrari, R.L. (1983) Finite element implementation of three dimensional electromagnetic problems, *IEEE Proceedings*, 78: 196-200.

17. Zhao, H., Turner, I.W. (1996) An analysis of the finite-difference time-domain method for modeling the microwave heating of dielectric materials within a three-dimensional cavity system, *Journal of Microwave Power and Electromagnetic Energy*, 31: 199-214.
18. Zhang, H., Taub, A.K., Doona, I.A. (2001) Electromagnetics, heat transfer and thermokinetics in microwave sterilization, *AIChE Journal*, 47: 1957-1968.
19. Ayappa, K.G., Davis, H.T., Davis, E.A., Gordon, J. (1992) Two-dimensional finite element analysis of microwave heating, *AIChE Journal*, 38: 1577-1592.
20. Ayappa, K.G., Brandon, S., Derby, J.J., Davis, H.T., Davis, E.A. (1994) Microwave driven convection in a square cavity, *AIChE Journal*, 40: 1268-1272.
21. Ayappa, K.G., Sengupta, T. (2002) Microwave heating in multiphase systems: evaluation of series solutions, *Journal of Engineering Mathematics*, 44: 155-171.
22. Basak, T., Ayappa, K.G. (1997) Analysis of microwave thawing of slabs with effective heat capacity method, *AIChE Journal*, 43: 1662-1667.
23. Ratanadecho, P., Aoki, K., Akahori, M. (2002) The characteristics of microwave melting of frozen packed beds using a rectangular waveguide, *IEEE Trans. on Microwave Theory and Techniques*, 50: 1495-1502.
24. Ratanadecho, P., Aoki, K., Akahori, M. (2002) Influence of irradiation time, particle sizes, and initial moisture content during microwave drying of multi-layered capillary porous materials, *Journal of Heat Transfer*, 124: 151-161.
25. Datta, A., Prosetya, H., Hu, W. (1992) Mathematical modeling of batch heating of liquids in a microwave cavity, *Journal of Microwave Power and Electromagnetic Energy*, 27: 38-48.

26. Ratanadecho, P., Aoki, K., Akahori, M. (2002) A Numerical and experimental investigation of the modeling of microwave heating for liquid layers using a rectangular wave guide (effects of natural convection and dielectric properties), *Applied Mathematical Modeling*, 26: 449-472.
27. Zhu, J., Kuznetsov, A.V., Sandeep, K.P. (2005) Numerical simulation of forced convection in a duct subjected to microwave heating, *Heat and Mass Transfer*, http://dx.doi.org/10.1007/s00231-006-0105-y (online first).
28. Basak, T., Ayappa, K.G. (2002) Role of length scales on microwave thawing dynamics in 2D cylinders, *International Journal of Heat and Mass Transfer*, 45: 4543-4559.
29. Ayappa, K.G., Davis, H.T., Barringer, S.A., Davis, E.A. (1997) Resonant microwave power absorption in slabs and cylinders, *AIChE Journal*, 43: 615-624.
30. Cheng, D.K. (1992) *Field and wave electromagnetics*, Addison-Wesley, New York.
31. Mur, G. (1981) Absorbing boundary conditions for the finite difference approximation of the time domain electromagnetic field equations, *IEEE Transactions on Electromagnetic Compatibility*, 23: 377-382.
32. Zhang, Q. (1998): *Numerical simulation of heating of a containerized liquid in a single-mode microwave cavity.* MS Thesis, Indiana University-Purdue University at Indianapolis, IN.
33. Bird, R.B., Stewart, W.E., Lightfoot, E.N. (2002) *Transport phenomena*, John Wiley & Sons, New York.
34. Kunz, K.S. Luebbers, R. (1993) *The finite difference time domain method for electromagnetics*, CRC, Boca Raton, FL.

35. Dey, S., Raj Mittra (1999) A conformal finite-difference time-domain technique for modeling cylindrical dielectric resonators, *IEEE Transactions on Microwave Theory and Techniques*, 47: 1737-1739.

36. Bykov, Y.V., Rybakov, K.I., Semenov, V.E. (2001) High-temperature microwave processing of materials, *Journal of Physics D: Applied Physics*, 34: 55-75.

4 NUMERICAL MODELING OF A MOVING PARTICLE IN A CONTINUOUS FLOW SUBJECT TO MICROWAE HEATING

ABSTRACT

In this chapter, microwave heating of a food particle and carrier liquid as they flow continuously in a circular pipe is investigated numerically. The three-dimensional transient fluid flow as well as electromagnetic and temperature fields are described by a model that includes coupled Maxwell, continuity, Navier-Stokes, and energy equations. The electromagnetic power and temperature distributions in both the liquid and the particle are taken into account. The hydrodynamic interaction between the solid particle and the carrier fluid is simulated by the force-coupling method (FCM). This chapter explores the effects of dielectric properties and the inlet position of the particle on microwave energy and temperature distributions inside the particle. The effect of the particle on power absorption in the carrier liquid is studied as well. The results show that electromagnetic power absorption by the particle is greatly influenced by the ratio of dielectric properties of the particle and the liquid as well as the distance between the particle and the location in the applicator where the electromagnetic power takes on its maximum value.

Nomenclature

A area, m^2

a_p particle radius, m

C_p specific heat capacity, $J/(kg \cdot K)$

c phase velocity of the electromagnetic propagation wave, m/s

$\mathbf{E}$	electric field intensity, V/m
f	frequency of the incident wave, Hz
$\mathbf{f}$	body force, N
$\mathbf{F}$	force monopole, N
$\mathbf{F}^{ext}$	external force, N
$\mathbf{g}$	gravity, m/s^2
h	effective heat transfer coefficient, $W/(m^2 \cdot K)$
$\mathbf{H}$	magnetic field intensity, A/m
k	thermal conductivity, $W/(m \cdot K)$
m	fluid consistency coefficient, $Pa\ s^n$
n	flow behavior index
N	number of time steps
p	pressure, Pa
P	microwave power, W
q	microwave power density, W/m^3
T	temperature, ^oC
t	time, s
$\tan\delta$	loss tangent
$\mathbf{u}$	fluid velocity vector, m/s
$\mathbf{V}$	velocity of the particle center, m/s
Z_{TE}	wave impedance, Ω

Greek symbols

η	apparent viscosity, $Pa \cdot s$
ε	electric permittivity, F/m
ε_r'	relative permittivity
ε_r''	relative loss factor
ε_{rad}	emissivity
λ_g	electromagnetic wavelength in the cavity, m
μ	magnetic permeability, H/m
ρ	density, kg/m^3
$\boldsymbol{\Omega}$	angular velocity, 1/s
σ_e	electric conductivity, S/m
σ_{rad}	Stefan-Boltzmann constant, $W/(m^2 K^4)$
σ, σ'	length scale, m
$\boldsymbol{\omega}$	vorticity, 1/s

Subscripts

∞	ambient
a	free space, air
0	initial condition
in	input (at the incident plane)
l	liquid
p	particle

n normal

t tangential

X,Y,Z projection on a respective coordinate axis

4.1 INTRODUCTION

Microwave heating of materials has been utilized in a wide range of industrial applications. Microwave technology makes it possible to heat the bulk of the material without any intermediate heat transfer medium. This results in high energy efficiency and a reduction in heating time compared to traditional heating techniques, where heat is transferred from a surface to the interior.

Modeling of microwave heating requires solving the energy equation with a source term, which describes microwave power absorption in the material. The power absorption can be evaluated by two methods, using the Lambert's law or by directly solving Maxwell's equations. Lambert's law has been extensively used in recent literature [1-4], mostly when the heated sample is large. In large samples microwave power absorption decays exponentially from the surface into the material. In small size samples, since the heat is generated by the resonance of standing waves, which Lambert's law can not adequately describe [5-6], the solution of Maxwell's equations is necessary to accurately determine the microwave power absorption [7-10].

Although most previous studies of microwave heating focused on solid materials, some effort for microwave heating of liquids is reported in [2, 3, 11, 12]. The analysis of microwave heating in liquids is more challenging due to the presence of fluid motion. Usually, a complete set of momentum, energy, and Maxwell's equations must be solved

to describe the complex interactions of flow, temperature, and microwave fields within the liquid. Complex interactions between electromagnetic field and convection during heating of liquids are addressed in [11-13].

Continuous processing of food is a promising alternative to traditional heating of food in containers. This technology has been successfully used for microwave heating of liquid foods. During this process, the liquid food flows in an applicator tube. When the flow passes through the section where the applicator is exposed to microwave radiation, the liquid absorbs microwave power and its temperature is quickly increased. Previous work [13] proposed a model describing forced convection heat transfer during the continuous flow microwave heating process. However, the previous investigation [13] only addresses a single phase flow in the applicator tube. To the best of the authors' knowledge, no modeling has been reported on microwave heating of a liquid with suspended particles. In this work, a three-dimensional model of heating of a liquid carrying a single solid particle as it passes a portion of the applicator subjected to microwave irradiation is proposed. The power and temperature distributions in both the liquid and solid particle are investigated. The effect of the particle on the microwave power absorption and temperature distribution of the liquid is studied.

4.2 MODEL GEOMETRY

Figure 4.1 shows the schematic diagram of the microwave system investigated in this research. The system consists of a waveguide, a resonant cavity, and a vertically positioned applicator tube that passes through the cavity. A liquid food, which is treated as a non-Newtonian fluid, carrying a solid food particle flows through the applicator tube

in the upward direction, absorbing microwave energy as it passes through the tube. The microwave operates in TE_{10} [14] mode at a frequency of 915 *MHz* with the input power of 7 *kW*, which is generated in the incident plane by imposing a plane polarized source. The microwave power is transmitted through the waveguide and directed on the applicator tube located in the center of the resonant cavity. An absorbing plane is located behind the incident plane to absorb the microwave energy reflected by the cavity. Parameters characterizing the geometry of the microwave system are listed in Table 4.1.

4.3 MATHEMATICAL MODEL

Two computational domains are utilized. The first domain, used for computing electromagnetic field, includes the region enclosed by the wall of the waveguide, resonant cavity, and incident plane. The second domain, used for solving the momentum and energy equations, coincides with the region inside the applicator tube. The origin of the coordinate system for the electromagnetic computational domain lies in the absorbing plane, as shown in Figure 4.1. The origin of the coordinate system for the inside of the applicator tube is in the center of the tube at the tube entrance.

A simulation begins when the particle enters the applicator and ends when the particle leaves the applicator.

4.3.1 ELECTROMAGNETIC FIELD

The electromagnetic field is governed by Maxwell's equations, which are presented in terms of the electric field, **E**, and the magnetic field, **H** [15]:

$$\varepsilon \frac{\partial \mathbf{E}}{\partial t} = \nabla \times \mathbf{H} - \sigma_e \mathbf{E} \tag{4.1}$$

$$\mu \frac{\partial \mathbf{H}}{\partial t} = -\nabla \times \mathbf{E} \tag{4.2}$$

$$\nabla \cdot (\varepsilon \mathbf{E}) = 0 \tag{4.3}$$

$$\nabla \cdot \mathbf{H} = 0 \tag{4.4}$$

where $\varepsilon = \varepsilon_a \varepsilon_r'$ is the electric permittivity (ε_a is the permittivity of free space, ε_r' is the relative permittivity of the material) and μ is the magnetic permeability. σ_e stands for the electric conductivity related to the loss tangent $\tan\delta$ by:

$$\sigma_e = 2\pi f \varepsilon \tan\delta \tag{4.5}$$

where

$$\tan\delta = \frac{\varepsilon_r''}{\varepsilon_r'} \tag{4.6}$$

In Eq. (4.6), ε_r'' stands for the relative loss factor.

At the inner walls of the waveguide and cavity, a perfect conducting condition is utilized. Therefore, normal components of the magnetic field and tangential components of the electric field vanish at these walls:

$$H_n = 0, \quad E_t = 0 \tag{4.7}$$

At the absorbing plane, Mur's first order absorbing condition [16] is utilized:

$$\left(\frac{\partial}{\partial Z}-\frac{1}{c}\frac{\partial}{\partial t}\right)E_Z\big|_{X=0}=0 \tag{4.8}$$

where c is the phase velocity of the propagation wave and t is the time.

At the incident plane, the microwave source is simulated by the following equations:

$$E_{Z,inc}=-E_{Zin}\sin\left(\frac{\pi Y}{W}\right)\cos\left[2\pi\left(ft-\frac{X_{in}}{\lambda_g}\right)\right] \tag{4.9}$$

$$H_{Y,inc}=\frac{E_{Zin}}{Z_{TE}}\sin\left(\frac{\pi Y}{W}\right)\cos\left[2\pi\left(ft-\frac{X_{in}}{\lambda_g}\right)\right] \tag{4.10}$$

where f is the frequency of the microwave, W is the width of the incident plane, X_{in} is the X-position of the incident plane, Z_{TE} is the wave impedance, λ_g is the wave length of a microwave in the waveguide, and E_{Zin} is the input value of the electric field intensity. By applying the Poynting theorem [11], the input value of the electric field intensity is evaluated by the microwave power input as:

$$E_{Zin}=\sqrt{\frac{4Z_{TE}P_{in}}{A}} \tag{4.11}$$

where P_{in} is the microwave power input and A is the area of the incident plane.

At $t=0$, all components of **E** and **H** are zero.

4.3.2 *HEAT TRANSFER MODEL*

The temperature distributions in the particle and carrier liquid are obtained by the solution of the following energy equations with a source term which accounts for internal energy generation due to the absorption of the microwave energy.

In the particle the energy equation is:

$$\rho_p C_{pp} \frac{\partial T_p}{\partial t} = \nabla \cdot \left(k_p \nabla T_p \right) + q_p(\mathbf{x}, t) \tag{4.12}$$

In the liquid the energy equation is:

$$\rho_l C_{pl} \left(\frac{\partial T_l}{\partial t} + \mathbf{u} \cdot \nabla T_l \right) = \nabla \cdot \left(k_l \nabla T_l \right) + q_l(\mathbf{x}, t) \tag{4.13}$$

where ρ is the density; C_p is the specific heat; k is the thermal conductivity; T is the temperature; and q is the microwave power density, representing the local electromagnetic heat generation intensity term, which depends on dielectric properties of the liquid and particle as well as the electric field intensity:

$$q = 2\pi f \varepsilon_0 \varepsilon_r' (\tan \delta) \mathbf{E}^2 \tag{4.14}$$

The following thermal boundary condition is proposed at the applicator wall. The wall is assumed to lose heat by natural convection and radiation:

$$-k \left. \frac{\partial T}{\partial n} \right|_{surface} = h\left(T - T_\infty\right) + \sigma_{rad} \varepsilon_{rad} \left(T^4 - T_\infty^4\right) \tag{4.15}$$

where h is the convection coefficient, T_∞ is the ambient air temperature (the waveguide walls are assumed to be in thermal equilibrium with the ambient air), σ_{rad} is the Stefan-Boltzmann constant, and ε_{rad} is the surface emissivity.

The inlet liquid temperature is assumed to be uniform and equal to the temperature in the free space outside the applicator, T_∞.

The thermal boundary condition at the surface of the particle is:

$$T_{r=a_p+0} = T_{r=a_p-0} \quad \text{and} \quad k_p \left.\frac{\partial T}{\partial n}\right|_{r=a_p-0} = k_l \left.\frac{\partial T}{\partial n}\right|_{r=a_p+0} \tag{4.16}$$

The initial temperatures of the liquid and the particle are defined as:

$$T_l = T_{l0} \ , \ T_p = T_{p0} \quad \text{at} \quad t = 0 \tag{4.17}$$

4.3.3 HYDRODYNAMIC MODEL

The movement of the liquid is determined by the continuity and momentum equations:

$$\nabla \cdot \mathbf{u} = 0 \tag{4.18}$$

$$\rho_l \left(\frac{\partial \mathbf{u}}{\partial t} + \mathbf{u} \cdot \nabla \mathbf{u} \right) = -\nabla p + \nabla \cdot \eta \nabla \mathbf{u} + \rho_l \mathbf{g} + \mathbf{f}(\mathbf{x}, t) \tag{4.19}$$

where η is the apparent viscosity of the non-Newtonian fluid, which in this chapter is assumed to obey the power-law, as:

$$\eta = m\left(\dot{\gamma}\right)^{n-1} \tag{4.20}$$

where m and n are the fluid consistency coefficient and the flow behavior index, respectively.

The effect of the particle on the fluid is represented by a localized body force $\mathbf{f}(\mathbf{x}, t)$ that transmits to the fluid the resultant force of the particle on the flow [17]. In this

chapter, a force-coupling method (FCM) developed by Maxey et al. [17-20] is utilized to simulate this source term $\mathbf{f}(\mathbf{x},t)$.

According to FCM, the body force $\mathbf{f}(\mathbf{x},t)$ is specified as

$$\mathbf{f}(\mathbf{x},t) = \mathbf{F}\Delta\left(\mathbf{x}-\mathbf{Y},\sigma\right) \tag{4.21}$$

where $\mathbf{Y}$ is the position of the particle and $\mathbf{F}$, the force monopole, represents the hydrodynamic drag on the particle. The localized force distribution for the particle is determined by the Gaussian function

$$\Delta\left(\mathbf{x}\right) = \left(2\pi\sigma^2\right)^{-3/2}\exp\left(-\mathbf{x}^2/2\sigma^2\right) \tag{4.22}$$

and the length scale σ is related to the radius of the particle, a_p, as

$$\sigma = \frac{a_p}{\sqrt{\pi}} \tag{4.23}$$

The force monopole is determined by the sum of the external force $\mathbf{F}^{ext}$ acting on the particle and the inertia of the particle:

$$\mathbf{F} = \mathbf{F}^{ext} - (4/3)\pi a_p{}^3(\rho_g - \rho_l)\frac{d\mathbf{V}}{dt} \tag{4.24}$$

where the only external force $\mathbf{F}^{ext}$ acting on the suspending particles is the buoyancy force:

$$F_b = (4/3)\pi a_p{}^3(\rho_l - \rho_g)\mathbf{g} \tag{4.25}$$

The velocity of the particle, $\mathbf{V}$, can be determined by a local average of the fluid velocity over the region occupied by the particle:

$$\mathbf{V}(t) = \int \mathbf{u}(\mathbf{x},t)\Delta(\mathbf{x}-\mathbf{Y},\sigma)d^3\mathbf{x} \tag{4.26}$$

The angular velocity of the particle, $\mathbf{\Omega}$, is calculated as

$$\mathbf{\Omega} = \frac{1}{2}\int \boldsymbol{\omega}(\mathbf{x},t)\Delta(\mathbf{x},\sigma')d^3\mathbf{x} \tag{4.27}$$

where $\boldsymbol{\omega}$ is the vorticity and the length scale σ' is

$$\sigma' = \frac{a_p}{\left(6\sqrt{\pi}\right)^{1/3}} \tag{4.28}$$

At the inner surface of the applicator tube, a hydrodynamic no-slip boundary condition is used. At the inlet to the applicator, a uniform, fully developed velocity profile is imposed, and specified by the inlet mean velocity, U_{mean}. The flow in the applicator is assumed to be hydrodynamically fully developed at $t = 0$. The inlet velocity of the particle is calculated as a volume average of the fluid velocity in a volume occupied by the particle, as stated by Eq. (4.26).

4.4 NUMERICAL PROCEDURE

The electromagnetic solver used in this work is based on the FDTD method [21]. A non-uniform structured mesh consisting of 1,236,000 cells in the electromagnetic computational domain is utilized. The volume occupied by the applicator pipe is refined with smaller cells in order to accurately evaluate the electromagnetic power distribution. The time step for the electromagnetic solver obeys the stability condition [21]:

$$\Delta t \le \frac{1}{c\sqrt{\frac{1}{\Delta X^2}+\frac{1}{\Delta Y^2}+\frac{1}{\Delta Z^2}}} \tag{4.29}$$

Since a non-uniform mesh is used, in Eq. (4.29) ΔX , ΔY , ΔZ represent the smallest space increments in *X*, *Y*, and *Z* directions, respectively. A portion of the boundary of the resonant cavity surface is curved, and the utilization of structured mesh results in a staircase approximation of the curved surface, so a contour-path integral FDTD method [22] is used to improve the approximation of the curved surface of the microwave cavity with traditional structured cells.

An implicit time-integration scheme and the time marching procedure introduced by Patankar and Spalding [23] are adopted to solve the continuity and momentum equations (4.18) and (4.19). At each time step, the continuity and momentum equations for the fluid phase are first solved in the absence of the particle. Once the hydrodynamic information about the fluid phase motion is obtained, the velocity of the particle is determined from Eq. (4.16). The continuity and momentum equations are then resolved with the particle source term. This procedure is repeated until the following convergence criterion is met

$$\frac{\left\|\hat{\mathbf{r}}^{(k)}\right\|_\infty}{\left\|\hat{\mathbf{r}}^{(0)}\right\|_\infty} \le 10^{-6} \tag{4.30}$$

where $\hat{\mathbf{r}}$ is the residual of the pressure correction equation and the superscripts (0) and (k) refer to the initial and *k*th iteration, respectively.

Energy equations (4.12) and (4.13) are discretized using a cell-centered finite volume approach and solved implicitly in the Cartesian coordinate system. The two

energy equations are coupled by the boundary condition given by Eq. (4.16). At each time step, Eqs. (4.12) and (4.13) are solved iteratively until boundary condition (4.16) is satisfied. The rotation of the particle is taken into account by rotating the temperature field in the particle at each time step.

Since microwave propagation is much faster than heat and mass transfer, different time steps of $\Delta t_1 = 1\ ps$ and $\Delta t_2 = 0.4\ ms$ are used for solving Maxwell's equations and heat and mass transfer equations, respectively. First, the distribution of the microwave power density, q, in the applicator is computed by iterating the electromagnetic solver until the sinusoidal steady state (pure time-harmonic) distribution of the electromagnetic field is attained. The temperature distributions in both the liquid and solid particle are then determined using this power distribution. Utilizing these temperature distributions, the liquid dielectric properties (which are temperature dependent) are updated. The updated dielectric properties are then used to update the electromagnetic field and the power density distributions in the applicator. This procedure is repeated at each time step. The details of the computational procedure are illustrated in Figure 4.2. Table 4.2 shows thermophysical and electromagnetic properties used in computations.

4.5 RESULTS AND DISCUSSION

In this chapter, three kinds of solid food particles and two kinds of liquid food products are considered. The properties of particles 1, 2, and 3 are representative for marinated shrimp, non-marinated shrimp, and potato, respectively. Liquids 1 and 2 have properties representative for two different soup products. Table 4.3 shows dielectric and thermal properties of these food products. Densities of particles 1, 2, and 3 are almost the

same, which results in their similar hydrodynamic behavior. Thermal and dielectric properties of the particles are also similar except for the loss tangent. Particles 1, 2 and 3 have a high loss tangent, medium loss tangent, and low loss tangent, respectively. The loss tangent of liquid 1 is twice as large as that of liquid 2 at $20\,^{\circ}C$. The particles are assumed spherical with a diameter of 0.9 *cm*. In each computed case, only one particle is introduced into the applicator tube. The flow in the applicator pipe is assumed initially to be hydrodynamically fully developed with a mean velocity of 6.0 *cm/s*. At t = 0, the particle is suddenly released at the inlet of the applicator. This makes the flow unsteady. The initial position of the particle is illustrated in Figure 4.3. Since the particle is released away from the pipe center, the flow is not axi-symmetric but three-dimensional with a plane of symmetry, which is the plane passing through $\theta = 0^{\circ}$ and $\theta = 180^{\circ}$, as shown in the section A-A of Figure 4.3. Also, at t = 0, the microwave energy is turned on. The initial temperatures of the particle and the carrier liquid are $T_{p0} = T_{l0} = 20\,^{\circ}C$. The temperature in the free space outside the applicator is also $T_{\infty} = 20\,^{\circ}C$. It is assumed that there is no phase change in either the particle or the carrier liquid during the heating process. Hydrodynamic, electromagnetic, and thermal interactions between the particle and the carrier liquid are investigated.

4.5.1 HYDRODYNAMIC INTERACTIONS BETWEEN THE PARTICLE AND LIQUID

The fluid flow in the applicator is initially fully developed, and then it is affected by the particle entering the applicator. In different simulated cases, the particle is released at different radial positions at the inlet. A typical flow field is shown is Figure 4.4, where the velocity contour lines of the fluid axial velocity and streamlines of the fluid velocity relative to the particle are given in the plane of symmetry. Figure 4.4 is computed for

particle 2 and liquid 1 with the particle initial position at $r = 0.67\ cm$ and $\theta = 0^{\circ}$. From the axial velocity distributions, it is evident that the particle does not greatly modify the fully developed velocity profile except in the immediate vicinity of the particle. The streamlines shown in Figure 4.4 indicate the difference in velocities of the liquid and the particle. The forward streamlines in the central area of the applicator pipe indicate a larger axial velocity of the liquid than that of the particle. It is also evident that there is a recirculation zone just downstream in relation to the particle, close to the wall of the pipe. This is because of the relative velocity between the particle and the liquid. Figure 4.5 shows streamwise velocities and trajectories of the particle for different particle initial positions. Since the flow is symmetric with respect to the plane of symmetry, there is no displacement of the particle in the θ direction. Therefore, the trajectories of the particle are shown in the plane of symmetry only.

4.5.2 ELECTROMAGNETIC POWER DENSITY AND TEMPERATURE PROFILES

The transient power and temperature distributions inside the applicator are shown in Figure 4.6. After the particle enters the applicator, both the particle and the liquid are subjected to microwave irradiation. A peak of the microwave power occurs near the center of the applicator pipe, and is located at $r = 0.67\ cm$ and $\theta = 0^{\circ}$. The temperature in the streamwise direction increases because a fluid volume absorbs microwave power as it is convected downstream. The contour lines of power density are parallel to each other except near the particle. This is because dielectric properties of liquid 1 are not very sensitive to temperature and the temperature of the liquid does not rise significantly during the short residence time of the particle inside the applicator. This also indicates that on average the particle does not affect significantly the power density distribution in

the applicator. There is a thermal wake in front of the particle that grows with time, which is due to the fact that the particle velocity decreases after the particle enters the applicator, which enhances convection between the particle and the surrounding liquid.

The power and temperature distributions inside the particle are shown in Figure 4.7. A peak of power density occurs in the left half of the particle. According to the power distributions shown in Figure 4.6, the magnitude of this power peak is much higher than the power density in the vicinity of the particle. This is attributed to higher loss tangent of the particle than that of the carrier liquid. The temperature distribution inside the particle is determined by the power density distribution, with the higher temperature values corresponding to higher power values. However, it is also evident in Figures 4.7 b(1) and b(2) that the temperature and power distributions in the upper and lower halves of the particle show less symmetry as the time increases. This is attributed to the effect of convection between the liquid and the surface of the particle. Since the streamwise velocity of the particle is smaller than the local velocity of the liquid, the lower half of the particle surface is upwind to the liquid flow. This causes more convection heat transfer between the lower particle surface and the surrounding liquid. This also results in the asymmetric power distribution in the upper and lower halves of the particle. Figure 4.8 shows the temperature distributions at the surface of the particle. It is evident that a region of the highest temperature appears at the upper part of the particle surface. Also, the surface temperature distributions indicate higher temperature in the left half of the particle than in the right half, which is consistent with the results shown in Figure 4.7.

4.5.3 *HEATING PATTERNS FOR PARTICLES WITH DIFFERENT DIELECTRIC PROPERTIES*

A comparison of the power and temperature distributions inside the particle for three particles with different dielectric properties is shown in Figure 4.9. Liquid 1 is used as the carrier liquid, and the particle is released at $r = 0.67\ cm$ and $\theta = 0^{\circ}$, same for particles 1, 2, and 3. It is evident that the highest temperature and power density are attained for particle 1. This is attributed to the highest loss tangent of particle 1. The mean power densities in the three particles are shown in Figure 4.10(a). It is evident that particle 1 has the largest mean power density, indicating the highest heating rate. Figure 4.5 shows that if the initial radial position of the particle is at $r = 0.67\ cm$, the radial displacement of the particle as it passes through the applicator is not large. Since dielectric properties of particles 1, 2 and 3 are temperature independent, the difference between mean power densities for each particle are attributed to the influence of the streamwise position of the particle. The effect of the particle on power absorption in the liquid is investigated by comparing the mean power densities between the cases with and without the particle, as shown in Figure 4.10(b). It is evident that particle 3 has most influence on the power absorption in the liquid. This is attributed to the large difference in the power absorption between the materials of particle 3 and liquid 1. For the extreme case when the applicator is filled by the material whose dielectric properties are identical to that of the particle, the mean power density is 46.19 W/cm^3 for the material of particle 1, 44.93 W/cm^3 for that of particle 2, and 36.56 W/cm^3 for that of particle 3. From Figure 4.10(b), it is evident that the mean power density in the liquid for the case with no particle is around 42.33 W/cm^3. The larger difference in power absorption between

particle 3 and liquid 1 results in particle 3 exhibiting more influence on the mean power density in the carrier liquid than particles 1 and 2.

4.5.4 *Effect of Dielectric Properties of the Carrier Liquid on Particle Heating*

The influence of dielectric properties of the carrier liquid on the power density and temperature distributions in the particle are investigated. Simulations are performed for particle 2 with both carrier liquids 1 and 2. Liquid 2 has lower loss tangent than liquid 1. Figure 4.11 compares the power density distributions in the cross-section at 1/2 height of the applicator in the two liquids at the moment then the particle passes the outlet of the applicator. It is evident that the power density distribution in liquid 2 is similar to that in liquid 1, but the magnitude of the power density is smaller in liquid 2 than in liquid 1. A comparison between the power density distributions in particle 1 with carrier liquids 1 and 2 is shown in Figures 4.12 a(1) and a(2). It is found that the power absorption by the particle in liquid 2 is much smaller than in liquid 1. This indicates that the dielectric properties of the liquid determine the power absorption in the particle. The particle absorbs more microwave energy in a high loss liquid than in a low loss liquid. This also results in particle 2 attaining higher temperature in liquid 2 than in liquid 1, as shown in Figures 4.12 b(1) and b(2).

4.5.5 *Effect of the Radial Position of the Particle on Power Absorption in bothe the Particle and Carrier Liquid*

The effect of particle position on power density and temperature distributions in the particle is studied. Simulations are performed for liquid 1 with particle 2. The results presented in Figure 4.12 show variations of power density distributions in the particle released at different inlet positions: (a) $r = 0.95\,cm$ and $\theta = 0^{\circ}$, (b) $r = 0.67\,cm$

and $\theta = 0^{\circ}$, (c) $r = 0.28\,cm$ and $\theta = 180^{\circ}$, (d) $r = 0.67\,cm$ and $\theta = 180^{\circ}$ and (e) $r = 0.95\,cm$ and $\theta = 180^{\circ}$. Results are shown in the plane of symmetry at the moment when the particle is passing ½ height of the applicator. The radial position of the particle for this moment of time is displayed in Figure 4.5. It is evident that the power peak inside the particle occurs in the left half of the particle in cases a) and b), but in the right half of the particle in cases c), d), and e). Recalling that the power peak in liquid 1 occurs at $r = 0.3\,cm$ and $\theta = 180^{\circ}$, this indicates that the power peak inside the particle always occurs in the half of the particle which is closer to the location of the power peak in the liquid. Also, the power density and temperature inside the particle are higher if the particle is closer to the position where the power peak in the liquid occurs. This indicates that the power distribution in the carrier liquid determines the power distribution inside the particle.

4.6 CONCLUSIONS

A numerical model is developed for simulating a 3D flow of a non-Newtonain fluid carrying a solid particle as the liquid and the particle pass the applicator tube subjected to microwave heating. The model takes into account hydrodynamic and thermal interactions between the particle and the carrier liquid. It is shown that the particle may get heated at a different rate than the carrier liquid. The results reveal that the power absorption in the particle is determined by the value of the loss tangents of the particle and the carrier liquid. The larger the loss tangent of the particle, the larger is the power absorption in the particle. The particle absorbs more microwave energy in a high loss liquid than in a low loss liquid. The power absorption in the liquid is also influenced by

the particle. The power density distribution inside the particle is determined by the power distribution in the liquid as the power peak inside the particle always occurs in the half of the particle which is closer to the position of the power peak in the liquid. Depending on the radial positions of the particle at the inlet of the applicator, power absorption in the particle may differ significantly. The power absorption in the particle shows a strong dependence on the distance between the particle and the location of the power peak in the liquid. The power density inside the particle is higher if the particle is closer to the position where the power peak in the liquid occurs.

Table 4.1 Geometric parameters.

Symbol	Description	Value (cm)
D	Applicator diameter	3.8
AD	Apogee distance of cavity	20.5
PD	Perigee distance of cavity	15.4
CH	Cavity and applicator height	12.5
WL	Waveguide length	34.7
WW	Waveguide width	24.4
WH1	Waveguide height 1	12.5
WH2	Waveguide height 2	5.1
TL	Total length of the system	66.1
IAD	Distance between the incident plane and absorbing plane	2.7

Table 4.2 Thermophysical and electromagnetic properties utilized in computations.

$\varepsilon_0 = 8.85419\times10^{-12}$ (F/m)	$\varepsilon_{rad} = 0.4$
$\mu = 4.0\pi\times10^{-7}$ (H/m)	$\sigma_{rad} = 5.67\times10^{-8}$ (W/(m$^2\cdot$K^4))
$h = 20$ (W/(m$^2\cdot$K))	$P_{in} = 7000$ (W)
$Z_{TE} = 377$ (Ω)	$f = 915$ (MHz)

Table 4.3 Thermophysical and dielectric properties of food products.

Product	Property	Value
Liquid food product 1	ρ, kg/m^3	1037
	m, Pa·s^n	0.0059
	n	0.98
	c_p, J/(kg · K)	3943.7
	k, W/(m · K)	0.5678
	ε_r'	-0.155T+72.5
	$\tan\delta$	0.0034T+0.18
Liquid food product 2	ρ, kg/m^3	1037
	m, Pa·s^n	0.0059
	n	0.98
	c_p, J/(kg · K)	3943.7
	k, W/(m · K)	0.5678
	ε_r'	-0.163T+76.8
	$\tan\delta$	0.12
Particle 1	ρ, kg/m^3	1069
	c_p, J/(kg · K)	2.5
	k, W/(m · K)	0.47
	ε_r'	68.4
	$\tan\delta$	0.86
Particle 2	ρ, kg/m^3	1069
	c_p, J/(kg · K)	2.5
	k, W/(m · K)	0.47
	ε_r'	65.8
	$\tan\delta$	0.48
Particle 3	ρ, kg/m^3	1065
	c_p, J/(kg · K)	3.5
	k, W/(m · K)	0.55
	ε_r'	52.5
	$\tan\delta$	0.26

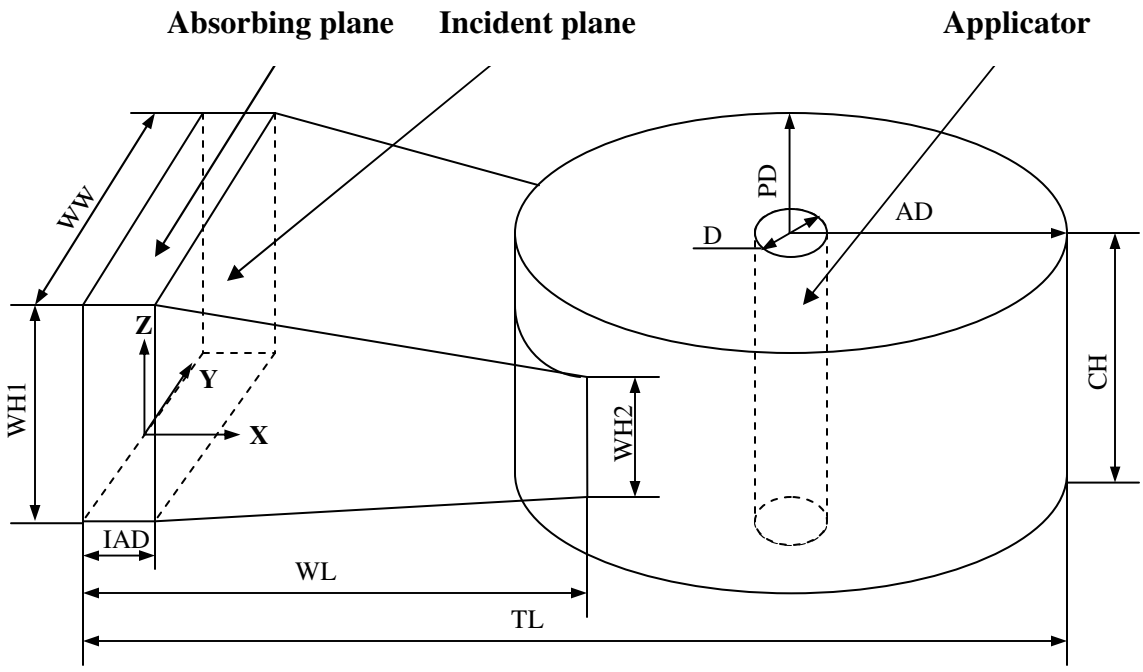

Figure 4.1 Schematic diagram of the microwave system.

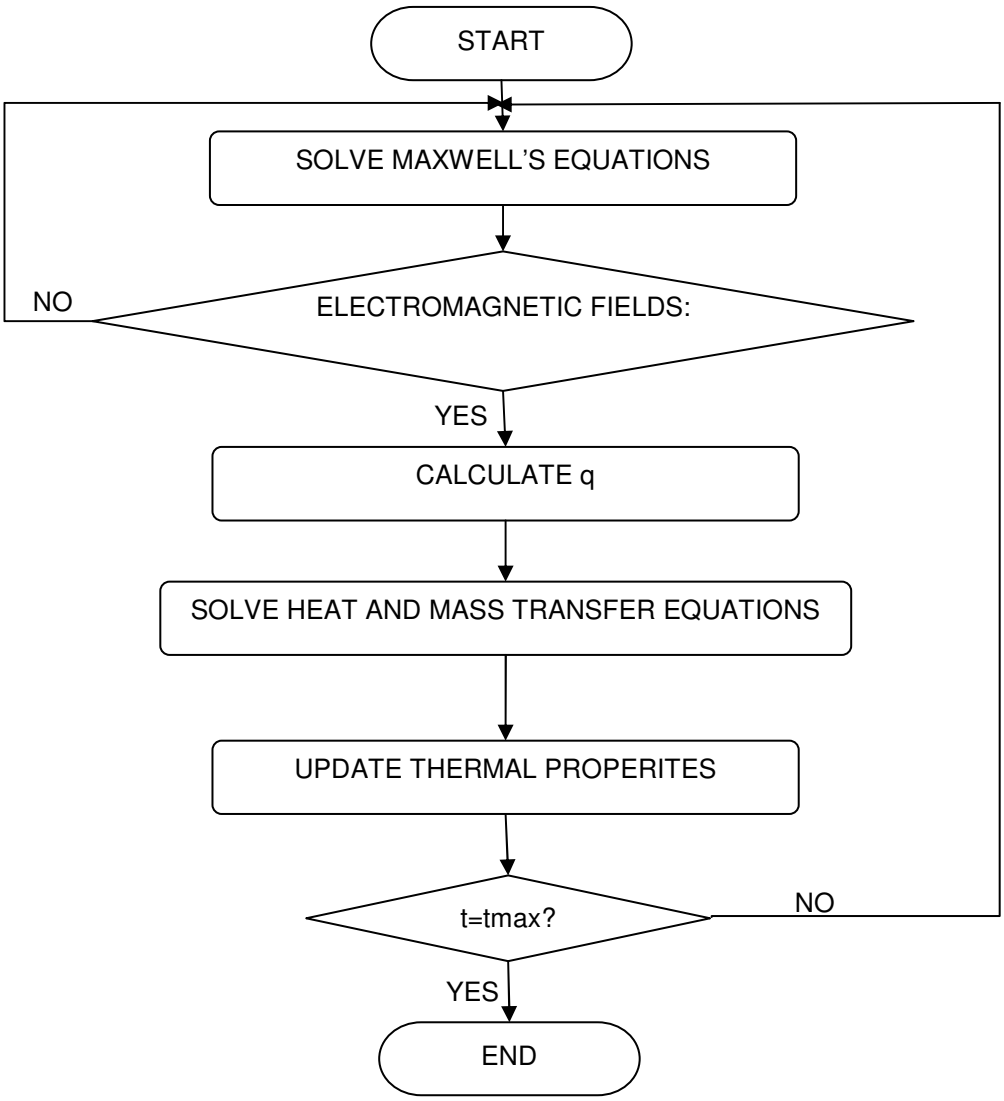

Figure 4.2 Computational algorithm.

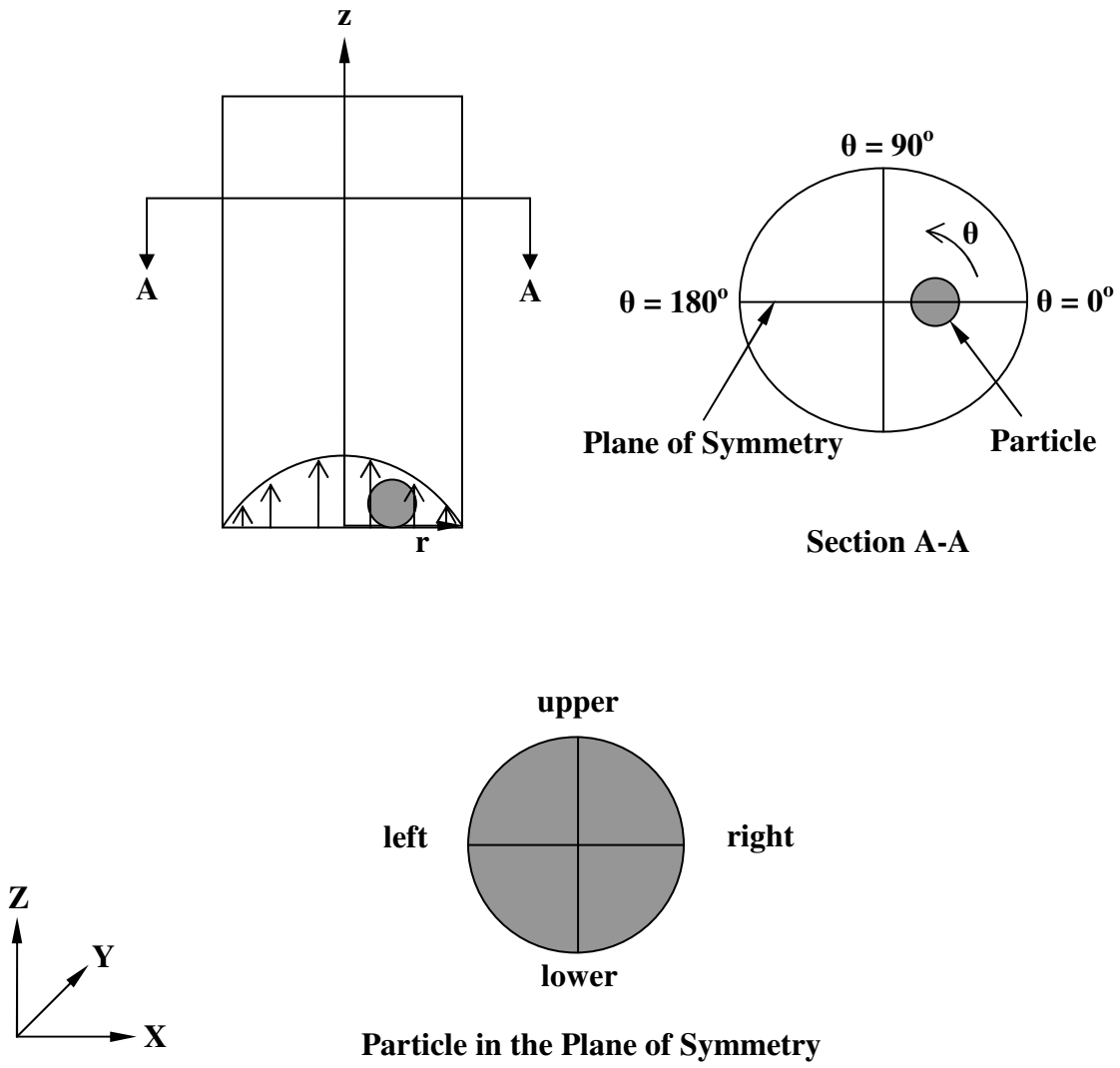

Figure 4.3 Basic arrangement for the particle inside the applicator.

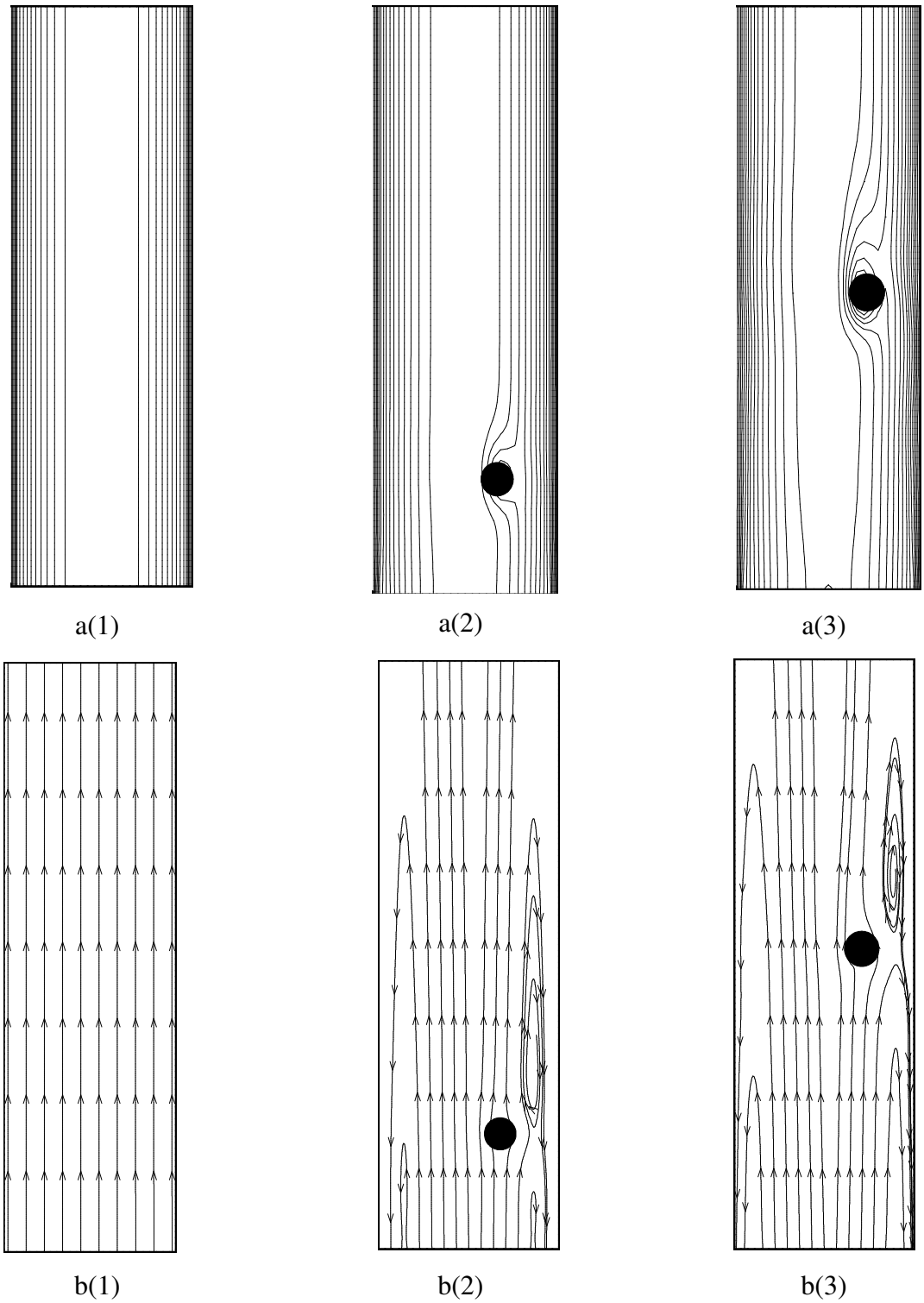

Figure 4.4 (a) Contour lines of the axial velocity of the fluid flow in the plane of symmetry of the applicator , and (b) streamlines in the plane of symmetry of the applicator: (1) before the particle entered the applicator; (2) $t = 0.2\ s$; (3) $t = 0.65\ s$.

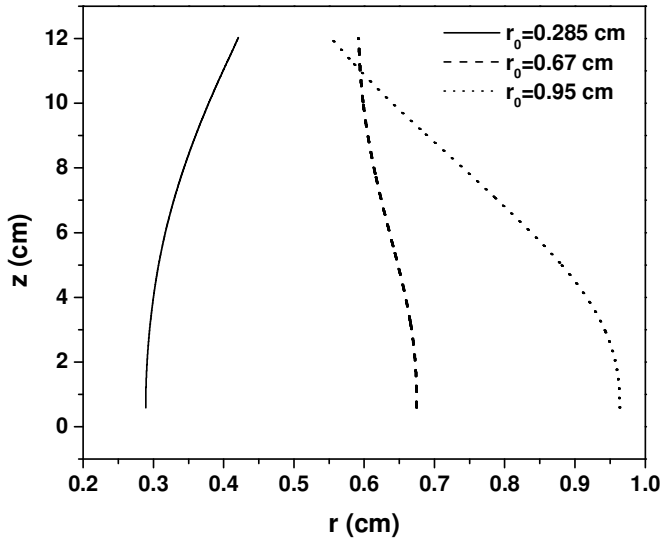

(a)

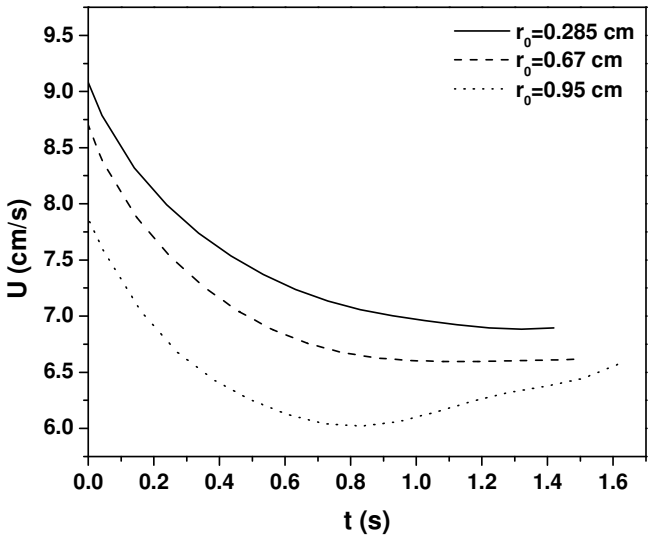

(b)

Figure 4.5 (a) Trajectory of the particle in the plane of symmetry; (b) streamwise velocity of the particle.

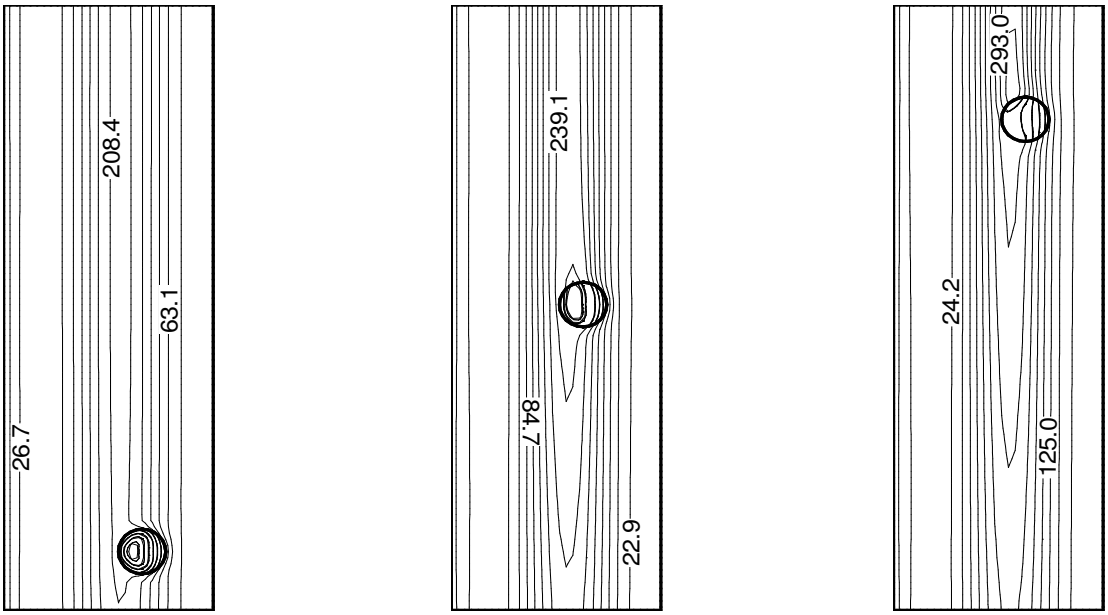

a(1) a(2) a(3)

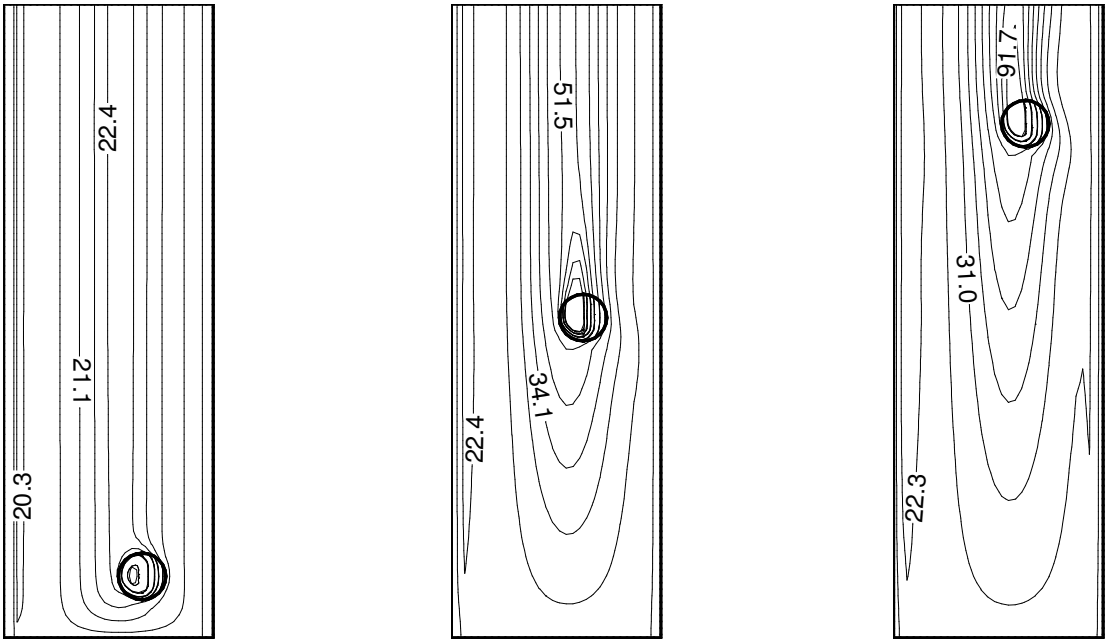

b(1) b(2) b(3)

Figure 4.6 (a) Power density distributions (W/cm^3) in the plane of symmetry of the applicator, and (b) temperature distributions (^oC) in the plane of symmetry of the applicator for: (1) t = 0.06 s; (2) t = 0.65 s; (3) t = 1.12 s.

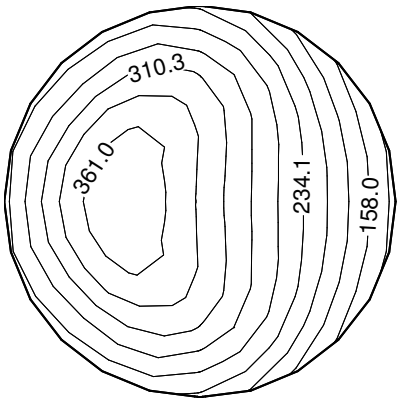

a(1)

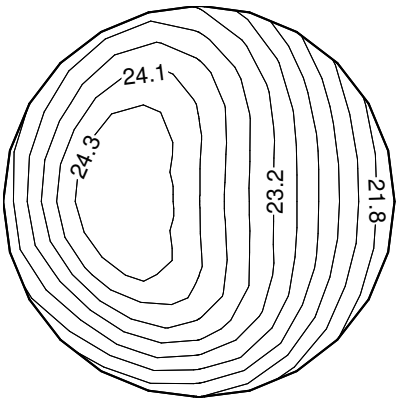

b(1)

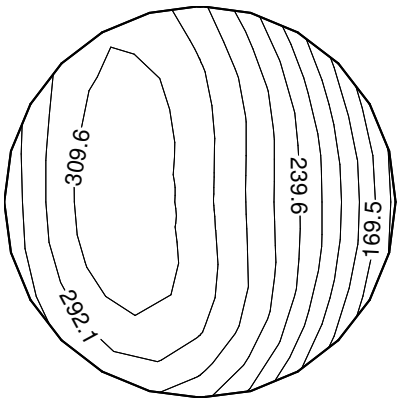

a(2)

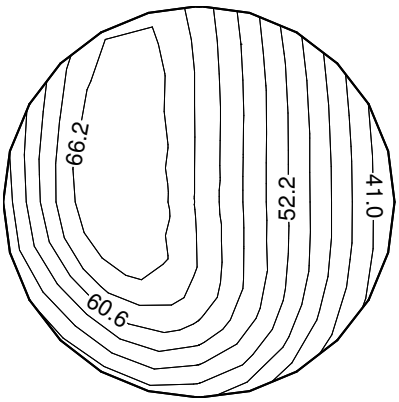

b(2)

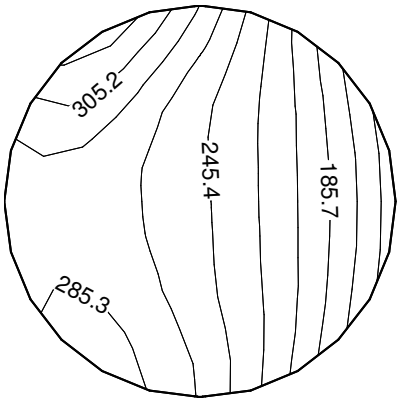

a(3)

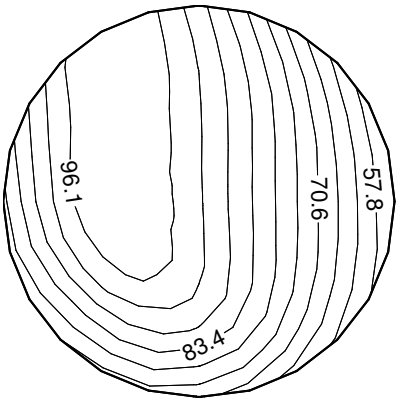

b(3)

Figure 4.7 (a) Power density distributions (W/cm^3) in the plane of symmetry of the particle, and (b) temperature distributions (^oC) in the plane of symmetry of the particle for: (1) $t = 0.06\ s$; (2) $t = 0.65\ s$; (3) $t = 1.12\ s$.

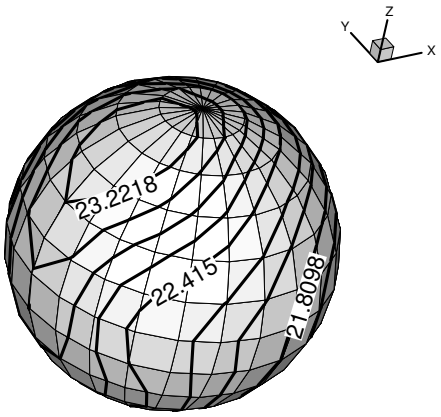

(a)

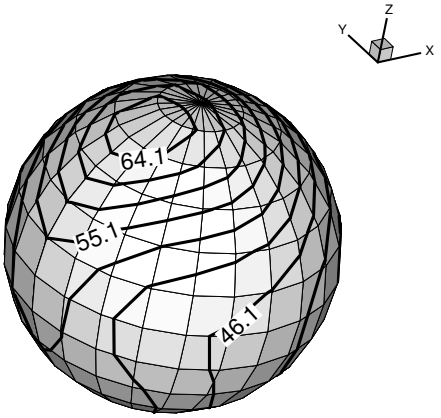

(b)

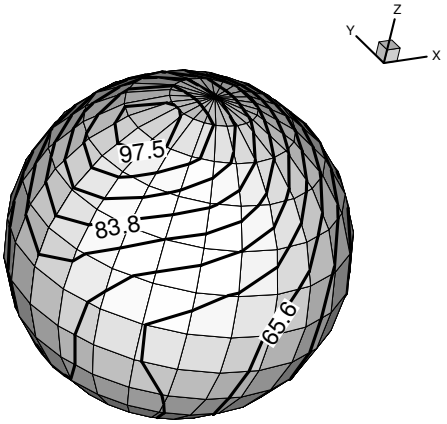

(c)

Figure 4.8 Surface temperature (^{o}C) of the particle for: (a) t = 0.06 s; (b) t = 0.65 s; (c) t = 1.12 s.

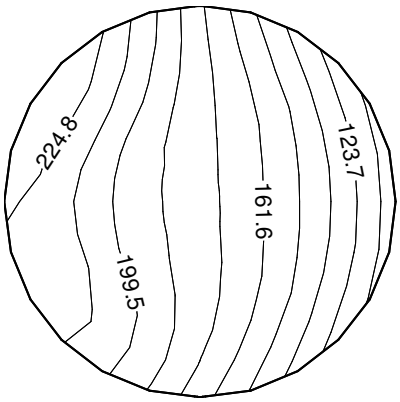

a(1)

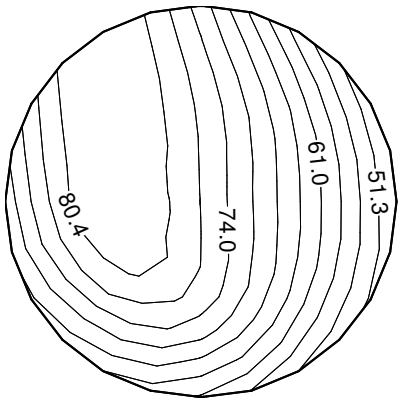

b(1)

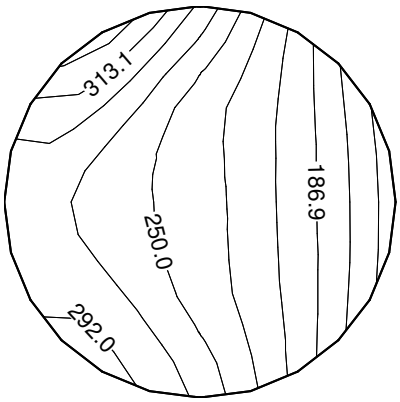

a(2)

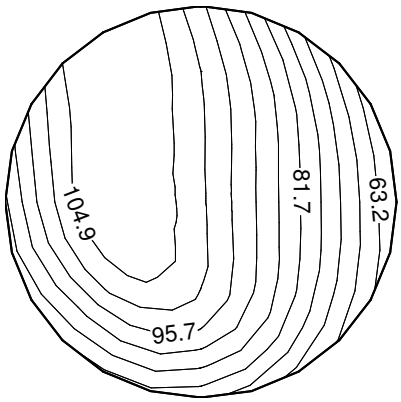

b(2)

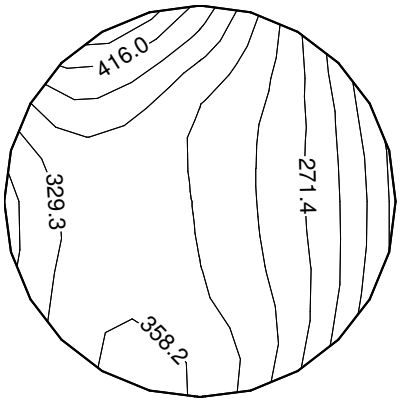

a(3)

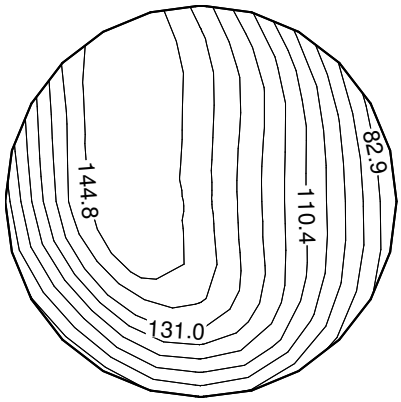

b(3)

Figure 4.9 (a) Power density distributions (W/cm^3) in the plane of symmetry of the particle, and (b) temperature distributions (^oC) in the plane of symmetry of the particle at t = 1.4 s in: (1) particle 1; (2) particle 2; (3) particle 3.

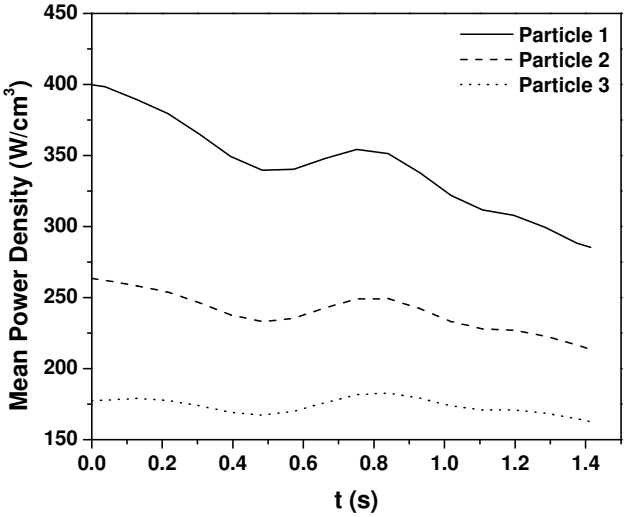

(a)

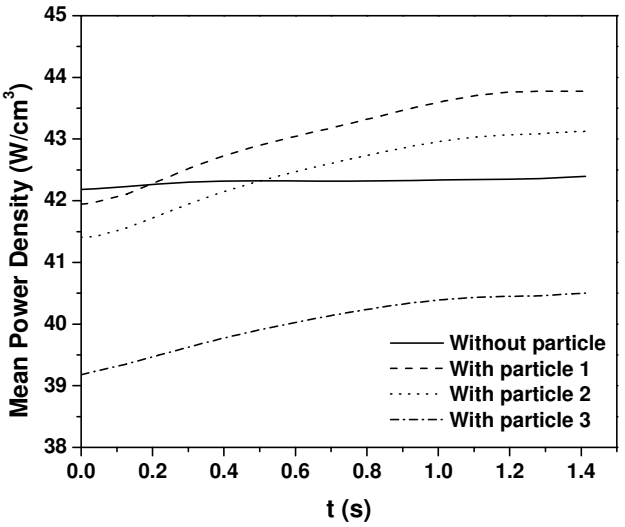

(b)

Figure 4.10 (a) Mean power density (W/cm^3) in the particle; (b) mean power density in the liquid.

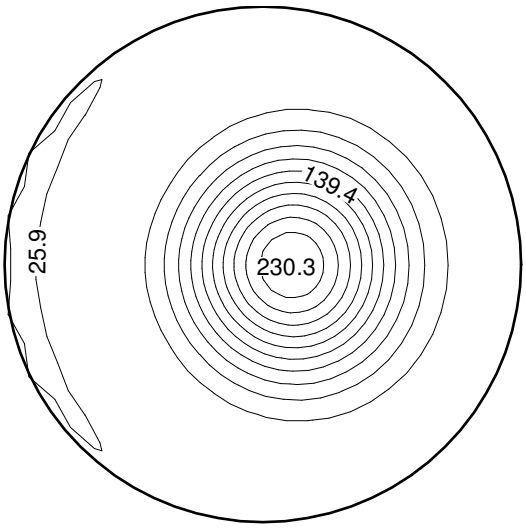

(a)

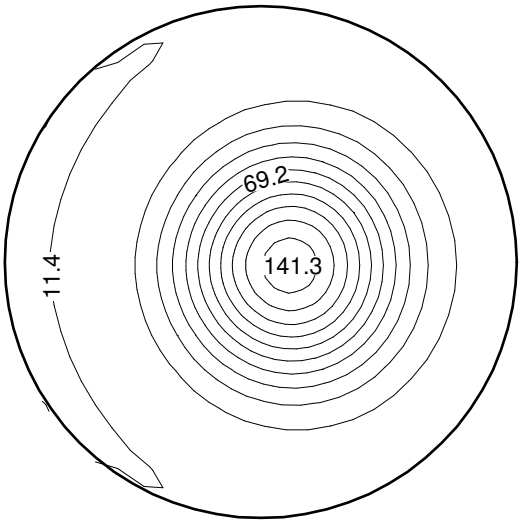

(b)

Figure 4.11 Power density distribution (W/cm^3) for: (a) liquid 1; (b) liquid 2.

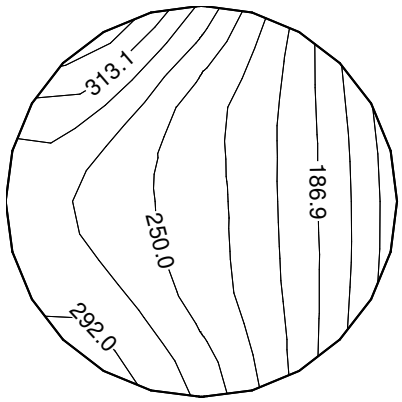

a(1)

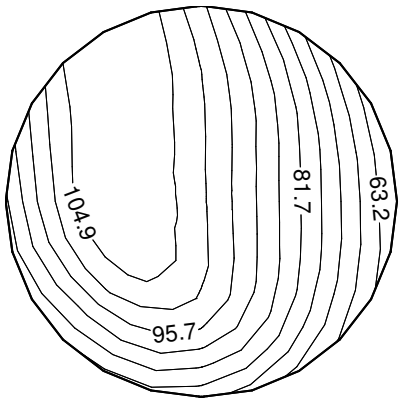

b(1)

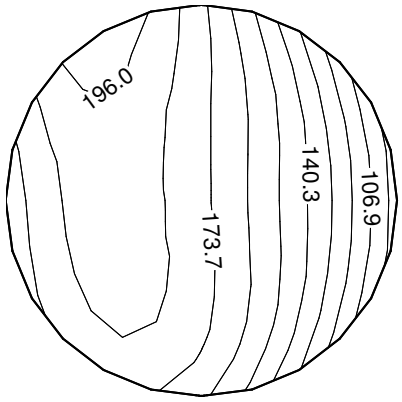

a(2)

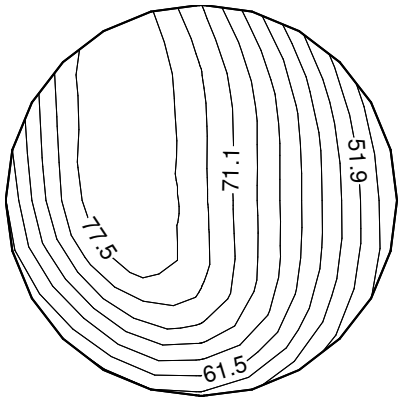

b(2)

Figure 4.12 (a) Power density distributions (W/cm^3) in the plane of symmetry of the particle, and (b) temperature distributions (^oC) in the plane of symmetry of the particle at t = 1.4 s with: (1) carrier liquid 1; (2) carrier liquid 2.

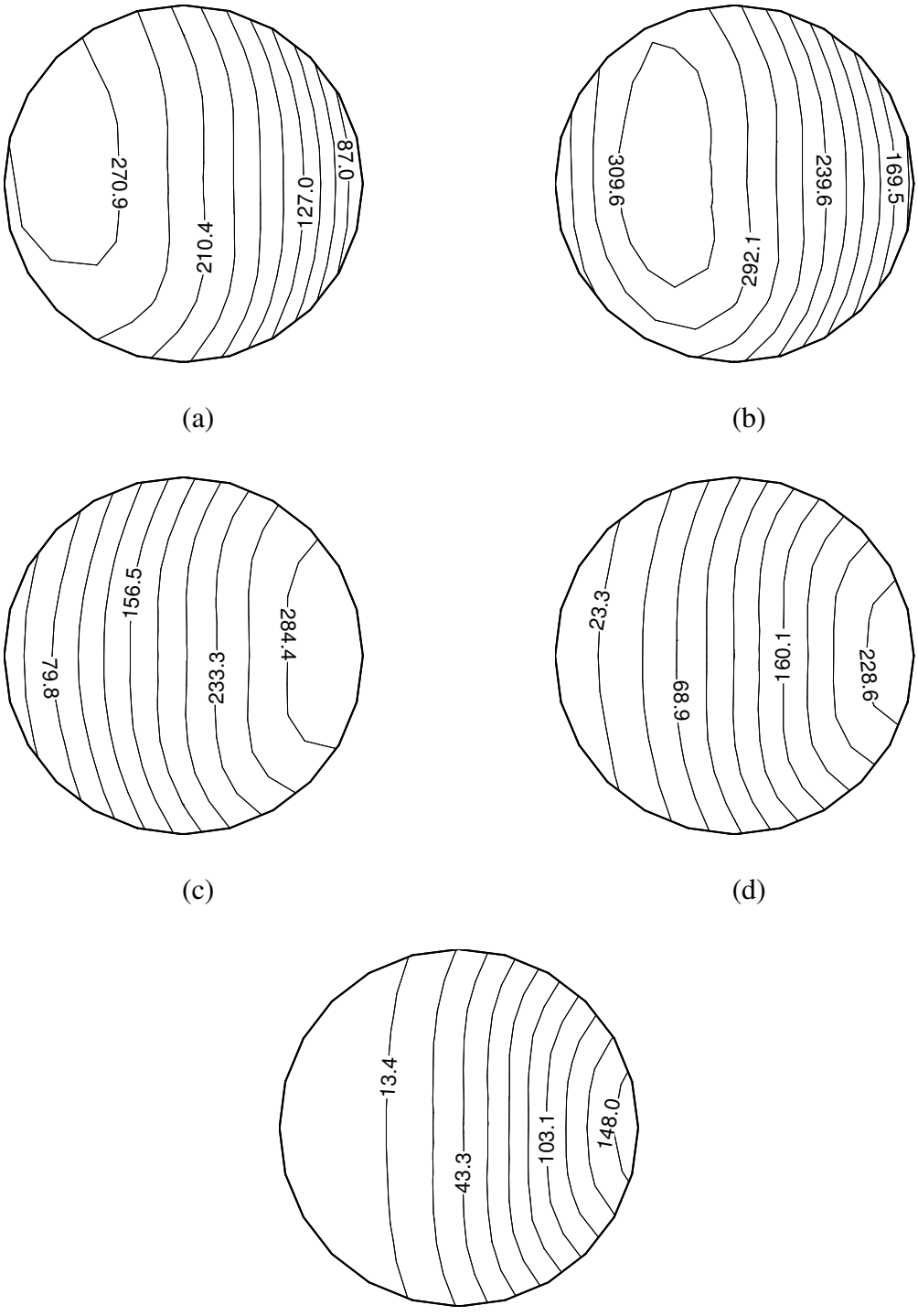

(a) (b) (c) (d) (e)

Figure 4.13 Power density distributions (W/cm^3) in the plane of symmetry of the particle with different initial positions of the particle: (a) $r = 0.95\ cm$ and $\theta = 0^\circ$; (b) $r = 0.67\ cm$ and $\theta = 0^\circ$; (c) $r = 0.28\ cm$ and $\theta = 180^\circ$; (d) $r = 0.67\ cm$ and $\theta = 180^\circ$; and (e) $r = 0.95\ cm$ and $\theta = 180^\circ$.

REFERENCES

1. Saltiel, C., Datta, A. (1997) Heat and mass transfer in microwave processing, *Adv. Heat Transfer*, 30: 1-94.
2. Ayappa, K.G., Brandon, S., et al. (1985) Microwave driven convection in a square cavity, *AIChE Journal*, 31: 842-848.
3. Franca, A.S., Haghighi, K. (1996) Adaptive finite element analysis of microwave driven convection, *International Communications in Heat and Mass Transfer*, 23: 177-186.
4. O'Brien, K.T., Mekkaoui, A.M. (1993) Numerical simulation of the thermal fields occurring in the treatment of malignant rumors by local hyperthermia, *Journal of Biomechanical Engineering*, 115: 247-253.
5. Ratanadecho, P., Aoki, K., Akahori, M. (2002) Influence of irradiation time, particle sizes, and initial moisture content during microwave drying of multi-layered capillary porous materials, *Journal of Heat Transfer*, 124: 151-161.
6. Ayappa, K.G., Davis, H.T., Davis, E.A., Gordon, J. (1991) Analysis of microwave heating of materials with temperature dependent properties, *AIChE Journal*, 37: 313-322.
7. Clemens, J., Saltiel, C. (1995) Numerical modeling of materials processing microwave furnaces, *International Journal of Heat and Mass Transfer*, 39: 1665-1675.
8. Basak, T., Ayappa, K.G., (2002) Role of length scales on microwave thawing dynamics in 2D cylinders, *International Journal of Heat and Mass Transfer*, 45: 4543-4559.

9. Barringer, S.A., Davis, E.A., et al. (1995) Microwave heating temperature profiles for thin slabs compared to Maxwell and Lambert law predictions, *Journal of Food Science*, 60: 1137-1142.

10. Aoki, K., Ratanadecho, P., Akahori, M. (2000) Characteristics of microwave heating for multi-layered materials using a rectangular wave guide, *Proceeding of the 4 th JSME-KSME Thermal Engineering Conference*, 2: 191-196.

11. Ratanadecho, P., Aoki, K., Akahori, M. (2002) A numerical and experimental investigation of the modeling of microwave heating for liquid layers using a rectangular wave guide (effects of natural convection and dielectric properties), *Applied Mathematical Modeling*, 26: 449-472.

12. Zhang, Q., Jackson, T.H., Ungan, A. (2000) Numerical modeling of microwave induced natural convection, *International Journal of Heat and Mass Transfer*, 43: 2141-2154.

13. Zhu, J., Kuznetsov, A.V., Sandeep, K.P. (2005) Mathematical modeling of continuous flow microwave heating of liquids (effects of dielectric properties and design parameters), *International Journal of Thermal Sciences*, In press.

14. Cheng, D. K. (1992) *Field and Wave Electromagnetics*, Addison-Wesley, New York.

15. Balanis, C.A. (1996) *Advanced Engineering Electromagnetics*, Wiley, New York.

16. Mur, G. (1981) Absorbing boundary conditions for the finite difference approximation of the time domain electromagnetic field equations, *IEEE Trans. Electromag. Compat.*, EMC-23, No. 4: 377-382.

17. Dance, S.L., Maxey, M.R. (2003) Force-coupling method for particulate two-phase flow: Stokes flow, *Journal of Computational Physics*, 184: 381-405.

18. Lomholt, S., Stenum, B., Maxey, M.R. (2002) Experimental verification of the force coupling method for particulate flows, *International Journal of Multiphase Flow*, 28: 225-246.

19. Dance, S.L., Maxey, M.R. (2003) Incorporation of lubrication effects into the force-coupling method for particulate two-phase flow, *Journal of Computational Physics*, 189: 212-238.

20. Maxey, M.R., Patel, B.K. (2001) Localized force representations for particles sedimenting in Stokes flow, *International Journal of Multiphase Flow*, 27: 1603-1626.

21. Kunz, K.S., Luebbers, R. (1993) *The Finite Difference Time Domain Method for Electromagnetics*, CRC, Boca Raton, FL.

22. Dey, S., Raj Mittra (1999) A conformal finite-difference time-domain technique for modeling cylindrical dielectric resonators, *IEEE Transactions on Microwave Theory and Techniques*, 47: 1737-1739.

23. Patankar, S.V., Spalding, D.B. (1972) A calculation procedure for heat, mass and momentum transfer in three-dimensional parabolic flows, *Journal of Heat and Mass Transfer*, 15: 1787-1806.

24. Olivera, M.E.C., Franca, A.S. (2002) Microwave heating of foodstuff, *Journal of food Engineering*, 53: 347-359.

5 INVESTIGATION OF A PARTICULATE FLOW SUBJECTED TO MICROWAVE HEATING

ABSTRACT

In this chapter, microwave heating of a liquid and large particles that it carries while continuously flowing in a circular applicator pipe is investigated. A three-dimensional model that includes coupled Maxwell, continuity, Navier-Stokes, and energy equations is developed to describe transient temperature, electromagnetic, and fluid velocity fields. The hydrodynamic interaction between the solid particles and the carrier liquid is simulated by the force-coupling method (FCM). Computational results are presented for the microwave power absorption, temperature distribution inside the liquid and the particles, as well as the velocity distribution in the applicator pipe and trajectories of particles. The effect of the time interval between consecutive injections of two groups of particles on power absorption in particles is studied. The influence of the position of the applicator pipe in the microwave cavity on the power absorption and temperature distribution inside the liquid and the particles is investigated as well.

Nomenclature

A	area, m^2
a_p	particle radius, m
C_p	specific heat capacity, $J/(kg \cdot K)$
c	phase velocity of the electromagnetic propagation wave, m/s
$\mathbf{E}$	electric field intensity, V/m
f	frequency of the incident wave, Hz

$\mathbf{f}$ body force, N

$\mathbf{F}$ force monopole, N

$\mathbf{F}^{ext}$ external force, N

$\mathbf{g}$ gravity, m/s^2

h effective heat transfer coefficient, $W/(m^2 \cdot K)$

$\mathbf{H}$ magnetic field intensity, A/m

k thermal conductivity, $W/(m \cdot K)$

m fluid consistency coefficient, $Pa\ s^n$

n flow behavior index

N number of time steps

p pressure, Pa

P microwave power, W

q microwave power density, W/m^3

T temperature, ^oC

t time, s

$\tan\delta$ loss tangent

$\mathbf{u}$ fluid velocity vector, m/s

$\mathbf{V}$ velocity of the particle center, m/s

Z_{TE} wave impedance, Ω

Greek symbols

η apparent viscosity, $Pa \cdot s$

ε electric permittivity, F/m

ε_r'	relative permittivity
ε_r''	relative loss factor
ε_{rad}	emissivity
λ_g	electromagnetic wavelength in the cavity, m
μ	magnetic permeability, H/m
ρ	density, kg/m^3
$\mathbf{\Omega}$	angular velocity, 1/s
σ_e	electric conductivity, S/m
σ_{rad}	Stefan-Boltzmann constant, W/(m^2 K^4)
σ, σ'	length scale, m
$\boldsymbol{\omega}$	vorticity, 1/s

Subscripts

∞	ambient
a	free space, air
0	initial condition
in	input (at the incident plane)
l	liquid
p	particle
n	normal
t	tangential
X,Y,Z	projection on a respective coordinate axis

5.1 INTRODUCTION

Microwave technology has been utilized in a wide range of industrial applications for decades. This technology has been extensively used in chemical engineering and food processing industries. Microwave heating of food is one of the most energy efficient methods of food processing; it can be employed for thawing, drying, cooking, baking, tempering, pasteurization, and sterilization of different kinds of foods. Unlike the traditional heating techniques, where heat is transferred from a surface to the interior, microwave technology makes it possible to heat the bulk of the material without any intermediate heat transfer medium. This results in a high energy efficiency and reduction in heating time. Extensive investigations devoted to modeling of microwave heating are reported in [1-5].

In order to determine temperature increase in a fluid passing in an applicator tube through a microwave cavity it is necessary to solve the energy equation with an electromagnetic heat generation term which describes microwave power absorption in the material. The power absorption can be evaluated by two methods, using the Lambert's law or by directly solving Maxwell's equations. Lambert's law has been extensively used in literature [6-9], it works the best when the heated sample is large. According to Lambert's law, microwave power absorption decays exponentially from the surface into the material. In order to use Lambert's law it is necessary to evaluate experimentally the amount of microwave radiation transmitted to the surface of the material. In small size samples, heat is generated by the resonance of standing waves, which Lambert's law cannot adequately describe [10-11], so the solution of Maxwell's equations is needed to

accurately determine the electromagnetic heat generation term. Modeling of microwave heating based on numerical solutions of Maxwell's equations is reported in [12-15].

Continuous processing of food is a promising alternative to traditional heating of liquid food in containers. During this process, liquid food flows in an applicator tube. When flow passes through the microwave cavity, the liquid absorbs microwave power and its temperature quickly increases. Compared to investigation of microwave heating of solid materials, the analysis of microwave heating of liquids is more challenging due to the presence of fluid motion. Research devoted to microwave heating of liquids is reported in [7, 8, 16, 17].

Modeling of microwave heating of liquids usually requires solving a complete set of momentum, energy, and Maxwell's equations to describe complex interactions of flow, temperature, and microwave fields as a liquid passes through the applicator [16,17]. Our previous work investigated continuous microwave heating of a single phase liquid flow in the applicator [18,19] and the case of a liquid carrying a single large solid particle, which represented a typical food particle with a diameter of 0.9 *cm* [20]. In this chapter, a three-dimensional model of microwave heating of a liquid carrying multiple large particles as it flows in the applicator subjected to microwave irradiation is proposed. The power absorption and temperature distributions in both the liquid and particles are investigated.

5.2 MODEL GEOMETRY

Figure 5.1(a) shows the schematic diagram of the continuous microwave heating system investigated in this research. The system consists of a waveguide, a resonant

cavity, and a vertically positioned applicator tube that passes through the cavity. A liquid food, which is treated as a non-Newtonian fluid, carrying multiple solid food particles flows through the applicator tube in the upward direction, absorbing microwave energy as it passes through the tube. The microwave operates in the TE_{10} [21] mode at a frequency of 915 *MHz* with the input power of 7 *kW*. The microwave power is transmitted through the waveguide and directed on the applicator tube located in the center of the resonant cavity. Parameters characterizing the geometry of the microwave system are listed in Table 5.1.

5.3 MATHEMATICAL MODEL

Two computational domains are utilized, as shown in Figure 5.1(a). The first domain, including the region enclosed by the walls of the waveguide, resonant cavity, and incident plane, is used for computing the electromagnetic field. The origin of the coordinate system of the first domain lies in the absorbing plane. The second domain, coinciding with the region inside the applicator tube, is used for solving the momentum and energy equations. The origin of the coordinate system of the second domain is in the center of the tube at the applicator inlet. A simulation begins when the first particle enters the applicator and ends when the last particle leaves the applicator.

5.3.1 MICROWAVE IRRADIATION

The electromagnetic field in the first domain is governed by Maxwell's equations, which are presented in terms of the electric field, **E**, and the magnetic field, **H** [21]:

$$\varepsilon \frac{\partial \mathbf{E}}{\partial t} = \nabla \times \mathbf{H} - \sigma_e \mathbf{E} \tag{5.1}$$

$$\mu \frac{\partial \mathbf{H}}{\partial t} = -\nabla \times \mathbf{E} \tag{5.2}$$

$$\nabla \cdot (\varepsilon \mathbf{E}) = 0 \tag{5.3}$$

$$\nabla \cdot \mathbf{H} = 0 \tag{5.4}$$

where μ is the magnetic permeability and $\varepsilon = \varepsilon_a \varepsilon_r'$ is the electric permittivity (ε_a is the permittivity of the free space and ε_r' is the relative permittivity of the material). σ_e stands for the electric conductivity related to the loss tangent $\tan\delta$ by:

$$\sigma_e = 2\pi f \varepsilon \tan\delta \tag{5.5}$$

where

$$\tan\delta = \frac{\varepsilon_r''}{\varepsilon_r'} \tag{5.6}$$

In Eq. (5.6), ε_r'' stands for the relative loss factor.

At the inner walls of the waveguide and cavity, a perfect conducting condition is utilized. Therefore, normal components of the magnetic field and tangential components of the electric field vanish at these walls:

$$H_n = 0, \quad E_t = 0 \tag{5.7}$$

At the absorbing plane, Mur's first order absorbing condition [22] is utilized:

$$\left(\frac{\partial}{\partial Z}-\frac{1}{c}\frac{\partial}{\partial t}\right)E_Z\big|_{X=0}=0 \tag{5.8}$$

where c is the phase velocity of the propagation wave.

At the incident plane, the microwave source is simulated by the following equations:

$$E_{Z,inc}=-E_{Zin}\sin\left(\frac{\pi Y}{W}\right)\cos\left[2\pi\left(ft-\frac{X_{in}}{\lambda_g}\right)\right] \tag{5.9}$$

$$H_{Y,inc}=\frac{E_{Zin}}{Z_{TE}}\sin\left(\frac{\pi Y}{W}\right)\cos\left[2\pi\left(ft-\frac{X_{in}}{\lambda_g}\right)\right] \tag{5.10}$$

where W is the width of the incident plane, f is the frequency of the microwave, Z_{TE} is the wave impedance, X_{in} is the X-position of the incident plane, λ_g is the wave length of a microwave in the waveguide, and E_{Zin} is the input value of the electric field intensity. According to the Poynting theorem [17], the input value of the electric field intensity is evaluated by the microwave power input as:

$$E_{Zin}=\sqrt{\frac{4Z_{TE}P_{in}}{A}} \tag{5.11}$$

where P_{in} is the microwave power input and A is the area of the incident plane.

At $t=0$, all components of **E** and **H** are zero.

5.3.2 HEAT TRANSFER

The temperature distributions in the particles and carrier liquid are obtained by the solution of the following energy equations.

In the particles the energy equation is:

$$\rho_p C_{pp} \frac{\partial T_p}{\partial t} = \nabla \cdot \left(k_p \nabla T_p \right) + q_p(\mathbf{x}, t) \tag{5.12}$$

In the liquid the energy equation is:

$$\rho_l C_{pl} \left(\frac{\partial T_l}{\partial t} + \mathbf{u} \cdot \nabla T_l \right) = \nabla \cdot \left(k_l \nabla T_l \right) + q_l(\mathbf{x}, t) \tag{5.13}$$

where ρ is the density, k is the thermal conductivity, C_p is the specific heat, T is the temperature, and q is the microwave power density:

$$q = 2\pi f \varepsilon_0 \varepsilon_r' (\tan \delta) \mathbf{E}^2 \tag{5.14}$$

The applicator wall is assumed to lose heat by natural convection and thermal radiation:

$$-k \left. \frac{\partial T}{\partial n} \right|_{surface} = h\left(T - T_\infty\right) + \sigma_{rad} \varepsilon_{rad} \left(T^4 - T_\infty^4\right) \tag{5.15}$$

where T_∞ is the ambient air temperature (the waveguide walls are assumed to be in thermal equilibrium with the ambient air), h is the effective convection coefficient that incorporates thermal resistance of the applicator wall, ε_{rad} is the surface emissivity, and σ_{rad} is the Stefan-Boltzmann constant.

The thermal boundary condition at the surface of the particle is:

$$k_p \left. \frac{\partial T}{\partial n} \right|_{r=a_p-0} = k_l \left. \frac{\partial T}{\partial n} \right|_{r=a_p+0} \quad \text{and} \quad T_{r=a_p+0} = T_{r=a_p-0} \tag{5.16}$$

Initially the particles and the liquid are assumed to be in thermal equilibrium, so

$$T_p = T_0 \quad \text{and} \quad T_l = T_0 \tag{5.17}$$

The inlet liquid temperature is assumed to be uniform and equal to the temperature in the free space outside the applicator, T_∞.

5.3.3 HYDRODYNAMICS

The fluid velocity field $\mathbf{u}(\mathbf{x},t)$ satisfies the Navier-Stokes equations:

$$\nabla \cdot \mathbf{u} = 0 \tag{5.18}$$

$$\rho_l \left(\frac{\partial \mathbf{u}}{\partial t} + \mathbf{u} \cdot \nabla \mathbf{u} \right) = -\nabla p + \nabla \cdot \eta \nabla \mathbf{u} + \rho_l \mathbf{g} + \mathbf{f}(\mathbf{x},t) \tag{5.19}$$

where η is the apparent viscosity of the non-Newtonian liquid, which in this chapter is assumed to obey the power-law:

$$\eta = m\left(\dot{\gamma}\right)^{n-1} \tag{5.20}$$

where m and n are the fluid consistency coefficient and the flow behavior index, respectively.

The effect of particles on the fluid is represented by a localized body force $\mathbf{f}(\mathbf{x},t)$ that transmits to the fluid the resultant force that particles impose on the flow [23]. In this chapter, a force-coupling method (FCM) developed by M.R. Maxey and his group in [23-26] is utilized to simulate this momentum source term $\mathbf{f}(\mathbf{x},t)$.

According to FCM, the body force $\mathbf{f}(\mathbf{x},t)$ is computed as

$$\mathbf{f}(\mathbf{x},t) = \sum_{n=1}^{N} \left[\mathbf{F}^{(n)} \Delta\left(\mathbf{x} - \mathbf{Y}^{(n)}, \sigma\right) \right] \tag{5.21}$$

where $\mathbf{Y}^{(n)}$ is the position of the *n*th particle and $\mathbf{F}^{(n)}$ is the force monopole representing the hydrodynamic drag on the *n*th particle. The localized force distribution for the particles is determined by the Gaussian function,

$$\Delta(\mathbf{x}) = \left(2\pi\sigma^2\right)^{-3/2} \exp\left(-\mathbf{x}^2 / 2\sigma^2\right) \tag{5.22}$$

and the length scale σ is related to the radius of the particle, a_p, as

$$\sigma = \frac{a_p}{\sqrt{\pi}} \tag{5.23}$$

The force monopole is determined by the sum of the external force $\mathbf{F}^{(n)ext}$ acting on the particle and the inertia of the particle:

$$\mathbf{F}^{(n)} = \mathbf{F}^{(n)ext} - (4/3)\pi {a_p}^3 (\rho_p^{(n)} - \rho_l) \frac{d\mathbf{V}^{(n)}}{dt} \tag{5.24}$$

where the only external force $\mathbf{F}^{(n)ext}$ acting on the suspending particles is the buoyancy force:

$$F_b = (4/3)\pi {a_p}^3 (\rho_l - \rho_p)\mathbf{g} \tag{5.25}$$

The velocity of the particle, $\mathbf{V}$, can be determined by a local average of the fluid velocity over the region occupied by the particle:

$$\mathbf{V}^{(n)}(t) = \int \mathbf{u}(\mathbf{x},t)\Delta(\mathbf{x} - \mathbf{Y}^{(n)}, \sigma) d^3\mathbf{x} \tag{5.26}$$

The angular velocity of the particle, $\mathbf{\Omega}$, is calculated as

$$\mathbf{\Omega}^{(n)}(t) = \frac{1}{2}\int \boldsymbol{\omega}(\mathbf{x},t)\Delta(\mathbf{x} - \mathbf{Y}^{(n)}, \sigma') d^3\mathbf{x} \tag{5.27}$$

where $\boldsymbol{\omega}$ is the vorticity and the length scale σ' is

$$\sigma' = \frac{a_p}{\left(6\sqrt{\pi}\right)^{1/3}} \tag{5.28}$$

In addition, to prevent particles from overlapping each other domains or penetrating into the wall, an additional inter-particle and particle-wall repulsive force $\mathbf{F}'$ [27] is added to the force $\mathbf{F}$ for each particle:

$$\mathbf{F}'^{(n)} = \sum_{\substack{n=1 \\ m \neq n}}^{N} \mathbf{F}^{P(n,m)} + \mathbf{F}^{W(n)} \tag{5.29}$$

In Eq. (5.29) $\mathbf{F}^{P(n,m)}$ represents the force exerted on the *n*th particle by the *m*th particle,

$$\mathbf{F}^{P(n,m)} = \begin{cases} 0, & d^{(n,m)} \geq a_p^{(n)} + a_p^{(m)} + \delta, \\ \dfrac{1}{\varepsilon_P}\left(\mathbf{Y}^{(n)} - \mathbf{Y}^{(m)}\right)\left(a_p{}^{(n)} + a_p{}^{(m)} + \delta - d^{(n,m)}\right)^2, & d^{(n,m)} \leq a_p^{(n)} + a_p^{(m)} + \delta, \end{cases} \tag{5.30}$$

where $d^{(n,m)} = \left|\mathbf{Y}^{(n)} - \mathbf{Y}^{(m)}\right|$ is the distance between the centers of the *n*th and *m*th particles, and ε_P is a small positive stiffness parameter. In Eq. (5.30), δ is the force range, the distance between the surfaces of two particles at which the contact force is activated; and δ is set to one mesh size in this chapter. The particle-wall force $\mathbf{F}^{W(n)}$ is modeled as the force between a particle and the imaginary particle located on the other side of the wall Γ (see Figure 5.2):

$$\mathbf{F}^{W(n)} = \begin{cases} 0, & d^{(n)'} \geq 2a_p^{(n)} + \delta \\ \dfrac{1}{\varepsilon_W}\left(\mathbf{Y}^{(n)} - \mathbf{Y}^{(n)'}\right)\left(2a_p{}^{(n)} + \delta - d^{(n)'}\right)^2, & d^{(n)'} \leq 2a_p^{(n)} + \delta \end{cases} \tag{5.31}$$

where $d^{(n)'} = \left| \mathbf{Y}^{(n)} - \mathbf{Y}^{(n)'} \right|$ is the distance between the centers of the nth particle and the center of its mirror image, $\mathbf{Y}^{(n)'}$ is the position of the imaginary particle, and ε_w is the second stiffness parameter. The stiffness parameters are taken as $\varepsilon_p = 8.15 \times 10^{-5}$ m^3 N^{-1} and $\varepsilon_w = \varepsilon_p / 2$.

A hydrodynamic no-slip boundary condition is used at the inner surface of the applicator tube. At the inlet to the applicator a uniform, fully developed velocity profile is imposed, and specified by the inlet mean velocity, U_{mean}. The flow in the applicator is assumed to be hydrodynamically fully developed at $t = 0$. The inlet velocity of the particle is calculated as a volume average of the fluid velocity in the volume occupied by the particle, as stated by Eq. (5.26).

5.4 NUMERICAL PROCEDURE

Maxwell's equations (5.1)-(5.4) are solved by the FDTD method [28]. A non-uniform structured mesh consisting of 1,236,000 cells in the electromagnetic domain is utilized. The time step for the electromagnetic solver obeys the stability condition [28]:

$$\Delta t \leq \frac{1}{c\sqrt{\frac{1}{\Delta X^2} + \frac{1}{\Delta Y^2} + \frac{1}{\Delta Z^2}}} \tag{5.32}$$

An implicit time-integration scheme and the time marching procedure [29] are adopted to solve the continuity and momentum equations (5.18) and (5.19). At each time step, the continuity and momentum equations for the fluid phase are first solved in the

absence of particles. The continuity and momentum equations are then solved again with the particles' source term. This procedure is repeated until convergence.

Energy equations (5.12) and (5.13) are discretized using a cell-centered finite volume approach and solved implicitly in the Cartesian coordinate system. The two energy equations are coupled by the boundary condition given by Eq. (5.16). At each time step, Eqs. (5.12) and (5.13) are solved iteratively until boundary condition (5.16) is satisfied. The rotation of the particles is taken into account by rotating the temperature field in each particle at every time step. Since microwave propagation is much faster than heat and mass transfer, different time steps of $\Delta t_1 = 1\ ps$ and $\Delta t_2 = 0.4\ ms$ are used for solving Maxwell's equations and heat and mass transfer equations, respectively.

5.5 CODE VALIDATION

The validation of the computer code developed for this chapter consists of two sections: 1) validation of the hydrodynamic solver; and 2) validation of the electromagnetic solver.

To validate the hydrodynamic solution in the applicator pipe a well-known case of a spherical particle positioned in the center of a pipe is tested and the results are compared to published data. The test is performed for the following geometry. The diameter ratio of the particle and pipe is 0.1. The length of the pipe is twice its diameter. A hydrodynamic fully developed velocity profile is imposed at the inlet. With this geometry, the flow is closely approximated by an externally unbounded uniform flow past a sphere. The drag coefficient on a sphere, C_D, defined by

$$C_D = \frac{F_D}{1/2\rho U_\infty A_s} \tag{5.33}$$

where F_D is the drag force, U_∞ is the mean flow velocity at the pipe entrance, A_s is the projection area of a sphere, πa_p^2, is computed and compared with published data [30] for two particle Reynolds number, $\mathrm{Re}_p = 10$ and $\mathrm{Re}_p = 100$. The particle Reynolds number is defined by

$$\mathrm{Re}_p = \frac{2U_\infty a_p}{\nu} \tag{5.34}$$

The algorithm for calculating the drag coefficient with the FCM method is described in [25]. Table 5.2 shows a comparison between predictions of the code and results published in [30]. The agreement in the value of the drag coefficient between published and computed results is within five percent.

The electromagnetic field in an empty rectangular waveguide is simulated to test the code's electromagnetic solver. The calculated results are compared with the analytical solution [21]. The waveguide is 30.5 *cm* in width (*x*-direction), 12.4 *cm* in height (*y*-direction) and 116.7 *cm* in length (*z*-direction). The microwave is excited in the TE_{10} mode [21] at a frequency of 915 *MHz*. Figure 5.3 provides a comparison of the numerical and analytical values of the *E* and *H* field components. Numerical results are in excellent agreement with the analytical solution.

5.6 RESULTS AND DISCUSSIONS

Table 5.3 summarizes the dielectric and thermal properties of the particles and the carrier liquid considered in this chapter. The particles are spherical with a diameter of 0.9 *cm*. The flow in the applicator pipe is assumed to be initially hydrodynamically fully developed with a mean velocity of 6.0 *cm/s*. At $t = 0$, the particles are suddenly released at the inlet of the applicator. This makes the flow unsteady. The particles are released into the liquid periodically. During each period only one group of four particles is released. Total of twenty particles enter the applicator in five groups for each computed case. In each group, the four particles are released at different angular positions of $\theta = 0^{\circ}$, $\theta = 90^{\circ}$, $\theta = 180^{\circ}$, and $\theta = 270^{\circ}$ respectively, and at the same radial position of $r = 0.67cm$. The inlet positions of the particles are illustrated in Figure 5.1(b), where positions I, II, III, and IV correspond to the inlet positions of four particles in each group (e.g. the third particle in the second group is particle # 7 ($4 \times 2 - 1 = 7$), and its inlet position is III).

A $t = 0$, the microwave energy is turned on. The initial temperature of the liquid, T_{l0}, and the temperature in the free space outside the applicator, T_{∞}, are both set to $20\,^{\circ}C$. The temperature of the particles at the moment when they enter the applicator, T_{p0}, is set to $20\,^{\circ}C$ as well. It is assumed that there is no phase change in either the particles or the carrier liquid during the heating process.

5.6.1 HYDRODYNAMIC FIELD

In this chapter, five groups of particles are released into the liquid periodically. Two cases, A and B, are simulated. The time interval between releasing two groups of

particles is 0.15 *s* for case A and 0.25 *s* for case B. The fluid flow in the applicator is initially fully developed, and then it changes because of the influence of the particles entering the applicator.

The flow field for case A is shown in Figure 4, where the velocity contour lines of the fluid axial velocity are given in $\theta = 0^{\circ}$ and 180° planes. It is evident that the particles do not greatly modify the fully developed velocity profile in the beginning. This is because at the inlet the particle velocity is set to the average fluid velocity in the volume occupied by the particle, so the particle does not initially move relative to the fluid. As time progresses, the velocity of particles decreases due to the larger density of particles than that of the liquid, which increases the velocity difference between the particles and the liquid.

From Figure 5.4, it is evident that the distance between the first and second groups of particles is the largest and the distance between groups of particles gets smaller with every new group entering the applicator. The particles' velocity is smaller than the velocity of the surrounding liquid, and the hydrodynamic wake is located downstream each particle. The particles released earlier experience a reduced drag force because they are in the hydrodynamic wakes of the particles released later (the particles released later shield particles released earlier from a fluid drag). This results in the particles released earlier having smaller streamwise velocity than the particles released later. This leads to collisions between particles. It is evident (see Figure 5.4, t = 2.12) that the fully developed velocity profile is greatly distorted downstream the particles after particles' collisions. This is because particles are more spread out after collisions. It is also found that after a collision the positions of particles and the velocity field are not axisymmetric.

This is because the outcome of a collision of two particles is sensitive to the velocities and positions of the particles, and small disturbances (naturally modeled by numerical errors) result in different separation velocities and paths of the particles.

It is found that there are no collisions between particles in case B. This can be attributed to the longer time interval between releasing groups of particles in case B, which enlarges the initial distance between each group of particles. A comparison of the residence time of each particle for cases A and B is shown in Figure 5.5. It is evident that the residence time distribution is more scattered in case A than in case B, which is due to the influence of particle collisions.

5.6.2 ELECTROMAGNETIC FIELD AND HEAT TRANSFER

Transient distributions of the microwave power density and temperature inside the applicator for case A are shown in Figure 5.6. After the particles enter the applicator, both the particles and the liquid are subjected to microwave irradiation. It is found that the region of high microwave power density is located in the central area of the applicator. The power densities in the particles are different from that in the surrounding liquid because of different dielectric properties of the particles and the liquid. It is also found that the injection of particles does not modify the power density distributions in the liquid except in the vicinity of the particles. A thermal wake is developed in front of each particle as the particle moves downstream the applicator, which is due to the increase of the velocity difference between the particle and the surrounding liquid.

Figure 5.7 shows the microwave power density and temperature distributions inside particles #15 and #19 in the planes corresponding to $\theta = 0^\circ$ and 180°. It is found that the power density inside the particles is greatly affected by the power density

distribution in the liquid. From Figures 5.6(a) and 5.7(a), it is evident that a region of higher power density occurs in the half of the particle which is closer to the centerline of the applicator. The power density inside a particle is high if the power density in the surrounding liquid is high (which is caused by high electromagnetic field intensity in this region). The power density in particle #15 is higher as the particle is closer to the central area of the applicator; the power density decreases as the particle moves toward the wall of the applicator, which happens after the collision between particles #15 and # 19. Since particle #15 is pushed toward the central area of the applicator by particle #19, the power density inside particle #15 increases. This trend is consistent with the observation that the power density distribution in the liquid in the central portion of the applicator is the highest. It is found that the temperature distribution inside the particle does not exactly follow the power density distribution, which is attributed to the effects of particle rotation as well as convection heat transfer between the surface of the particle and the surrounding liquid.

The mean temperature of particles at the outlet of the applicator for cases A and B is shown in Figure 5.8(a). It is found that the mean particle temperature distribution is more scattered in case A. That is attributed to a wider residence time distribution of particles for case A. Distribution of the mean power density in the mixture that includes both the liquid and particles is shown in Figure 5.8(b). It is found that the mean power density increases as time progresses in the beginning, then the mean power density remains almost constant, and finally it decreases as the particles start leaving the applicator. This can be attributed to the higher loss tangent of the particles than that of the liquid.

5.6.3 *EFFECT OF THE APPLICATOR POSITION IN THE MICROWAVE CAVITY*

The effect of the applicator position on power density and temperature distributions in both the liquid and particles is studied for case B. Ten different locations of the applicator are investigated. The position with the applicator in the center of the microwave cavity is treated as the base case; other nine cases correspond to -11.6 *cm*, -9.0 *cm*, -4.5 *cm*, +4.5 *cm*, +9.0 *cm*, and +11.6 *cm* applicator shift in the *X*-direction, and -4.5 *cm*, -7.0 *cm* and -8.4 *cm* applicator shift in the *Y*-direction. Figure 5.9 shows the power density distribution at the outlet of the applicator for different applicator positions at t=0.5 *s*. It is evident that the power density decreases significantly as the applicator is shifted from the base case location in either *X*- or *Y*-direction. It is also found that as the applicator is shifted in the *Y*-direction, the symmetry of the power density distribution in the planes corresponding to $\theta = 0^\circ$ and 180° breaks down, which does not happen if the applicator is displaced in the *X*-direction. This is because when the applicator is shifted away from the base position in the *Y*-direction, the symmetry of dielectric properties in the microwave cavity is broken, which distorts the electromagnetic field in the cavity. Figure 5.10 shows the electromagnetic filed in the plane located at 50% height of the microwave cavity perpendicular to the flow direction. It is evident that the electromagnetic field is not symmetric with respect to the *X*- axis. This results in the power density distribution in the applicator being asymmetric with respect to the planes corresponding to $\theta = 0^\circ$ and 180°. Since the electromagnetic field intensity is larger in the central area along the *X*-axis, as shown in Figure 5.10, the applicator shift away from the base position in the *Y*-direction significantly decreases the power absorption by the particulate flow in the applicator.

The temperatures inside the particles are greatly affected by the power density distribution in the applicator and are quite sensitive to the variation of the applicator position. Table 5.4 shows the mean temperature of particles # 1 and # 3 at the moment of them leaving the applicator. It is found that in cases of the applicator shift in the *X*-direction the mean temperature of particle #3 is higher than that of particle #1. For cases of the applicator shift in the *Y*-direction, the mean temperature of particle #1 is higher than that of particle #3. This is because the peak of the microwave power in the applicator occurs closer to the exposed surface of the applicator wall (for the definition of the exposed and unexposed surfaces see Figure 5.1(b)) when the applicator is shifted in the *X*-direction away from the base position, and particle #1 is closer to the exposed surface than particle #3. As the applicator is shifted in the *Y*-direction from the base position, the power peak occurs closer to the unexposed surface, and particle #3 is closer to the unexposed surface than particle #1. The inlet positions of particles #1 and #3 are illustrated in Figure 5.1(b).

5.7 CONCLUSIONS

Continuous microwave heating of a non-Newtonian liquid that carries large solid particles as it passes through the applicator pipe is investigated using a three-dimensional model. The model takes into account hydrodynamic, thermal, and electromagnetic fields in the liquid and particles. The results reveal that the particles are mainly heated by the microwave irradiation and not so much by convection with the surrounding liquid as it happens in traditional heating methods. The power absorption in the particles is determined by dielectric properties of the particles and the power density distribution in

the liquid. More power absorption in the particle occurs if the particle's path is close to the area of the highest power density in the liquid. It is also found that collisions between particles make the group of particles spread out in the radial direction and result in widening the residence time distribution of the particles. The collisions also result in enlarging the difference in the power absorption by different particles. It is also found that the power absorption in both the liquid and particles is greatly attenuated by shifting the applicator away from the center of the microwave cavity. Shifting the applicator affects the power density distribution in both the liquid and the particles.

Table 5.1 Geometric parameters of the microwave system.

Symbol	Description	Value (cm)
D	Applicator diameter	3.8
AD	Apogee distance of cavity	20.5
PD	Perigee distance of cavity	15.4
CH	Cavity and applicator height	12.5
WL	Waveguide length	34.7
WW	Waveguide width	24.4
WH1	Waveguide height 1	12.5
WH2	Waveguide height 2	5.1
TL	Total length of the system	66.1
IAD	Distance between the incident plane and absorbing plane	2.7

Table 5.2 Comparison of the drag coefficient, C_D, predicted by the code with published data [30].

Case	$\mathrm{Re}_p = 10$	$\mathrm{Re}_p = 100$
Present work	4.02	1.06
Published	4.26	1.11

Table 5.3 Thermophysical and electromagnetic properties utilized in computations.

$\varepsilon_0 = 8.85419\times10^{-12}$ (F/m)	$\varepsilon_{rad} = 0.4$
$\mu = 4.0\pi\times10^{-7}$ (H/m)	$\sigma_{rad} = 5.67\times10^{-8}$ (W/(m$^2\cdot$K^4))
$h = 20$ (W/(m$^2\cdot$K))	$P_{in} = 7000$ (W)
$Z_{TE} = 377$ (Ω)	$f = 915$ (MHz)
$k_p = 0.47$ W/(m$\cdot$K)	$k_l = 0.57$ W/(m$\cdot$K)
$C_{pp} = 2500$ J/(kg$\cdot$K)	$C_{pl} = 3944$ J/(kg$\cdot$K)
$\rho_p = 1069$ kg/m^3	$\rho_l = 1037$ kg/m^3
$\varepsilon_r' = 68.4$ (particles)	$\varepsilon_r' = -0.155T + 72.5$ (liquid)
$\tan\delta = 0.86$ (particles)	$\tan\delta = 0.0034T + 0.18$ (liquid)
$m = 0.0059$ Pa$\cdot s^n$	$n = 0.98$

Table 5.4 Particles' mean temperature at the applicator outlet, $^\circ C$.

Particles	Applicator shift in the *X*-direction (cm)						Base case	Applicator shift in the *Y*-direction (cm)		
	-11.6	-9.0	-4.5	+4.5	+9.0	+11.6	no shift	-4.5	-7.0	-8.4
#1	23.0	25.7	52.0	29.4	23.0	22.0	71.7	80.8	49.8	33.6
#3	54.1	57.1	78.1	72.3	49.1	39.6	68.8	25.3	25.2	24.9

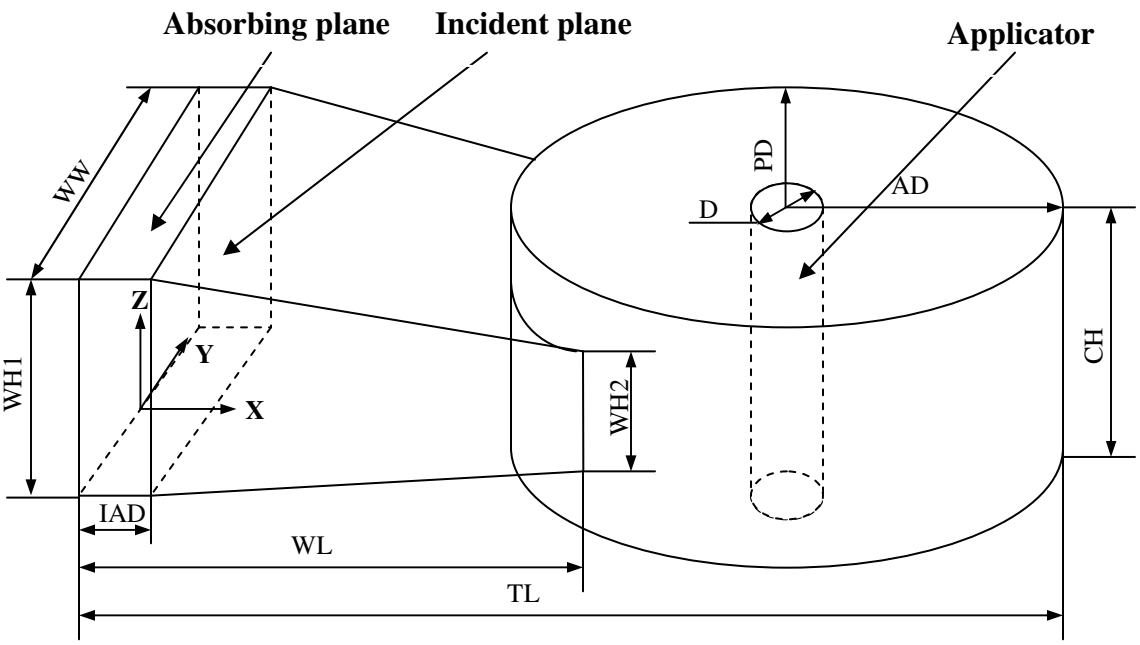

(a)

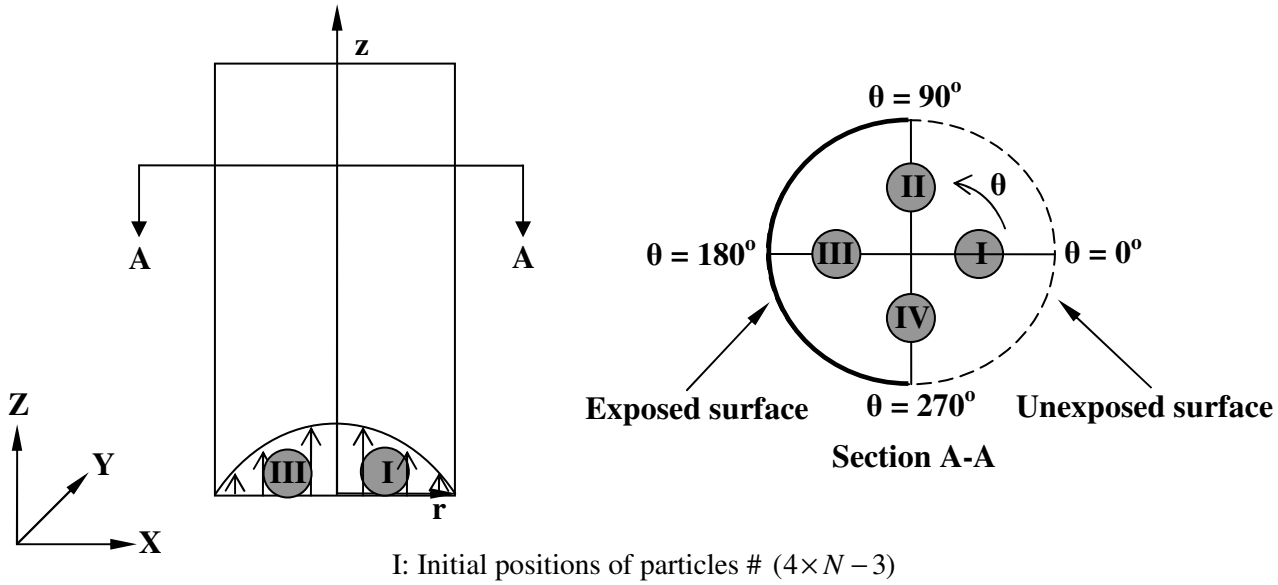

I: Initial positions of particles # $(4\times N-3)$

II: Initial positions of particles # $(4\times N-2)$

III: Initial positions of particles # $(4\times N-1)$

IV: Initial positions of particles # $(4\times N)$

(b)

Figure 5.1 (a) Schematic diagram of the microwave system; (b) Basic arrangement for the particles inside the applicator.

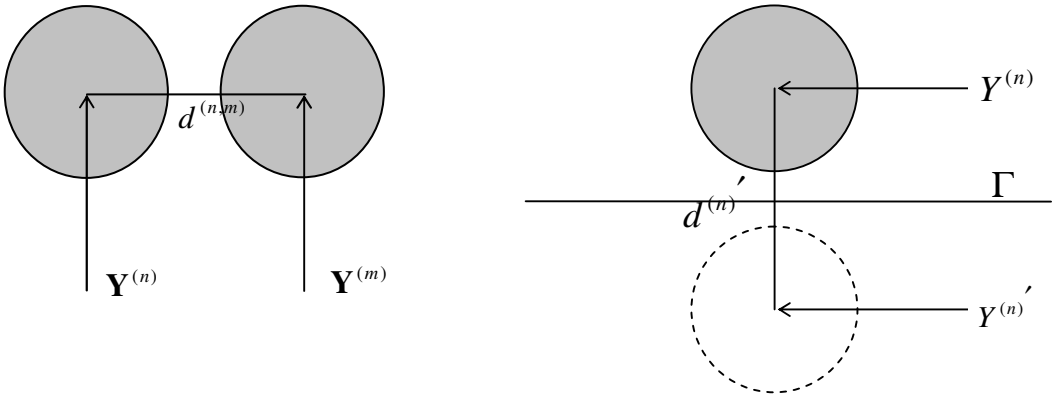

Figure 5.2 Schematic diagram for calculating contact forces of the inter-particle and particle-wall collisions.

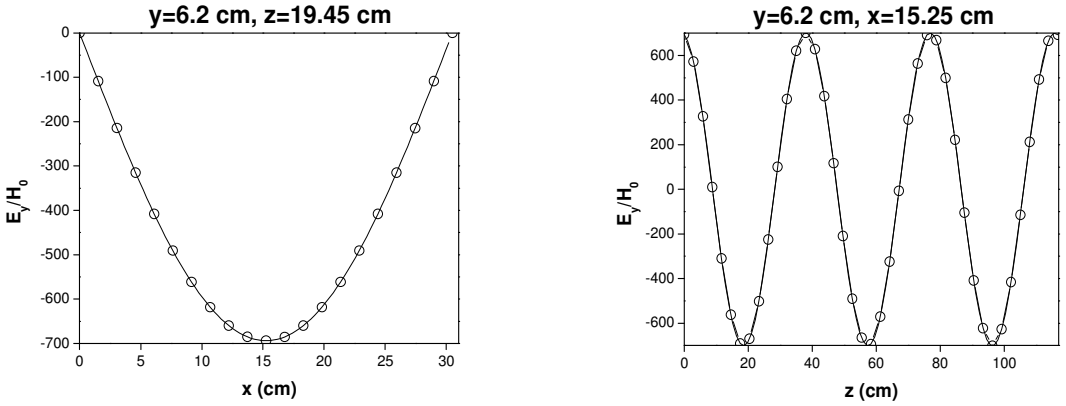

(a) E_y component

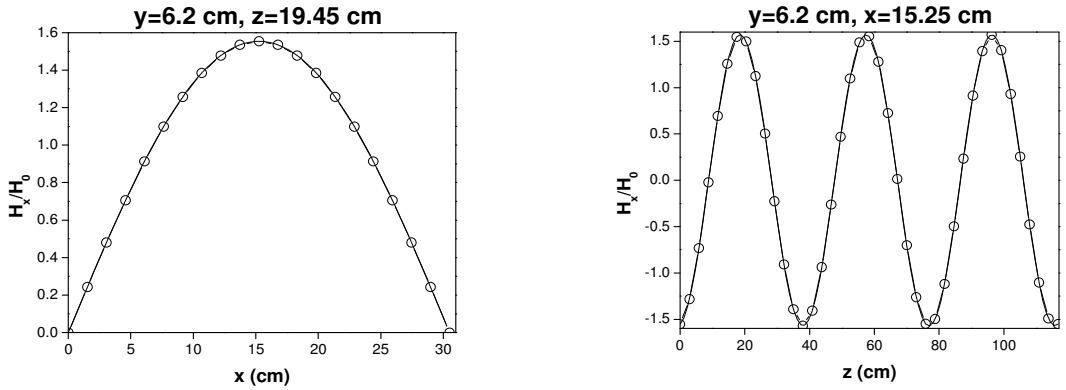

(b) H_x component

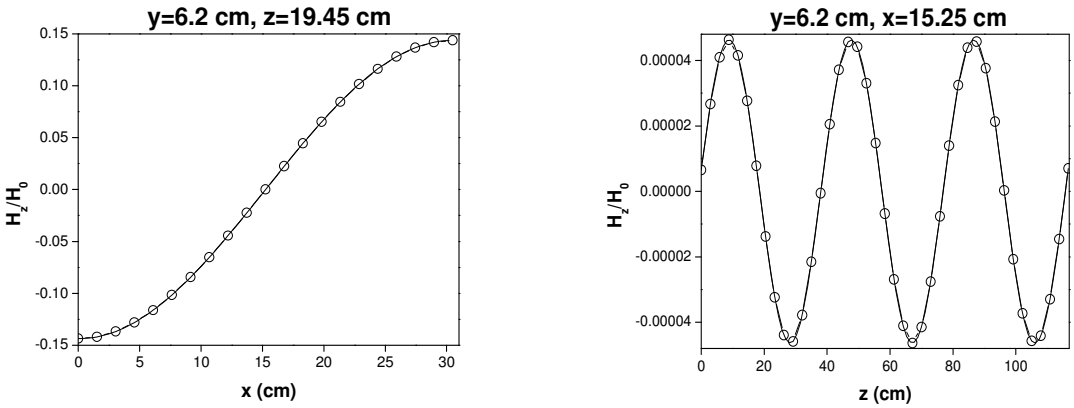

(c) H_z component

Figure 5.3 Comparison of numerical and analytical solutions for field components. Solid line: numerical solution; circles: analytical solution.

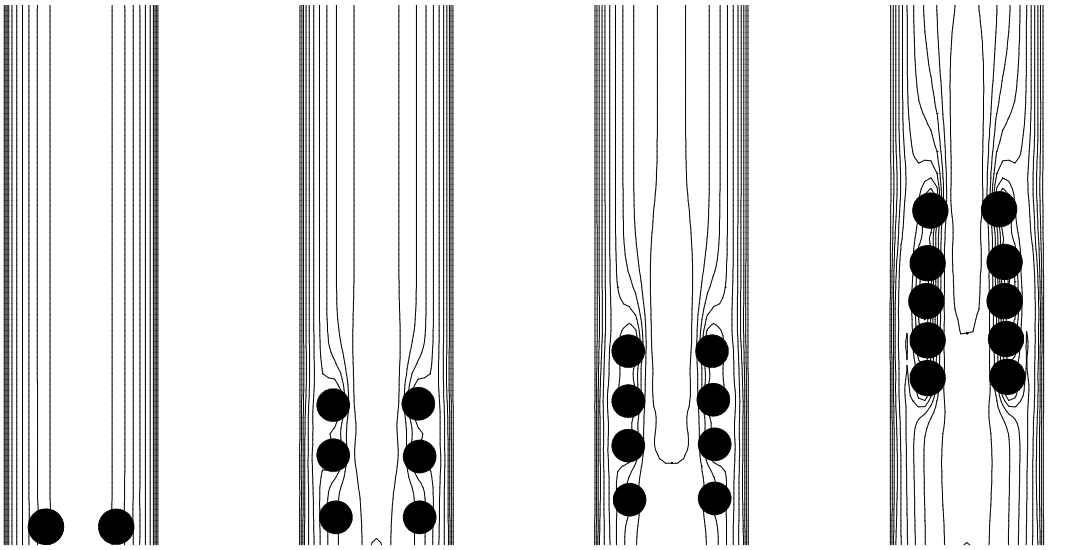

t = 0.004 s t = 0.31 s t = 0.50 s t = 0.99 s

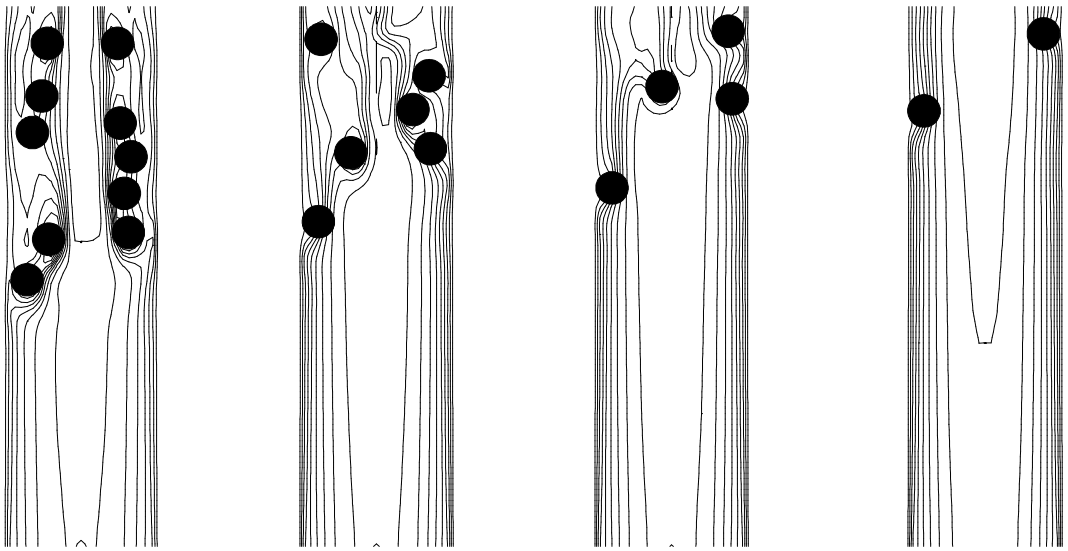

t = 1.73 s t = 2.12 s t = 2.36 s t = 2.72 s

Figure 5.4 Contour lines of the axial velocity of the fluid flow in the planes corresponding to $\theta = 0^{\circ}$ and 180°.

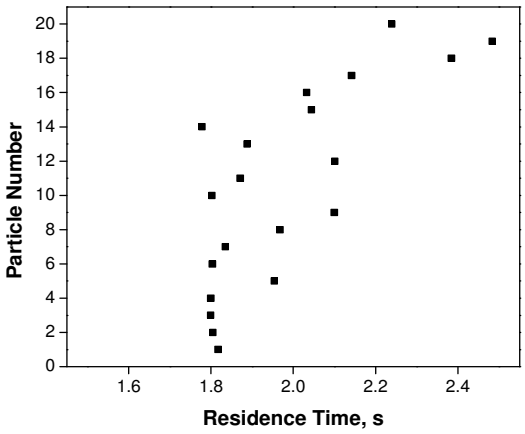

(a)

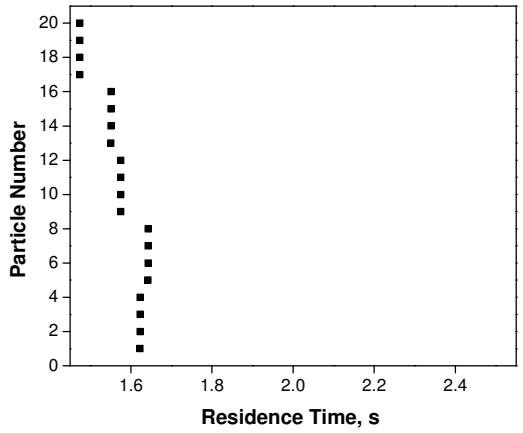

(b)

Figure 5.5 Residence time distribution of the particles : (a) case A, (b) case B.

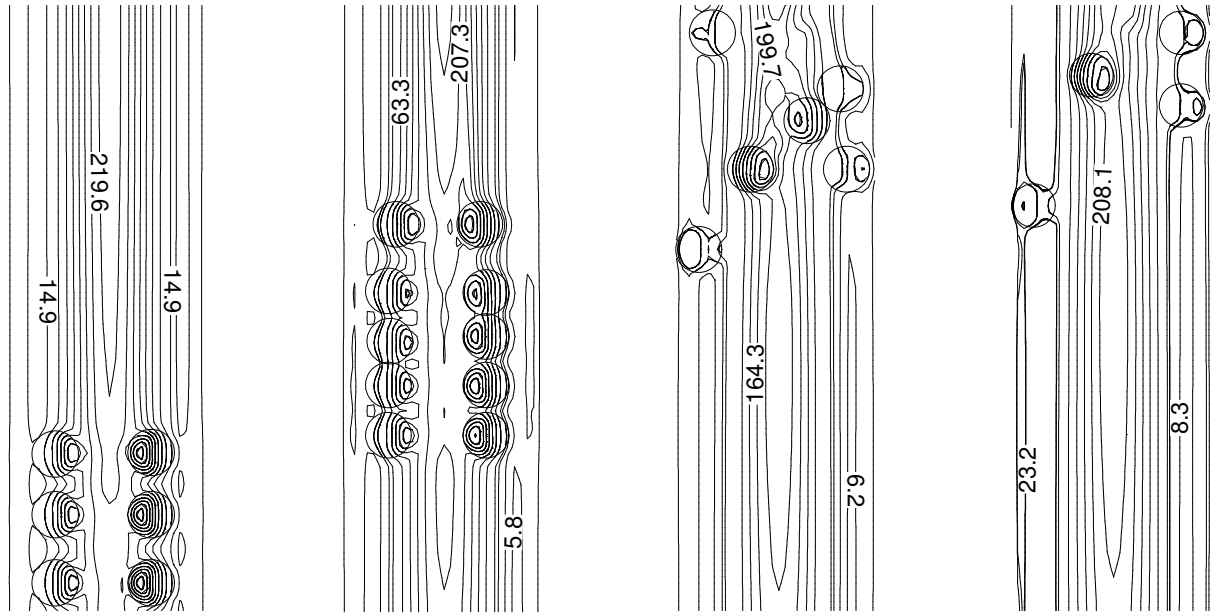

$t = 0.31\ s$ $t = 0.99\ s$ $t = 2.12\ s$ $t = 2.36\ s$

(a)

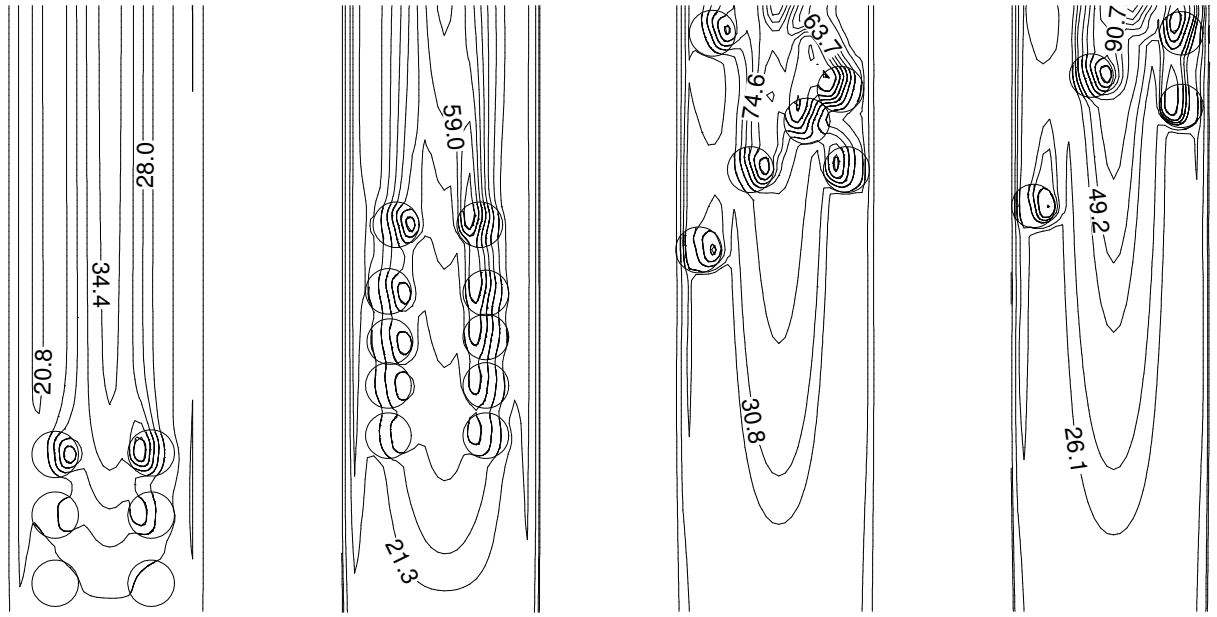

$t = 0.31\ s$ $t = 0.99\ s$ $t = 2.12\ s$ $t = 2.36\ s$

(b)

Figure 5.6 Transient distributions: (a) microwave power density, W/cm^3, (b) temperature, $^{\circ}C$.

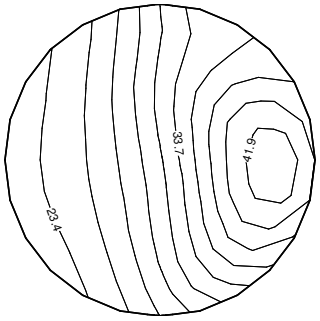

Temperature, $^{\circ}C$, t = 0.99 s

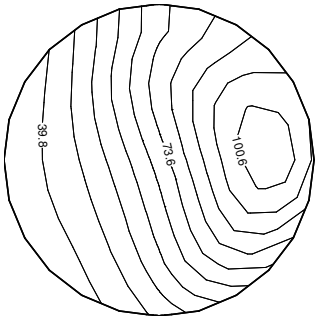

Temperature, $^{\circ}C$, t = 2.12 s

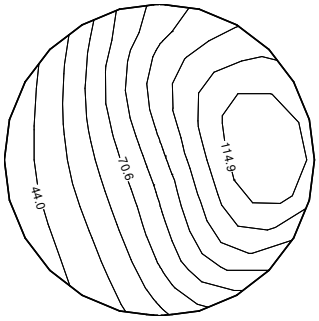

Temperature, $^{\circ}C$, t = 2.36 s

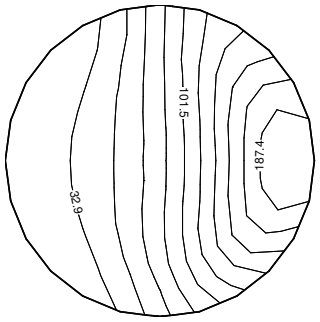

Power density, W/cm^3, t = 0.99 s

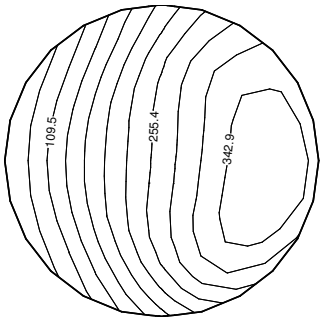

Power density, W/cm^3, t = 2.12 s

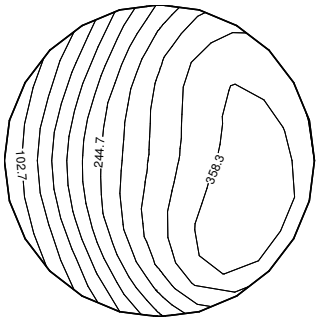

Power density, W/cm^3, t = 2.36 s

(a)

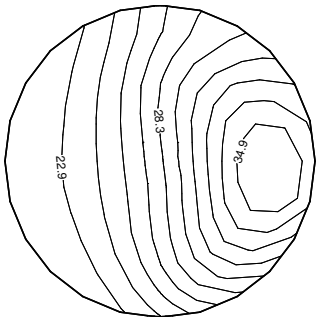

Temperature, $^{\circ}C$, t = 0.99 s

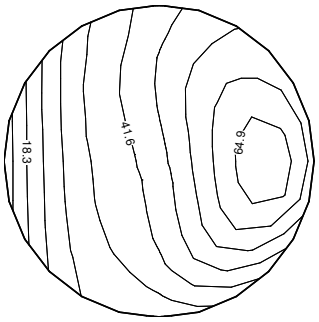

Temperature, $^{\circ}C$, t = 2.12 s

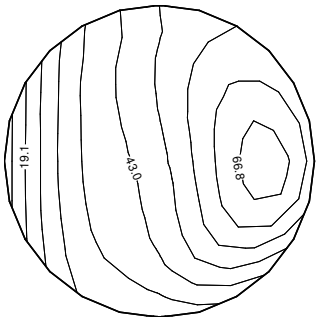

Temperature, $^{\circ}C$, t = 2.36 s

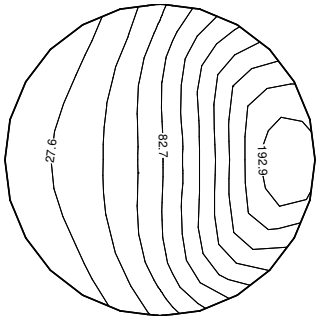

Power density, W/cm^3, t = 0.99 s

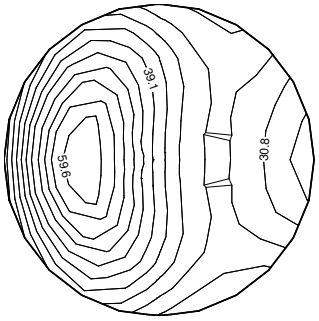

Power density, W/cm^3, t = 2.12 s

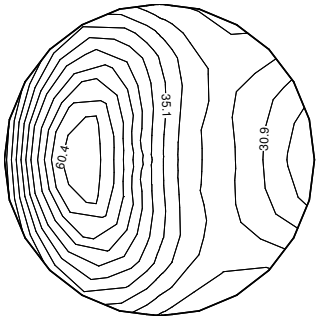

Power density, W/cm^3, t = 2.36 s

(b)

Figure 5.7 Microwave power density and temperature distributions inside particles: (a) particle #15, (b) particle #19.

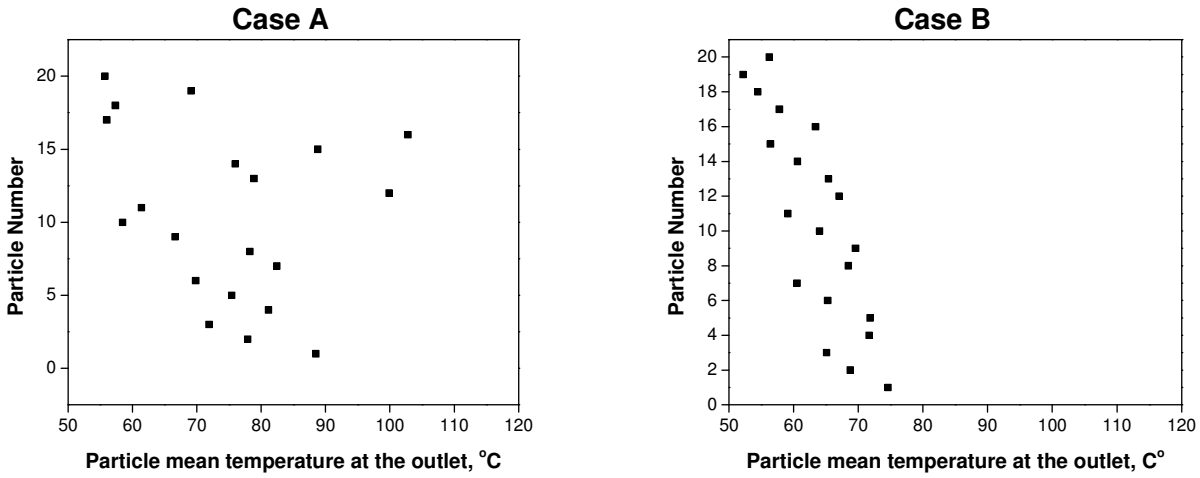

(a)

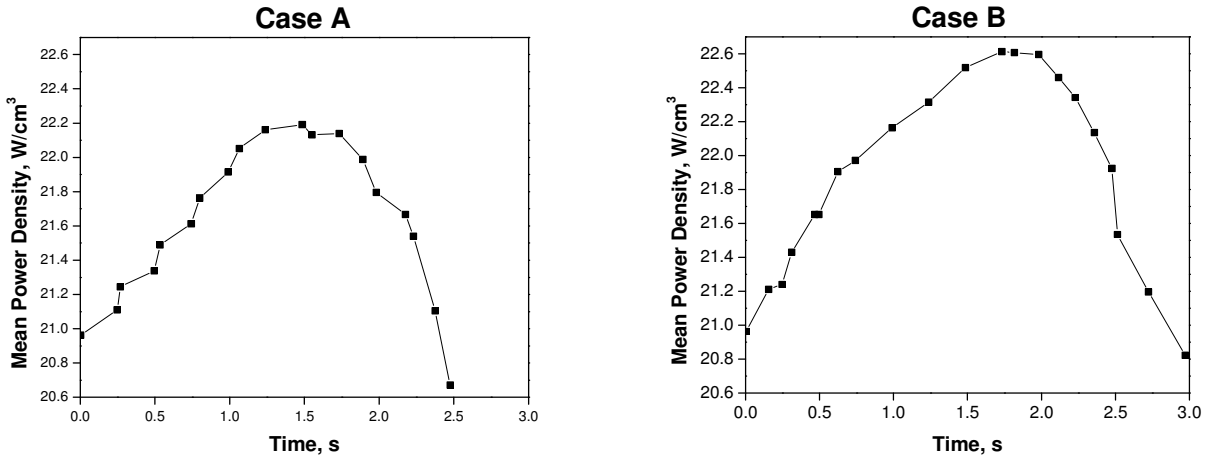

(b)

Figure 5.8 (a) Particles' mean temperature at the outlet of the applicator, $^{\circ}C$; (b) Mean power density in the mixture of the liquid and the particles, W/cm^3.

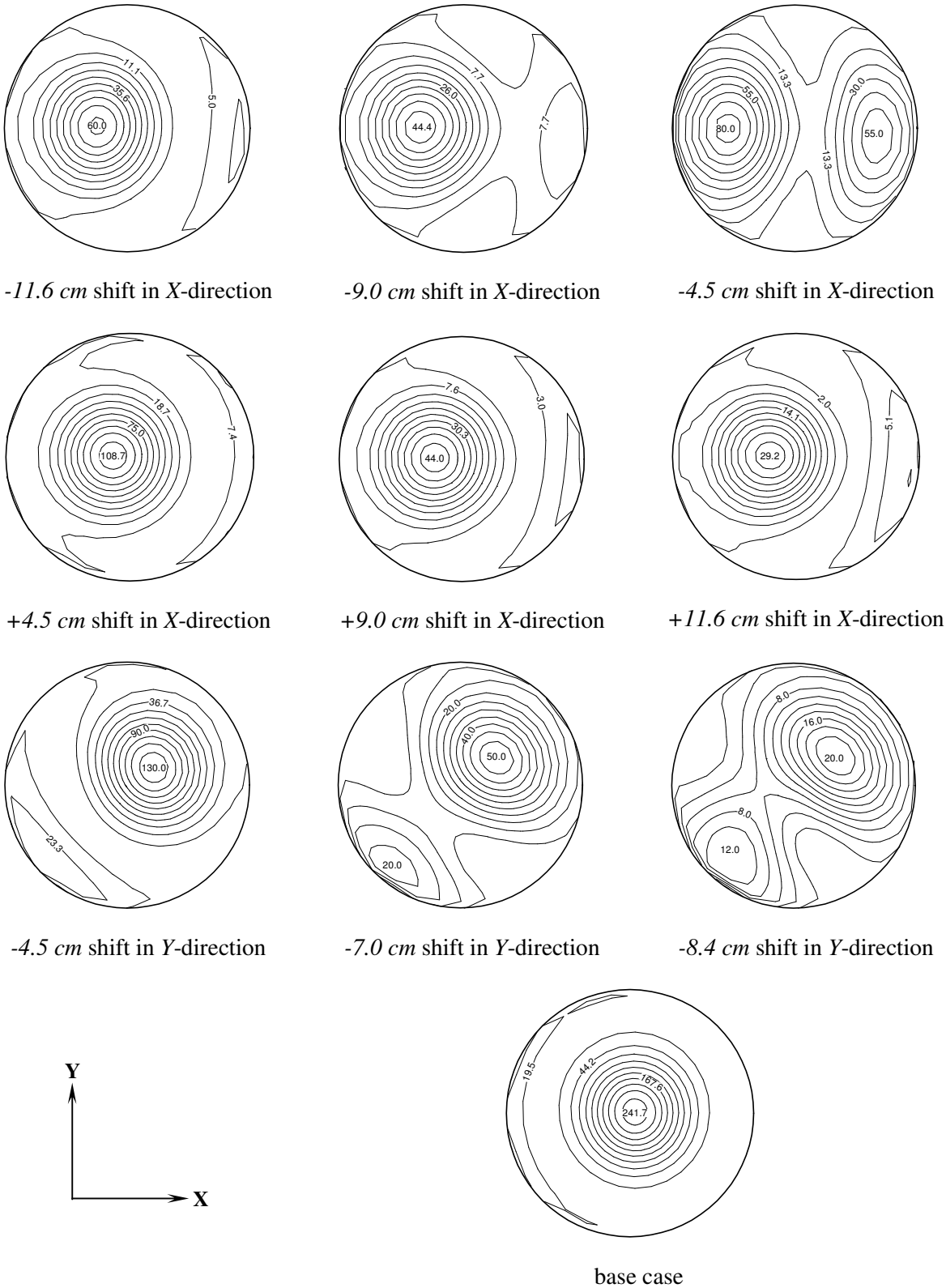

Figure 5.9 Power density distribution at the outlet of the applicator, W/cm^3.

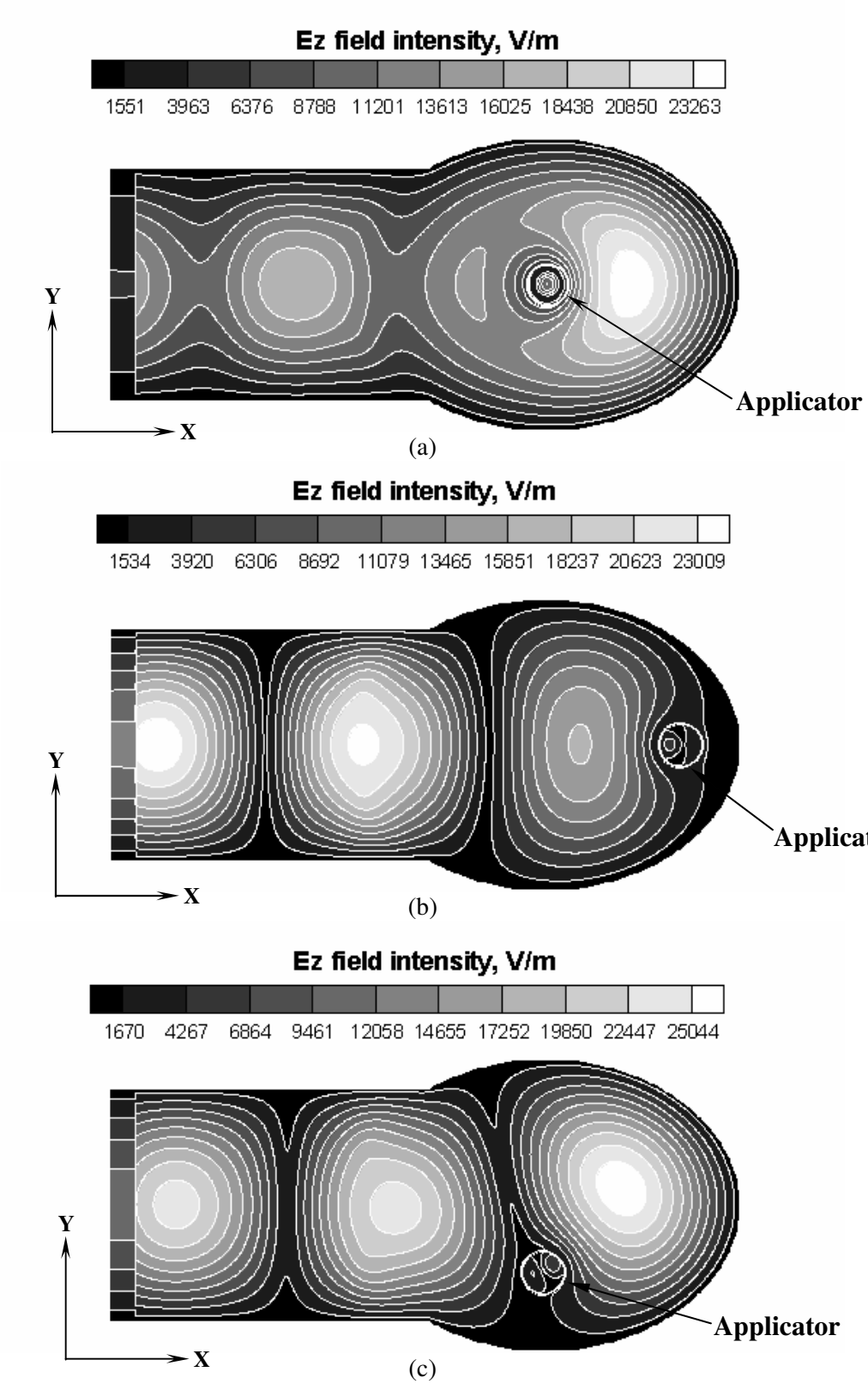

Figure 5.10 Distribution of electric field component, E_z, (V/m): (a) base case; (b) +11.6 *cm* applicator shift in the *X*-direction; (c) – 7.0 *cm* applicator shift in the *Y*-direction.

REFERENCES

1. Ayappa, K.G., Davis, H.T., Davis, E.A., Gordon, J. (1992) Two-dimensional finite element analysis of microwave heating, *AIChE Journal*, 38: 1577-1592.
2. Ayappa, K.G., Sengupta, T. (2002) Microwave heating in multiphase systems: evaluation of series solutions, *Journal of Engineering Mathematics*, 44: 155-171.
3. Kriegsmann, G.A. (1997) Cavity effects in microwave heating of ceramics, *Journal of Applied Mathematics*, 57: 382-400.
4. Araneta, J.C., Brodwin, M.E., Kriegsmann, G.A. (1984) High-temperature microwave characterization of dielectric rods, *IEEE Transactions on Microwave Theory and Techniques*, 32: 1328-1335.
5. Basak, T., Ayappa, K.G. (1997) Analysis of microwave thawing of slabs with effective heat capacity method, *AIChE Journal*, 43: 1662-1667.
6. O'Brien, K.T., Mekkaoui, A.M. (1993) Numerical simulation of the thermal fields occurring in the treatment of malignant rumors by local hyperthermia, *Journal of Biomechanical Engineering*, 115: 247-253.
7. Ayappa, K.G., Brandon, S., Derby, J.J., Davis, H.T., Davis, E.A. (1994) Microwave driven convection in a square cavity, *AIChE Journal*, 40: 1268-1272.
8. Franca, A.S., Haghighi, K. (1996) Adaptive finite element analysis of microwave driven convection, *International Communications in Heat and Mass Transfer*, 23: 177-186.
9. Saltiel, C., Datta, A. (1997) Heat and mass transfer in microwave processing, *Adv. Heat Transfer*, 30: 1-94.

10. Ayappa, K.G., Davis, H.T., Davis, E.A., Gordon, J. (1991) Analysis of microwave heating of materials with temperature dependent properties, *AIChE Journal*, 37: 313-322.
11. Ratanadecho, P., Aoki, K., Akahori, M. (2002) Influence of irradiation time, particle sizes, and initial moisture content during microwave drying of multi-layered capillary porous materials, *Journal of Heat Transfer*,124: 151-161.
12. Clemens, J., Saltiel, C. (1995) Numerical modeling of materials processing microwave furnaces, International Journal of Heat and Mass Transfer 39: 1665-1675.
13. Basak, T., Ayappa, K.G. (2002) Role of length scales on microwave thawing dynamics in 2D cylinders, *International Journal of Heat and Mass Transfer*, 45: 4543-4559.
14. Barringer, S.A., Davis, E.A., et al. (1995) Microwave heating temperature profiles for thin slabs compared to Maxwell and Lambert law predictions, *Journal of Food Science*, 60: 1137-1142.
15. Aoki, K., Ratanadecho, P., Akahori, M. (2000) Characteristics of microwave heating for multi-layered materials using a rectangular wave guide, *Proceeding of the 4 th JSME-KSME Thermal Engineering Conference*, 2: 191-196.
16. Zhang, Q., Jackson, T.H., Ungan, A. (2000) Numerical modeling of microwave induced natural convection, *International Journal of Heat and Mass Transfer*, 43: 2141-2154.
17. Ratanadecho, P., Aoki, K., Akahori, M. (2002) A numerical and experimental investigation of the modeling of microwave heating for liquid layers using a

rectangular wave guide (effects of natural convection and dielectric properties), *Applied Mathematical Modeling*, 26: 449-472.

18. Zhu, J., Kuznetsov, A.V., Sandeep, K.P. (2005) Numerical simulation of forced convection in a duct subjected to microwave heating, *Heat and Mass Transfer*, http://dx.doi.org/10.1007/s00231-006-0105-y, (online first).
19. Zhu, J., Kuznetsov, A.V., Sandeep, K.P. (2005) Mathematical modeling of continuous flow microwave heating of liquids (effects of dielectric properties and design parameters), *International Journal of Thermal Sciences*, In press.
20. Zhu, J., Kuznetsov, A.V., Sandeep, K.P. (2006) Numerical modeling of a moving particle in a continuous flow subjected to microwave heating, *Numerical Heat Transfer, Part A*, Submitted.
21. Cheng, D.K. (1992) *Field and Wave Electromagnetics*, Addison-Wesley, New York
22. Mur, G. (1981) Absorbing boundary conditions for the finite difference approximation of the time domain electromagnetic field equations, *IEEE Trans. Electromag. Compat.*, EMC-23, No. 4, pp. 377-382.
23. Maxey, M.R., Patel, B.K. (2001) Localized force representations for particles sedimenting in Stokes flow, International Journal of Multiphase Flow 27: 1603-1626
24. Lomholt, S.B., Stenum, Maxey, M.R. (2002) Experimental verification of the force coupling method for particulate flows, *International Journal of Multiphase Flow*, 28: 225-246.
25. Dance, S.L., Maxey, M.R. (2003) Force-coupling method for particulate two-phase flow: Stokes flow, *Journal of Computational Physics*, 184: 381-405.

26. Dance, S.L., Maxey, M.R. (2003) Incorporation of lubrication effects into the force-coupling method for particulate two-phase flow, *Journal of Computational Physics*, 189: 212-238.

27. Glowinski, R., Pan, T.W., Hesla, T.I., Joseph, D.D. (1999) A distributed Lagrange multiplier/fictitious domain method for particulate flows, *International Journal of Multiphase Flow*, 25: 755-794.

28. Kunz, K.S., Luebbers, R. (1993) *The Finite Difference Time Domain Method for Electromagnetics*, CRC, Boca Raton, FL.

29. Patankar, S.V., Spalding, D.B. (1972) A calculation procedure for heat, mass and momentum transfer in three-dimensional parabolic flows, *Journal of Heat and Mass Transfer*, 15: 1787-1806.

30. Clift, R., Grace, J.R., Weber, M.E. (1978) *Bubbles, Drops, and Particles, Academic Press*, San Diego, CA.

6 CONCLUSIONS

This dissertation investigates heat transfer in liquids as they flow continuously in a duct that is subjected to microwave heating; microwave heating of a food particle or particles and carrier liquid as they flow continuously in a circular pipe. Mathematical modeling and numerical results are presented.

6.1 REMARKS ON HEAT TRANSFER IN LIQUIDS AS THEY FLOW CONTINUOUSLY IN A DUCT THAT IS SUBJECTED TO MICROWAVE HEATING

Continuous processing of food is a promising alternative to traditional heating of liquid food in containers. During this process, liquid food flows in an applicator tube. When flow passes through the microwave cavity, the liquid absorbs microwave power and its temperature quickly increases. A 3D numerical model is set up for simulating heat transfer in a non-Newtonian liquid continuously flowing in an applicator that is subjected to microwave heating. The results reveal a complicated interaction between electromagnetic field and convection. The spatial variation of the electromagnetic field and temperature field was obtained by solving coupled momentum, energy and Maxwell's equations.

It is found that dielectric properties of the liquid determine the ability of the liquid to absorb the microwave energy; the geometry of the microwave system has great effect on the power absorption and distribution as well. Enlarging the size of the applicator increases the effective surface available to absorb the microwave energy, usually increases the power absorption in the liquid. However, beyond the critical size of the applicator, an opposite trend is observed. The critical size of the applicator depends on

the geometry of the resonant cavity and dielectric properties of the liquid flowing in the applicator. The microwave power absorption is also sensitive to the location of the applicator and the shape of the resonant cavity, which affect the microwave propagation and resonance.

6.2 Remarks on Microwave Heating of a Food Particle or Multiple Particles and Carrier Liquid as They Flow Continuously in a Circular Pipe

A three-dimensional model of microwave heating of a liquid carrying a single large particle or multiple large particles as it flows in the applicator subjected to microwave irradiation is proposed. The power absorption and temperature distributions in both the liquid and particles are investigated. The model takes into account hydrodynamic and thermal interactions between the particle and the carrier liquid. It is shown that the particle may get heated at a different rate than the carrier liquid. And the particle is mainly heated by the microwave irradiation and not so much by convection with the surrounding liquid as it happens in traditional heating methods. The results reveal that the power absorption in the particle is determined by the value of the loss tangents of the particle and the carrier liquid. The particle absorbs more microwave energy in a high loss liquid than in a low loss liquid. The power absorption in the liquid is also influenced by the particle. The power density distribution inside the particle is determined by the power distribution in the liquid. Depending on the radial positions of the particle at the inlet of the applicator, power absorption in the particle may differ significantly. The power absorption in the particle shows a strong dependence on the distance between the particle and the location of the power peak in the liquid.

It is also found that collisions between particles make the group of particles spread out in the radial direction and result in widening the residence time distribution of the particles. The collisions also result in enlarging the difference in the power absorption by different particles. It is also found that the power absorption in both the liquid and particles is greatly attenuated by shifting the applicator away from the center of the microwave cavity. Shifting the applicator affects the power density distribution in both the liquid and the particles.